



**POLITECNICO**  
MILANO 1863

SCUOLA DI INGEGNERIA INDUSTRIALE  
E DELL'INFORMAZIONE

# Design, Realization and Control of an Aquatic Snake robot

TESI DI LAUREA MAGISTRALE IN  
MECHANICAL ENGINEERING-INGEGNERIA  
MECCANICA

Author: **Kavinda Pradeep Herath Herath Mudiyanse Lage**

Student ID: 10730809  
Advisor: Simone Cinquemani  
Co-advisor: Bianchi Giovanni  
Academic Year: 2020-21



# Abstract

The conventional aquatic robots encounter several challenges such as versatility of operations, flexibility of usages, and adaptability on all kind of aquatic environments. In this dissertation, an aquatic snake robot was designed, realized, and controlled to face these issues. This bioinspired aquatic snake robot is modular, remotely operated, slightly buoyant, and waterproof. Power and control are distributed, and the aquatic snake robot has a laterally compressed body. It is equipped with sensors such as a camera, ultrasonic sensor, and inertial measurement unit sensor. In this thesis, a kinematic model and a dynamic model are presented. The control algorithm necessary to achieve forward motion and turning has been developed for two different swimming gaits. These algorithms have been simulated by using MATLAB to observe the behaviors of the aquatic snake robot while performing the swimming gaits. The aquatic snake robot has been manufactured, and its electronic circuit has been realized integrating the sensors and the communication with the external device. The developed control algorithm implemented using a high-level feedforward system and a low-level feedback system. Two different swimming patterns have been tested in an aquatic environment, and it has been observed that aquatic snake robot is able to propel forward in water.

**Keywords:** Bioinspired Robotics, Aquatic Snake Robot, Snake Swimming Gait, Modular Robot.



## Abstract in lingua italiana

I robot acquatici convenzionali affrontano diverse sfide come la versatilità delle operazioni, la flessibilità degli usi e l'adattabilità a tutti i tipi di ambienti acquatici. In questa tesi un robot serpente acquatico è stato progettato, realizzato e controllato. Questo robot serpente acquatico di ispirazione biologica è modulare, comandato a distanza, leggermente galleggiante e impermeabile. La potenza e il controllo sono distribuiti e il robot serpente acquatico ha un corpo compresso lateralmente. È dotato di sensori tra cui una macchina fotografica, un sensore a ultrasuoni e un sensore per unità di misura inerziale. In questa tesi vengono presentati un modello cinematico e un modello dinamico. L'algoritmo di controllo necessario per ottenere il movimento in avanti e le manovre è stato sviluppato per due diverse tipologie di nuoto. Questi algoritmi sono stati simulati utilizzando MATLAB per osservare i comportamenti del robot serpente acquatico durante l'esecuzione dei movimenti di nuoto. Il robot serpente acquatico è stato costruito, ed è stato realizzato il suo circuito elettronico integrando i sensori e la comunicazione con un dispositivo esterno. L'algoritmo di controllo è stato implementato utilizzando un sistema feedforward di alto livello e un sistema di feedback di basso livello. Sono stati sperimentati due diversi modelli di nuoto in ambiente acquatico ed è stato osservato che il robot serpente acquatico è in grado di nuotare in avanti.

**Parole chiave:** Robotica Bioispirata, Robot Serpente Acquatico, Nuoto Del Serpente, Robot Modulare.



# Contents

<b>Abstract.....</b>	i
<b>Abstract in lingua italiana .....</b>	iii
<b>Contents .....</b>	v
<b>Introduction.....</b>	1
Objective of the thesis .....	2
Thesis Organization .....	3
<b>1. Physical principles of aquatic snake locomotion .....</b>	5
1.1 Sea Snake Anatomy .....	6
1.2 Swimming gait .....	8
1.3 Motivation for Biomimicry .....	9
<b>2. State of the Art.....</b>	11
2.1 Terrestrial snake robot .....	11
2.1.1 Passive wheels .....	12
2.1.2 Wheel less .....	12
2.1.3 Active wheel.....	14
2.1.4 Elongation.....	15
2.2 Amphibious and aquatic snake robot.....	15
2.2.1 Passive propeller .....	16
2.2.2 Propeller less .....	18
2.2.3 Active propeller .....	20
<b>3. Design of the Robot.....</b>	21
3.1 Design requirements .....	21
3.2 Head design.....	23
3.2.1 Ultrasonic sensor .....	24
3.2.2 Camera .....	25

3.2.3	Inertial measurement unit.....	25
3.2.4	Bluetooth module .....	25
3.2.5	Microcontroller. ....	26
3.2.6	Head outer cover .....	26
3.3	Module design.....	27
3.3.1	Servo.....	28
3.3.2	Microcontroller .....	28
3.3.3	Module outer cover.....	29
3.4	Design of the Assembly .....	30
<b>4.</b>	<b>Modeling of an aquatic snake robot.....</b>	<b>33</b>
4.1.	Kinematic Model .....	33
4.2.	Dynamic Model .....	38
<b>5.</b>	<b>Control algorithm.....</b>	<b>47</b>
5.1	State of art of Control algorithm.....	47
5.1.1	Feedforward control .....	47
5.1.2	Feedback control.....	50
5.2	Implemented Control Algorithm .....	51
5.2.1	Lateral undulation.....	51
5.2.2	Eel motion.....	53
5.2.3	Simulation.....	54
5.3	Gait implementation .....	64
5.3.1	High level feedforward system .....	65
5.3.2	Low level feedback system .....	66
<b>6.</b>	<b>Construction of the robot and the Experimental tests .....</b>	<b>71</b>
6.1	Fused deposition modeling.....	71
6.2	Head assembly .....	73
6.3	Module assembly .....	76
6.4	Snake Robot Assembly.....	79
6.5	Experimental tests .....	81
6.5.1	Eel-Like motion.....	82
<b>7.</b>	<b>Conclusion and future development .....</b>	<b>85</b>

7.1	Conclusion .....	85
7.2	Future development.....	86
	<b>Bibliography.....</b>	<b>89</b>
	<b>List of Figures.....</b>	<b>101</b>
	<b>List of Tables .....</b>	<b>105</b>
2.	<b>Acknowledgements .....</b>	<b>109</b>



# Introduction

Aquatic robots have been a prominent robotic research area for several decades. These robots provide the ability for data collection, inspection, construction in aquatic environments and maintenance of the aquatic equipment's. In designing the aquatic robot, scientific community has gained inspiration from nature on many occasions. This process is known as bioinspiration. The unique nature of locomotion that can be observed in the sea snakes provides them the ability to move through constraint and narrow spaces and different environments in the water. This nature has inspired the scientific community to mimic this abilities and create aquatic robots with a similar characteristic. These robots are known to be aquatic snake robots, water snake robots, ocean snake robots, etc.

Aquatic snake robots receive a special attention since they perform better than the conventional aquatic robots in many areas thanks to their physical properties which are listed below.

- Hyper-redundancy:

Being inspired from the biological sea snake, snake robots are designed to have many degrees of freedoms (DOFs). These DOFs provide the snake robot the ability to move through constraint spaces. Due to its hyper-redundancy the aquatic snake robot (ASR) can be used as a manipulator. Further in modular ASR, since the robot is composed of individual links, a malfunction of one or many links does not affect the function of the whole ASR.

- Compactness:

The cross-section of the sea snake is very small compared to the length of its body. This property grants sea snake the ability to swim through constrained spaces. Similarly, ASRs can navigate in narrow locations where the bulky conventional robots cannot move.

- Propulsion:

Most of the conventional underwater robots have only one means of propulsion and most of them achieve motion with actuated propellers. On the other hand, ASR can be propelled by an actuated propeller or through the serpentine movement performed using the actuated joints. Therefore,

ASRs are more flexible in operation compared to the conventional underwater robots.

- Fluid proof:

ASRs are built to operate in water. Therefore, they are built with good fluid sealing such that water does not interfere with the electronics. Since ASRs are fluid proof, ASRs can work in environments where toxic and non-toxic fluids are present.

Aquatic snake robots have the potential to be used in several industries. Pipe relates industries is one of the promising industries where the ASRs can be used. These ASRs can be used to inspect the pipelines and perform several tasks such as clearing obstacles, repairs, wear assessment, etc. Further, they can be developed into Underwater snake robots (USR) and used in the under-water pipes

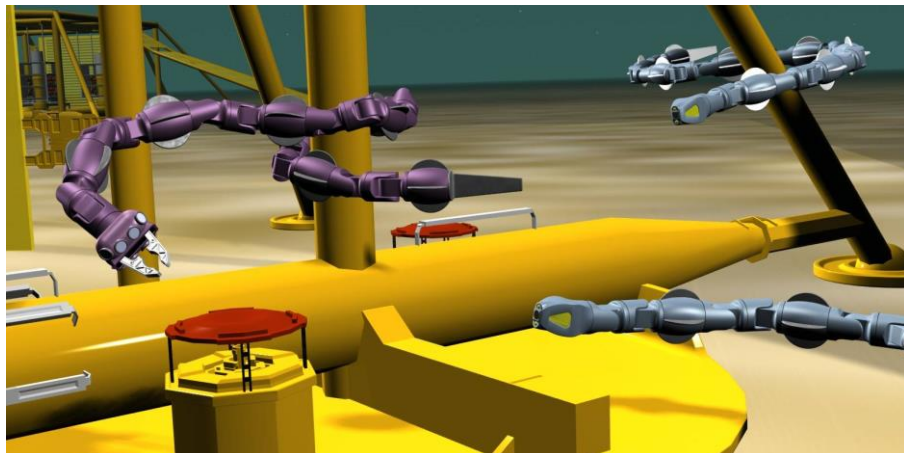


Figure 0.1: Simulation of snake robot working on underwater pipes.

The wildlife photography community has a high appreciation for ASRs. Wildlife photographers are interested in capturing nature without provoking nature. To get better images they had used bioinspired robots. These robots move closer to the subject without provoking them. ASRs can be used to photograph sensitive amphibious animals and marine animals

These ASR can be also used in hazardous environments such as nuclear power plants to work on pipes and in the case of nuclear accidents where the radiation is very high and lethal for humans. ASRs can be used to explore the water caves and can be used for search and rescue purposes.

## Objective of the thesis

In this thesis, we aim to design, manufacture, and control an aquatic snake robot. We need this aquatic snake robot to be modular, waterproof, slightly buoyant, power distributed and wirelessly operable. We will design a snake robot to achieve above

goals. We will develop motion control to achieve different swimming gaits and the motion of the aquatic snake robot in aquatic environment. We will manufacture the aquatic snake robot while constructing and integrating circuits and sensors respectively. We will implement the motion control on aquatic snake robot to achieve forward motion and turning for different swimming gaits.

## Thesis Organization

- Chapter 1 In this chapter, we introduce the sea snake and discuss the anatomy of the sea snake. Further, we discuss the swimming gaits of the sea snakes and motivations for bioinspiration.
- Chapter 2 In this chapter, we discuss the existing work done on the terrestrial, amphibious, and aquatic snake robots. Further, a classification is made on the existing work.
- Chapter 3 In this chapter, we present a kinematic model for the snake robot that can swim in the water. Then a dynamic model for an aquatic snake robot is presented with an analytical formulation to derive the complex fluid forces and moments acting on the aquatic snake robot.
- Chapter 4 In this chapter, we discuss the design constraints and the design of the aquatic snake robot. Then we perform an assessment of the used components.
- Chapter 5 In this chapter, we discuss the existing work done on the motion control of an aquatic snake robot. Then we discuss the implemented control system and the implementation of the control system.
- Chapter 6 In this chapter, we discuss the process and the techniques we used in manufacturing and assembling the aquatic snake robot. Further, we discuss the experimental activities done with aquatic snake robot to test the eel-like motion.
- Chapter 7 In this chapter, we present the conclusion of the thesis and the future developments that can be done to improve and continue the work.



# 1. Physical principles of aquatic snake locomotion

The sea snake belongs to the family *Hydrophiinae* which is a sub-family of the *Elapidae*. Sea snakes have a close resemblance to the terrestrial snakes. The sea snakes had begun their evolution from terrestrial snake about 8-17 million years ago and about 60% of their species had started to become speciating about 1.5-7.5 million years ago[1]. Most of these snakes are completely adapted for the water except for a few of them. Most of the snakes are venomous and completely adapted to the water and only a few can survive on the land[2]. Sea snakes mostly prefer warm and shallow water and prefer to live close to the coastal area. They are widely spread around the world and can be found from the Indian Ocean to the Pacific Ocean[3]. Figure 1.1 shows the distribution of the *Pelamis Platurus* also known as the Yellow-Bellied Sea snake, around the world[4].

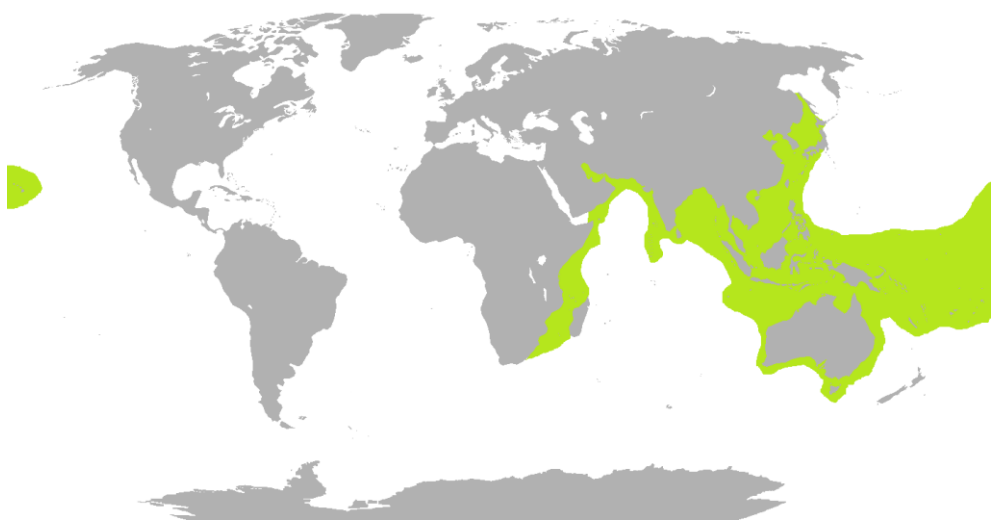


Figure 1.1: The distribution of the Yellow-Bellied Sea snake around the world.

Most adult sea snake species grow between 120 and 150 cm in the length. The largest *Hydrophis Spiralis* can grow up to 3m in length[5], [6]. The Yellow-Bellied Sea snake is

one of the most investigated sea snakes which is also known as the *Pelamis platurus* [7][8]. These snakes can grow of about 45-70 cm, and they can swim as fast as  $20\text{cms}^{-1}$  [7]. The species *Hydrophis major* also known as olive head sea snake can grow up to 1.5m in length [9].



(a) *Hydrophis major*.



(b) *Pelamis platurus*.

Figure 1.2: Different species of Sea snakes

## 1.1 Sea Snake Anatomy

The body of the sea snake has evolved in a way such that its body is horizontally compressed to provide them the better ability in swimming. The evolution of the sea snake's body with lateral compression had gotten rid of the ventral scales which can be found in terrestrial snakes. Ventral scales are the enlarged transversely elongated scales that extend down to the underside of the body from the neck to the anal scale as shown in figure 1.3.

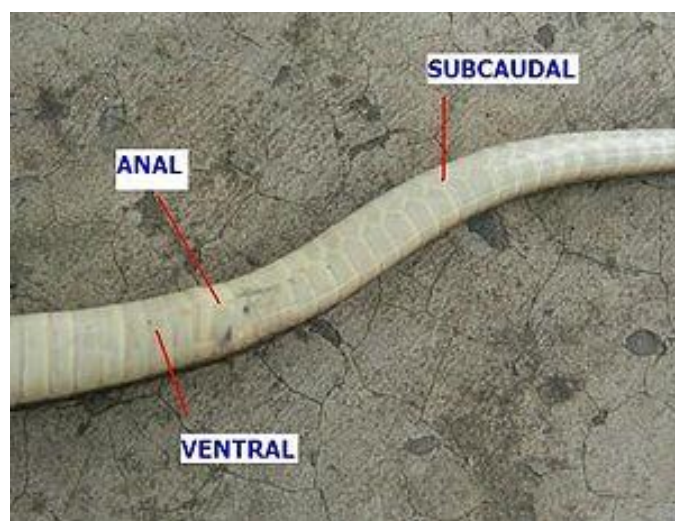


Figure 1.3: Ventral scales of Snakes and Sea Kraits.

The lack of ventral scales on sea snakes makes it difficult for them to survive on land. Sea snakes have also developed a flat tail compared to terrestrial snakes[10]–[12]. Some of the sea snakes were able to retain their ventral scales and therefore they have become amphibious such as *Laticauda*. These animals are also known as the Sea Kraits[13].

These marine animals are different from the eel fish although they share the swimming style. Sea snakes have no gills therefore to breathe, they must surface often. Even though sea snakes must surface to breathe, they can remain submerged for several hours depending on the temperature of the water and the degree of the activities. They can swim up to depths of 90m[6]. Its nostrils have valves consisting of a special spongy tissue to exclude water and the windpipe can be drawn up to where the short nasal passage opens into the roof of the mouth. This is an important adaptation for an animal that must surface to breathe. These animals must partially submerge when breathing. They have evolved to have long lungs and they are almost the length of the body of the snake. It is believed that the rear portion of the lung is used to balance the buoyancy of the Sea snake[5], [12], [14]. Some of the sea snakes can have cutaneous respiration. For example, *Pelamis Platurus* obtain about 25% of its oxygen using cutaneous respiration[15]. Cutaneous respiration is the respiration performed through the skin.

Scalation among the sea snake is highly variable. They have developed their own scaling to protect against abrasion. Reef dwelling species have adapted imbricate scales to protect against the sharp corals. Some species have developed scales such as keeled, spiny, smooth, or granular. Pelamis has body scales that are ‘peg-like’ while those on its tail are juxtaposed hexagonal plates[12].

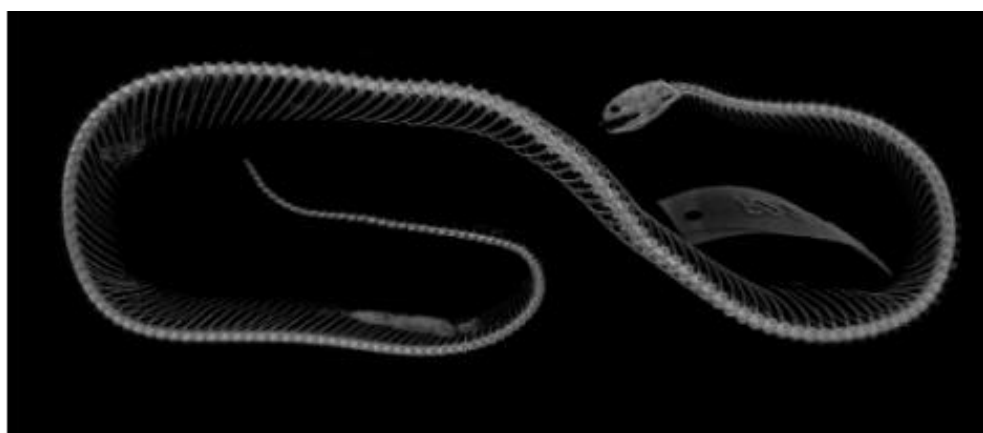


Figure 1.4: Skeleton of a snake.

The sea snake is equipped with several sensors. Out of them vision chemoreception and hearing are important senses. But since these sensors are become diluted under

the water, they have adapted to improve their sensitivity. The olive snake is reported to have photoreceptors on the tail of the snake[16].

The sea snake prefers to swim between coral reefs and caves to catch its prey. It is extremely flexible, and it has the ability to swim across through narrow spaces and take a sharp turn while it is in motion. Snakes receive their unique ability due to the structure of their skeleton. Figure 1.4 shows the skeleton of a snake. The Snake skeleton is consisted of at least 130 vertebrae and can exceed even 400. The range of the motion of a joint is about 10 to 20 degrees on the horizontal plane and about 2 to 3 degrees on the vertical plan [17].

## 1.2 Swimming gait

The swimming pattern of the snake is known as Anguilliform [17]. Anguilliform is a swimming gait performed by bending the body into backward moving propulsive waves along the body. Sea snakes can swim backward and forward by simply changing the direction of the propagation of the wave. Unlike the fish, the sea snakes use the whole body to generate large amplitude undulations. Sfakiotakis et al say that at least one complete wavelength can be observed on the sea snakes on the motion, and it results in the cancelation of the lateral force which helps to minimize the recoil on the body [18].

The swimming style of the snake change depending on the depth of water [7]. When the sea snakes swim, they tend to have their head above the water and their body slightly above water and tail completely immersed in the water as shown in figure 1.5[7]. Ming et al say that this sort of the swimming form is more efficient since the ratio between work and distance is small [19].



Figure 1.5: A Sea snake performing lateral undulation.

The main swimming pattern of the sea snake observed in planar swimming is known as lateral undulation swimming. It is basically a traveling sine wave along its body as shown in figure 1.5. Another marine animal that performs an Anguilliform swimming gait is the eel. Although eels are not in the same category of sea snakes their motion patterns are similar. Eel motion can be seen as a derivative of the lateral undulation [20]. The main difference between these motions is that the head of eel in eel motion has relatively low oscillation than the undulatory swimming. Figure 1.6 shows an eel performing its swimming gait. Eel motion can be also observed in sea animals like lampreys[21].



Figure 1.6: An Eel performing an eel like motion.

Unlike terrestrial snakes, sea snakes have a limited number of gaits. Terrestrial snakes have several gaits such as lateral undulation, concertina, sidewinding and rectilinear. These gaits cannot be seen in sea snakes. But the researchers have tried to implement these gaits in the aquatic snake robots, and this will be discussed in chapter 5 [22].

### 1.3 Motivation for Biomimicry

Modern aquatic robots have evolved through time to an advanced state. Nevertheless, its advancement still these robots face several issues. It is the versatility of robots in all environments. Most conventional aquatic robots cannot move in constraint or narrow space. To solve this kind of issues we need to take look into the best engineering works in the world which is the nature.

Sea snakes are marvelous inventions of the nature. These marine animals are efficient swimmers in all environments. Sea snakes can use their body for both locomotion and manipulation. They are able travel through very constrained spaces taking very

sharp directional changes. Also, they have developed sensors that are required to catch its prey in dark places such as caves. Sea snakes are good surface and underwater swimmers.

Obtaining inspiration from the sea snake we can build better aquatic robots. The structure of the sea snake skeleton, which is composed of hundreds of vertebrae with limited rotation on each has inspired many to build modular snake robots. Moreover, the adaptability for different environments and robustness in operation have inspired many researchers to work on aquatic snake robots.

## 2. State of the Art

There are several works done on aquatic snake robots. Based on the environment where these robots can operate prior work done on the snake robots can be categorized into terrestrial, amphibious, and aquatic snake robots. In general, several actuating techniques have been used to construct the snake robots. Some of these methods are Piezoelectric-based (PZT) [23], Pneumatic-based [24], modular-based, etc. In this dissertation, we focus only on modular snake robots. The modular snake robot is composed of identical links where the joints can be actuated or not actuated.

This chapter is organized as follows: section 2.1, investigates the work of the terrestrial snake robot, section 2.2 investigates the work of the amphibious snake robot and aquatic snake robots.

### 2.1 Terrestrial snake robot

Terrestrial snake robots were the first snake robots to be studied. Compared to the aquatic snake robots and the amphibious snake robots there are many works done on the terrestrial snake robots. The existing works on terrestrial robots can be classified into four main categories based on the interaction with the ground. They are as follows,

- Passive-wheels

Passive-wheel robots have non-actuated wheels, and the robot is solely propelled using the internal torque generated through actuated joints [25]–[30].

- Wheels-less

Wheel-less snake robots do not have wheels. These robots also move using internal joints. Due to the absence of wheels in these robots, they meet higher friction than the passive wheel snake robots [31]–[38].

- Active-wheels

This kind of robots have actuated wheels on the robot. Other than the internal torque these wheels contribute to the motion of robot [39]–[41].

- Elongation

Elongation-type robots have linear actuators in between the modules in addition to the actuated joints [42].

### 2.1.1 Passive wheels

Hirose receives the honor to have made the world's first snake robot in 1972, which is ACM-3 [43]. ACM-3 is composed of 20 links and passive wheels, and it was powered and controlled by a cable. It was capable of 2D motion. This snake robot weighs 28kg and about 2000mm long. ACM-3 was able to achieve a maximum speed of about  $400\text{mms}^{-1}$  [28], [44]. Hirose and his team invented ACM-R3, a snake robot controlled remotely and got passive wheels. The main difference between ACM-R3 to the ACM-3 is that ACM-R3 can move in 3D space. ACM-R3 robot was total of 12.1 kg weight and length was about 1755mm [25], [26], [44]. Zhu et al had worked on a passive-wheel snake robot with 4 links. This snake robot has an onboard power source and it can be controlled wirelessly with a computer [27].



(a) ACM-3, developed by Hirose.



(b) ACM-R3, developed by Hirose.

Figure 2.1: Different Snake Robots developed by Hirose.

### 2.1.2 Wheel less

Bayraktaroglu et al has developed a snake robot with no wheels. This snake is composed of 9 modules and is only able to move in a 2D plane. This snake robot was

about 900g in weight and the total length was about 600mm. Its maximal speed along linear trajectory was about  $0.05 \text{ ms}^{-1}$  [31]. Yim et al have developed a snake robot with no wheel known as PolyBot [32] and another robot known as Polypod [33]. Worst and Linnemann had worked on a snake-like robot controlled by a computer via a CAN bus data connection [34]. Wright et al had worked on a snake robot where and developed a skin to the snake robot. This skin was able to provide more friction to the snake robot although it can hinder the movement of the joint and cause heating issues[35].

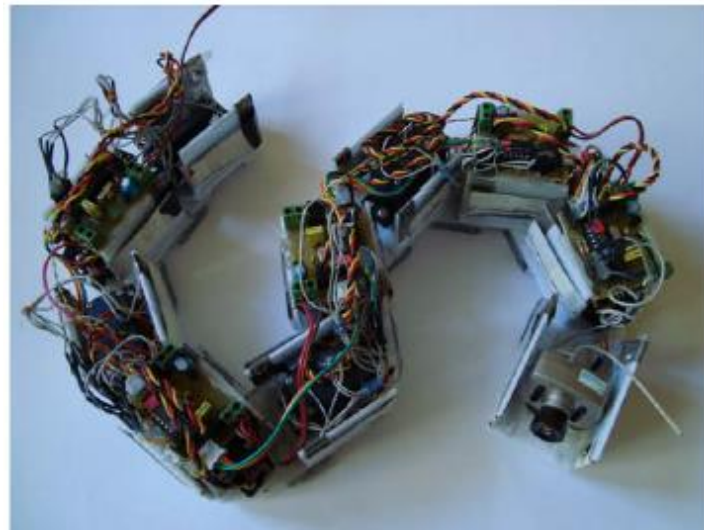


Figure 2.2: Snake robot developed by Bayraktaroglu.

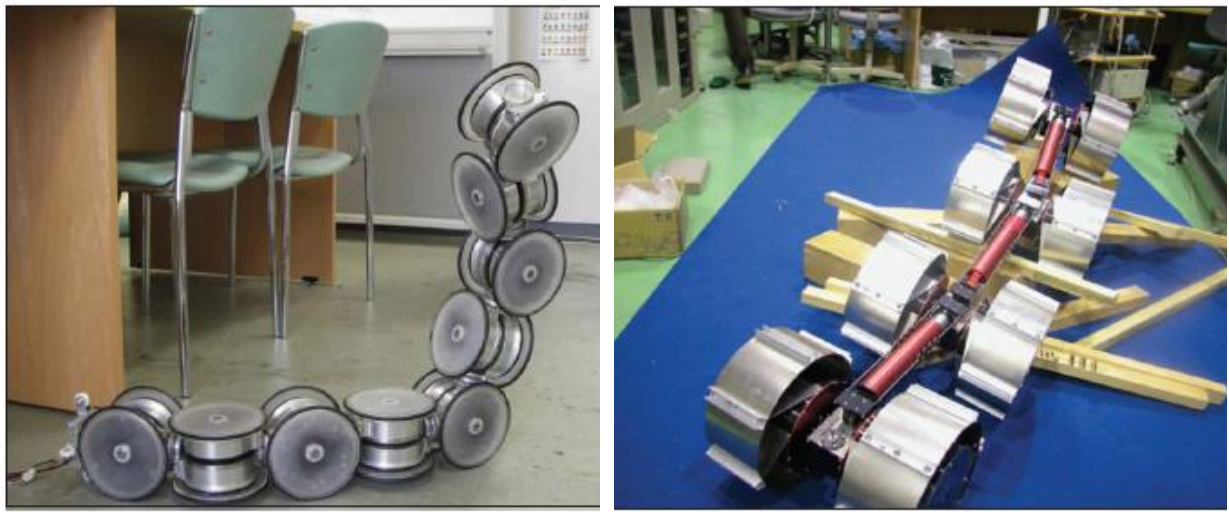


Figure 2.3: Snakey robot developed by Wakimoto et al.

Wakimoto et al had developed a snake robot specialized in movement inside the pipelines. This snake robot is composed of 13 links, 1187 mm long, and weighs about 1.1kg. This snake robot exploits the friction in the pipe walls to achieve its motion and was able to achieve a top speed of about  $48.5 \text{ mms}^{-1}$ . To increase the adhesion, they had used silicone rubber on the outer cover of the snake. Hence the snake uses the traction in the pipe to travel, the diameter of the pipe influences the velocity of the snake. It was found that an increase in the diameter of the pipe tends to decrease the velocity of the snake robot. Wakimoto et al plan to build a waterproof model of the snake robot to increase the versatility of the snake robot[38].

### 2.1.3 Active wheel

Mamba was a snake robot developed by Liljebäck et al. This robot can be changed into both passive and active wheel snake robots [39].



(a) ACM-R4, developed by Hirose.

(b) Genbu-3, developed by Hirose.

Figure 2.4: Different Snake Robots developed by Hirose.

ACM-R4 is a snake robot developed by Hirose and his team. This snake has the ability to drive its wheels and due to this feature, the snake robot ACM-R4 does not require many links to generate the internal torque used to propel the snake robot. This robot has a length of 1100mm and weighs about 9.5 Kg [41]. Genbu-3 is another snake robot that is developed by Hirose and his team. This snake robot has relatively large wheels and they are independently driven. It is equipped with its own power source but controlled via a cable. It is 1700mm long and weighs about 35kg [40].

### 2.1.4 Elongation

Snake robot developed by Wang et al, can elongate between the modules, other than performing the simple serpentine movement using the actuated joints. This modification has granted the snake robot the ability to move as fast as  $20\text{mm s}^{-1}$  in the rectilinear motion [42].

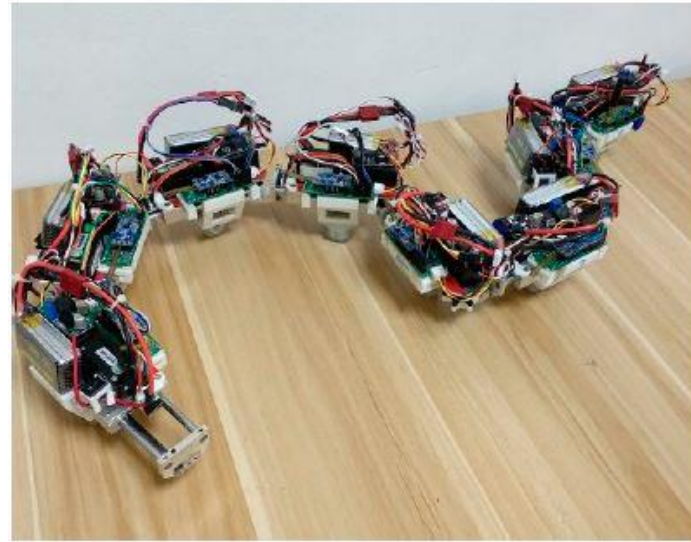


Figure 2.5: Snake robot which can elongate, developed by Wang et al.

## 2.2 Amphibious and aquatic snake robot

The amphibious snake robots can move in the water and on the land. Aquatic snake robots are the snake robots designed solely to navigate in water. Amphibious snake robots can be assigned into both classifications of aquatic snake robots and terrestrial snake robots. Compared to the terrestrial snake robot there are only few works that had been done on the amphibious snake and aquatic snake robot. The aquatic snake robots can be classified in mainly three types depending on the method of propulsion. They are as,

- Active propeller

The active propellers snake robots consist of an actuated mechanism attached to the snake robot to generate thrust in addition to the serpentine movement [45], [46].

- Passive propeller

The passive propellers snake robots consist of non-actuated mechanisms such as fins attached to the snake robot which passively generate a thrust in addition to the serpentine movement [29], [47].

- Propeller less

Propeller-less snake robot does not have any other means of generating thrust except for the serpentine movement [20], [30], [36], [37], [48].

### 2.2.1 Passive propeller

ACM-R5 is an amphibious snake robot developed by Hirose et al. It was designed to have almost the same specific weight of water. This snake has the ability to dive into the water and swim sub-surface and on the surface of the water.



Figure 2.6: ACM-R5 amphibious snake robot, developed by Hirose et al.

ACM-R5 is composed of universal joints hence it can move in 3D space. The robot is equipped with passive wheels in order to facilitate ground movement. The solid extrusions which are supporting the wheels are designed in the shape of dorsal fins. Dorsal fins are acting as passive fins. They were able to achieve a velocity of about  $0.4\text{ms}^{-1}$  both on the ground and in the water [29], [44].

Mamba snake robot was initially developed as a terrestrial snake robot was and later modified as an amphibious snake robot. Since this snake robot was modular, they had conducted several experiments with different numbers of links. It has been found that increasing the number of body links from 10 to 20, the snake was able to increase its forward velocity by 20%. This snake robot was powered and controlled via a cable. The cable was neutrally buoyant, but it had a considerable effect on the snake robot while in motion. It was tested in both eel-like motion and lateral undulation. Researchers had tested the mamba snake robot with the caudal fin

attached as passive propellers. This snake robot was able to achieve a top speed of  $93.6 \text{ mms}^{-1}$  in lateral undulation and about  $92.5 \text{ mms}^{-1}$  in eel-like motion without the caudal fins. With the caudal fins attached to the snake robot, it was able to obtain speeds of about  $198.3 \text{ mms}^{-1}$  and  $177.3 \text{ mms}^{-1}$  for the lateral undulation and eel-like motion respectively. The use of passive propellers increases the power consumption of the snake robot. Qualisys motion capture system was placed in the basin, and it was used to obtain the real-time motion capture data. Those data were used to build a feedback system where the snake was able to navigate to a given position [20], [47], [49].



Figure 2.7: Mamba snake robot with passive propellers.

Ma et al had worked on an amphibious snake robot in 2008. This robot has the freedom to move in the three-dimensional space thanks to its 2-servo motor acting as a universal joint. The snake robot they developed is 1.74 m long and each module was equipped with four passive wheels. In their work, they had experimented with different process parameters, and they have analyzed effects on the speed of the snake robot with different process parameters [50].



Figure 2.8: Snake robot developed by Ma et al.

## 2.2.2 Propeller less

AmphiBot 1 is a modular amphibious snake robot developed by Crespi et al. This snake robot was able to move only on the 2D plane and it was a wheelless robot. This robot was built slightly buoyant so that the robot would passively float on water. This robot was able to achieve a maximum speed of about  $35 \text{ mms}^{-1}$  on the surface of the water[37]. AmphiBot 2 is the newer version of the AmphiBot 1, and it can connect its modules without soldering to each other through connectors. The AmphiBot 2 robot is equipped with passive wheels and a water detector in case of water leaks into the snake robot. It was composed of motors with higher torque than the predecessor. It can move at a maximum velocity of about  $400 \text{ mms}^{-1}$  on the land and the water about  $230 \text{ mms}^{-1}$  [30].



(a) AmphiBot 1.



(b) AmphiBot 2.

Figure 2.9: AmphiBot family robots, developed by Crespi et al.



Figure 2.10: Snakey robot, developed by Jasni et al.

Snakey was a robot developed by Jasni et al. It has the capability to perform amphibious locomotion. They had achieved a maximum velocity of motion of about  $1.2 \text{ mms}^{-1}$  on the land and about  $3\text{mms}^{-1}$  in the water. This snake was designed for

surface swimming. Since this was powered and controlled through a cable, their space of operation was hindered and the lack of sensors other than a camera make it difficult to navigate [36].

Wright et al have worked on a series of snake robots where their latest one is waterproof. These snake robots consist of 8 modules, and it is powered by custom servo motors which were designed and built by them. To facilitate the communication between the modules RS485 protocol was used. To make the snake waterproof they have constructed a skin for the snake robot using several materials such as nylon, polyester, microfiber, etc. They have discovered that the skin has caused heat issues for the snake modules[51].



(a) Series of Robots.



(b) Unified Snake Robot.

Figure 2.11: Snake robots, developed by Wright et al.

Further, Wright et al have worked on another amphibious snake robot called Unified Snake. This robot consists of 16 modules, and it weighs about 3 kg. It is 94 cm long and has a diameter of 5.1 cm. This snake robot is equipped with brakes which provide the snake robot to hold into one position for a long time without consuming energy. The brake consumes energy only to be activated and deactivated. This feature is useful for holding into sometime for a long time. This amphibious snake robot has designed to be fully enclosed and used humidity sensors to detect the water leak into the module. But they point out that due to the lack of airflow these sensors do not perform well. Apart from the humidity sensor, they have also used several other sensors. RS-485 serial protocol was used to communicate with the snake and the external computers. There was no evidence found that these robots were used in swimming although they are waterproof.[52].

### 2.2.3 Active propeller

Gravdahl et al had worked on an articulated autonomous underwater vehicle (AIAUV) shown in figure 2.12. This robot is equipped with thrusters attached to the body in order to generate the thrust. These thrusters are placed along the axis of the snake robot and along directions perpendicular to the axis of the underwater snake robot. It is composed of 5 links and in the case of non-actuated thruster it can generate the thrust by performing the serpentine movement [45]. A simulation study of an underwater swimming manipulator (USM) has been done by Kelsaidi et al. They had explored the ability to use this robot in oil exploration. Similar to AIAUV, USM is composed of thrusters other than actuated links. This robot design is composed of an actuated arm on one end of the robot [46].



Figure 2.12: Snake robot with active propellers

## 3. Design of the Robot

In this chapter, we discuss the design of the aquatic snake robot. Our goal was to design an aquatic snake robot that can swim on the surface of water. And this had to be accomplished without neither active nor passive propellers.

This chapter is organized as follows: Section 3.1 describes the design requirements which influence the design of the aquatic snake robot, Section 3.2 describes the design of the head module, Section 3.3 describes the design of the module and Section 3.4 describe the design of the assembly of the aquatic snake robot and the design of its outer most cover.

### 3.1 Design requirements

In designing the snake robot, we considered several requirements which are listed below.

- Modular aquatic snake robot.
  - In designing the aquatic snake robot, the main requirement is to satisfy the reconstruction of the serpentine curve using modular links. This ability is influenced by the number of links that ASR contains. Also, the length of the link influences the shape of the serpentine curve. Figure 3.1 shows a reconstruction of the serpentine curve in 4 different scenarios, and 5,6,7, and 8 links were used respectively. The length of the links of the ASR is equal and set to 130mm. From figure 3.1, it is evident that a higher number of links provides higher DOFs and a better approximation of the serpentine curve. ASR with the shorter links and many links can approximate the serpentine curve better. In this dissertation, the aquatic snake robot consists of 8 modules except for the head. Since the robot is modular, one can easily increase the number of modules in the ASR. Since the snake robot is modular, the defective modules can be easily replaced.

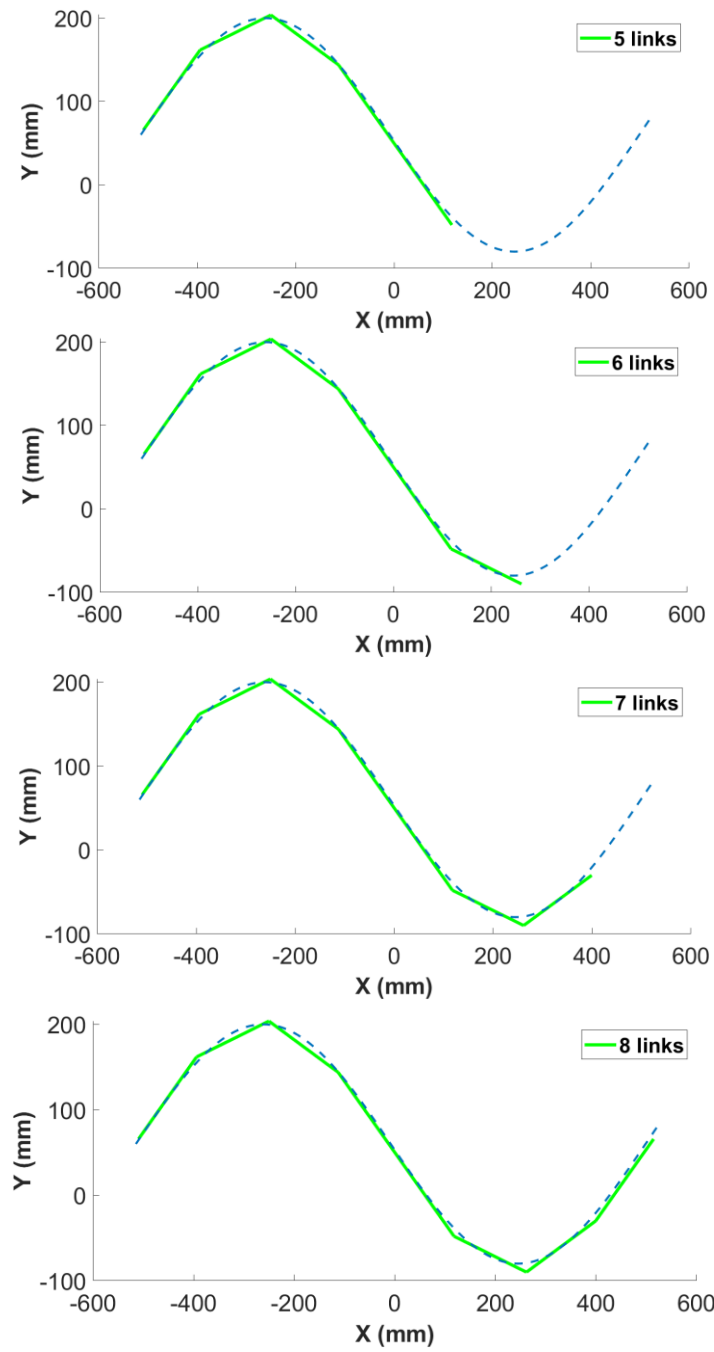


Figure 3.1: Different number of the links in a robot.

- Slightly buoyant snake robot.
  - Since this snake robot is designed to operate in water, the design of the snake robot is influenced by the properties of water. As stated above to surface swim in the water, buoyancy calculations were done to make

sure the snake robot is not completely sinking and neither completely floating. Further, to avoid the rollover of the snake robot in the water we make sure that the center of gravity of the snake robot is placed on the bottom of the aquatic snake robot.

- Distributed actuation power and control.
  - Each module is equipped with an onboard energy source and an actuating device. This property is useful since disabling one or a few modules do not hinder the operation of the total snake robot. In such situations, we can make a compromise using the other modules.
- Waterproof.
  - The aquatic snake robot is equipped with several sensors which are used for the navigation of the ASR. Waterproofing of the ASR is essential to protect the electronic components from short-circuiting. Further, it avoids the rusting of the metal components that were used in the ASR.
- Controlled remotely.
  - The snake robot is controlled remotely. This eliminates the necessity of wires for communication with the ASR. Such communication is needed for the control of the ASR and to receive data from the sensors. Thanks to this feature it is much easier for the snake robot to be waterproofed.
- Laterally compressed body.
  - In designing the outer cover of the ASR, we designed it such that it is compressed laterally. This feature can be observed in sea snakes and due to such a form, the aquatic snake robot can swim efficiently.

## 3.2 Head design

The head module is the front-most module of the ASR, and its purpose is to act as the brain of the ASR. It can control other modules and inspect the environment. It can receive commands from a user or a higher computational node in the case of autonomous driving.

The head module of the ASR does not consist of a servo motor hence it is not actuated. The head module of the ASR equipped with an onboard power source and several sensory devices that are useful in navigation. And these sensors can be used for autonomous driving. Figure 3.1 shows an exploded view of CAD of the ASRs head module with its components. The list of components used in the head module of ASR is shown in table 3.1.

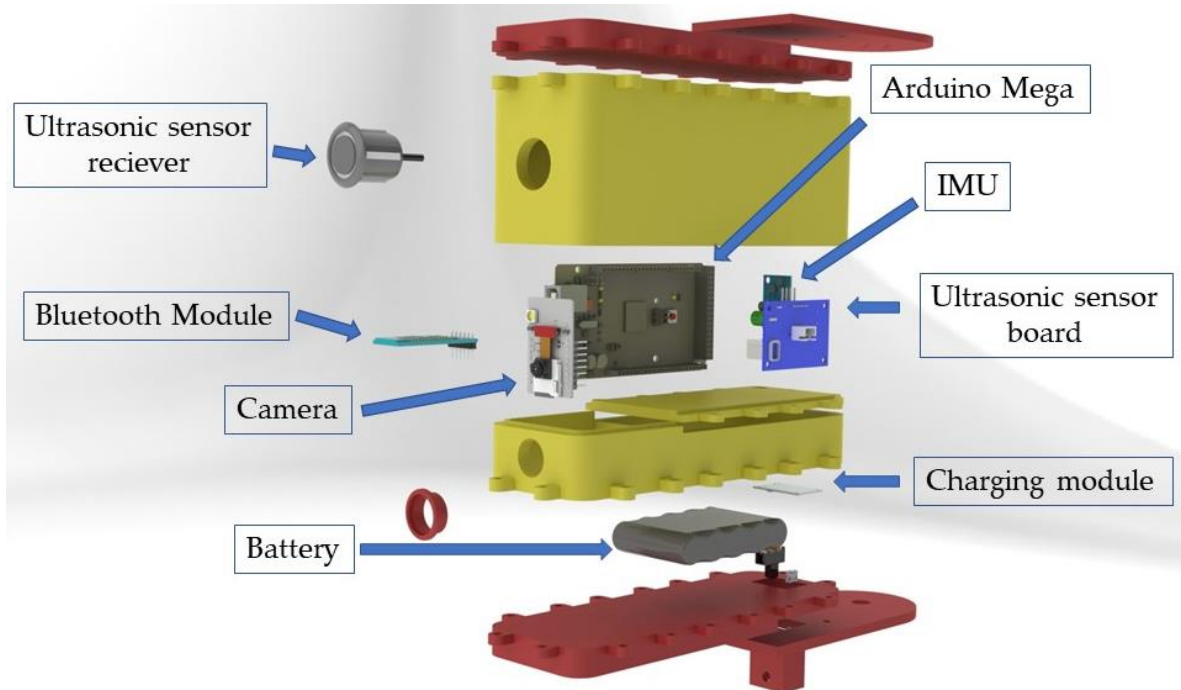


Figure 3.2: Exploded view of Head.

Components	Model
Ultrasonic sensor	JSN-S4RT
Inertial Measurement Unit	IMU 9250
Micro-controller	Arduino Mega
Bluetooth module	HM-05
Battery	2000mAh 6v
Camera	ESP32-CAM
5 cell charger modules	NIUP11TA
Switch	-
USB female adapter	-
Head outer cover	-

Table 3.1: List of components used in head module.

### 3.2.1 Ultrasonic sensor

The ultrasonic sensor is a sensor used to detect the distance to objects in its range of operation. Using the ultrasonic sensor, we can detect the distance for an obstacle. Hence this sensor can be very useful in obstacle avoidance driving and autonomous driving. The ultrasonic sensor measures the time it takes to observe the echo which is

originated due to the sound wave produced by the sensor. Using this time to observe echo, we can calculate the distance to the obstacle using equation 3.1.

$$d_{obs} = \frac{V_{sound} \times T}{2} \quad (3.1)$$

$d_{obs}$  is the distance measured from the face of head module to the obstacle. The unit of measurement is centimeters.  $V_{sound}$  is the speed of the sound in water and  $T$  is echo time measured in microseconds. The ultrasonic sensor we used in the robot was JSN-S4RT. This sensor was built with a waterproof feature hence it can be used underwater. This sensor consists of two elements, the receiver, and the circuit board. Only the receiver is waterproof therefore the circuit is placed inside the head module housing. The receiver's face is exposed to water so it can obtain measurements. Its range of operation is about 20cm to 70cm with an accuracy of 1 cm. it has a measuring range of angle of about 75 degrees

### 3.2.2 Camera

The camera can provide the controller of the robot a view in front of the snake and control the snake according to the visual feedback. The camera module we had used in the snake robot was ESP32-CAM. This camera module operates with 5v and also 3.3v. ESP32 can be programmed to connect with Wi-Fi and the image can be sent wirelessly. Further, this camera module consists of a SD card reader and the images can be stored to a SD card.

### 3.2.3 Inertial measurement unit

The inertial measurement unit is used to obtain several inertial measurements and it is very useful in the case of autonomous driving. It can provide information about the orientation of the ASR, the accelerations, and angular velocities acting on the ASR. The sensor we used in the project is IMU9250 and it is a 9-axis sensor that consists of 3 axis gyroscope, 3 axis accelerometer, and 3 axis magnetometers. It can measure acceleration, angular velocity, and magnetic orientation. This sensor works with 5v and consumes a current of about 1A.

### 3.2.4 Bluetooth module

The Bluetooth module allows the microcontroller in the head module to communicate with an external computer. This is useful for the remote control of the ASR and in the case of autonomous driving. The computation needed to generate the trajectory can be done on an external computer and can be transmitted to the

microcontroller. Further, it transmits the data obtained from the sensors to the external computer which can be used in remote control or autonomous driving. The model we used in this project is HC-05. It has a working range of about 100cm and this range can be increased by using an external antenna. The operating voltage of the module is 3.3v - 5v. This Bluetooth module cannot be used to communicate to the ASR while underwater but since our aquatic snake robot is swimming on the surface of water, it was usable.

### 3.2.5 Microcontroller.

The angles needed to perform the serpentine curve is generated by the microcontroller they are transmitted for the other modules using the I2C communication protocol. And further it gathers the all-sensing data and send it to the external computer. The model we used in this project is Arduino Mega. It has enough computational power and memory to deliver our needs. The Arduino Mega has an operating voltage range of 7v – 12v.

### 3.2.6 Head outer cover

The head outer cover is used to place the components and protect the internal components. The model is drawn using SolidWorks. In designing the dimension of the outer cover, attention was paid to calculate the buoyancy force acting on the head module. It was designed such that the buoyancy force is slightly larger than that of the gravity force. In designing the head module an extended arm is added to the head module design to attach the consecutive modules. The bottom extended arm is fixed to the module while the top extended arm is easily removable apart from the lid of the snake robot and it is fixed to the lid through screws. This feature allows easy assembly of the snake robot. Further, appropriate holes are designed to place the camera and the UV sensor. Brackets are designed to hold the internal components of the head module. Figure 3.3 shows an assembled version of the head using CAD. CAD images shown in figures 3.2 and 3.3 was rendered in Solid works.

To power the head module a 2000mAh NiMH battery was used and it is expected to have an operational period of the module up to 1.5h. In deciding the capacity of the battery, we summed all the current that is consumed by the electronic components and multiplied it by the time we need the ASR to operate. To charge the battery of the head module, a charger module was included in the design. The charger module safeguards the battery life and operational life. A switch is used to open the circuit while charging the battery.



Figure 3.3: CAD head assembled.

### 3.3 Module design

The module is the single segment of the body of the ASR. The body of the ASR is composed of 8 other modules. The collective contribution of these modules generate the swimming gaits so the ASR can move through the water. The module is designed to follow the command from the microcontroller in the head module.

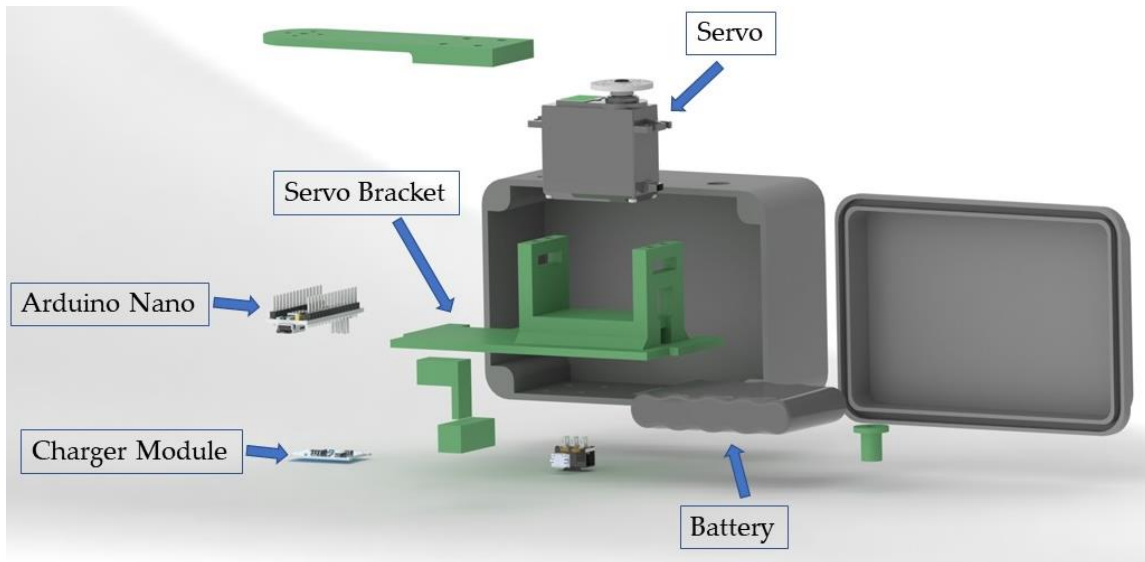


Figure 3.4: Module CAD exploded view

The head module feeds the target angle to the microcontroller on the module, and it is equipped with a feedback controller to command the servo motor. The ASR is

composed of 8 such modules and all modules are identical to one another. Figure 3.4 shows a CAD exploded view of the ASR module. The components used to make the module are shown in table 3.2.

Components	Model
Servo	FeeTech FB5311M-360
Microcontroller 2	Arduino Nano
Battery	2000mAh 6v
5 cells battery charger module	NIUP11TA
Switch	-
Charger module	-
Module outer cover	-

Table 3.2: List of components used in the module.

### 3.3.1 Servo

The servomotor provides the actuating power needed for the motion of aquatic snake robot. The servomotor used on the ASR was FeeTech FB5311M-360. The servo FeeTech FB5311M-360 is a continuous servo motor. The servomotor is equipped with an in-built encoder. It can provide a position feedback which allows to implement a control on the angle position. The specifications of the servo motor are given in table 3.3.

Components	Model
Voltage	4.8v
Idle current	4mA
No load speed	50 rpm
Stall torque	15kgcm
Stall current	1500mA
Running current (no load)	130mA

Table 3.3: The specifications of the servo motor.

### 3.3.2 Microcontroller

The microcontroller placed in the modules act as a receiver of the microcontroller in the head module and control the servo. Further, it is used to implement the algorithm necessary to have a feedback angle control on the servo motor. For this purpose, Arduino Nano is used due to its small dimension, low power consumption, and computation power.

### 3.3.3 Module outer cover

Similar to the head design a module outer cover is designed for the module. Here much more attention is paid to the structure since there is torque generated by the servomotor. A separate bracket is designed to place the servomotor as shown in figure 3.4. Further, a buoyancy calculation is performed on the dimension of the module outer box to make sure that it is slightly larger than that of the gravitational force.

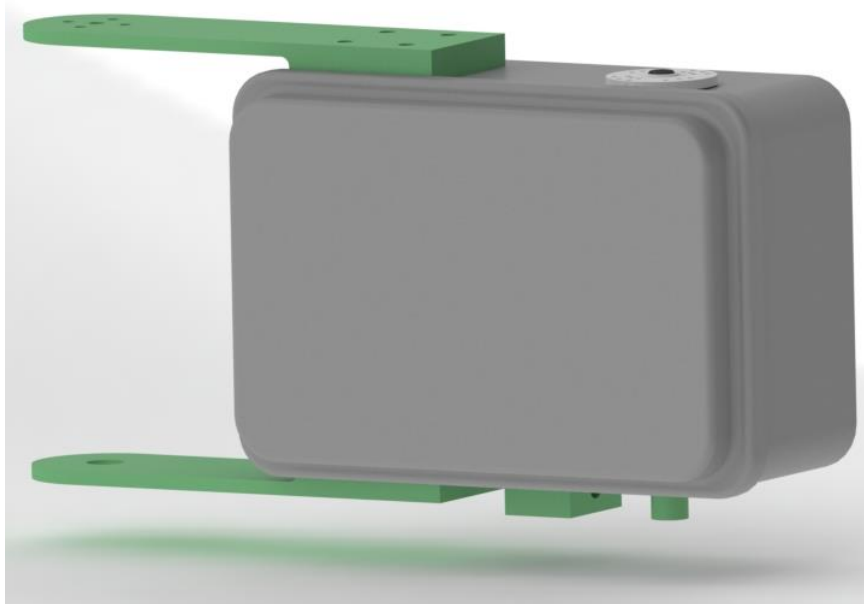


Figure 3.5: CAD of the assembled module.

A premanufactured box was obtained based on the calculated dimension. The spacers and brackets to hold other components were designed. In designing the module an extended arm is added similar to that of the head module. The extended arm is suspended to the module through M3 screws which make it easily removable to attach to the next module. This feature allows easy assemble of the aquatic snake robot. Figure 3.5 represents an assembled CAD version of the module.

The battery is the onboard power source and, it powers the servomotor and the microcontroller of the module. It has a capacity of about 2000mAh NiMH battery. The battery charger module is used to charge the battery. To charge the battery a female USB adapter is used in the circuit. A switch is included to interrupt the current to the circuit which is useful in the case of over charging.

### 3.4 Design of the Assembly

The designed head module and the modules of the ASR are assembled. The design of the assembly is shown in figure 3.6. The assembly of the ASR is designed such that each module can be easily taken apart and assembled easily, the extended arm designed to the module and the head modules are used to connect to each other module. To connect the wiring two connectors are designed on each module to connect the neighboring modules.

In designing the modules and head we make the module have an optimum turning angle when assembled. Further, to have symmetry in the ASR, the consecutive modules are connected with a 180-degree rotation. Due to this rotation, the odd number of actuated modules have their lid on one side and even on the other side. Further, due to this rotation, the mass of the aquatic snake robot is distributed evenly.

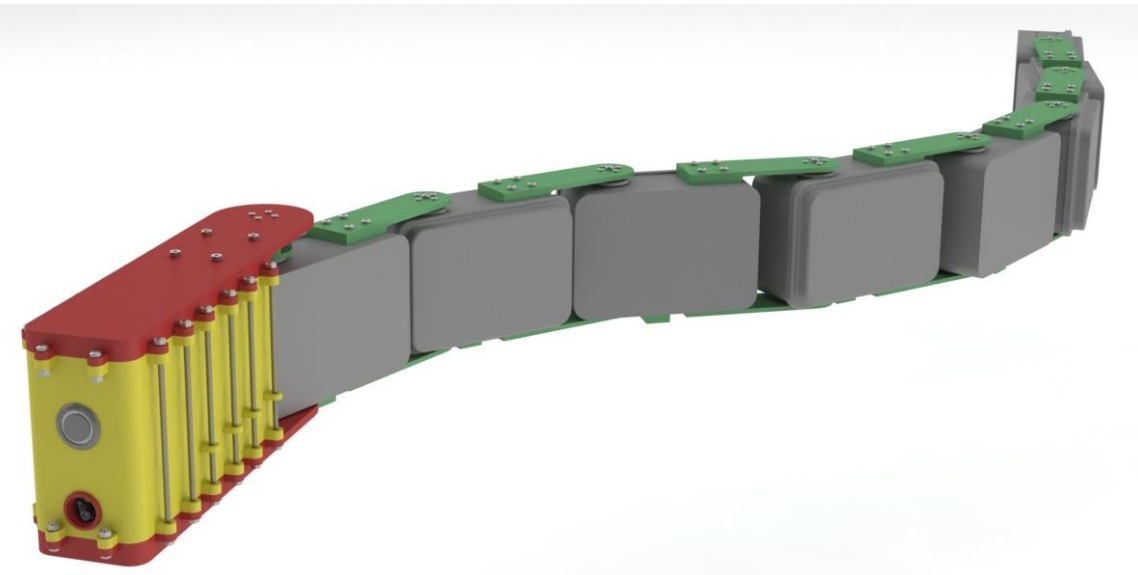


Figure 3.6: CAD of assembly.

To improve the aesthetic aspect of the ASR and support the polythene cover, which is used to waterproof the ASR, a plastic cover was designed. This cover was designed such that it can be easily taken apart when we need to access the electronic components inside the box. Figure 3.7 shows the assembly of the snake robot with the designed cover. A tubular polythene cover was added to cover the ASR. This tubular polythene cover is sealed on both ends and a zipper is added to open the cover so that the ASR can be taken out and placed in easily.

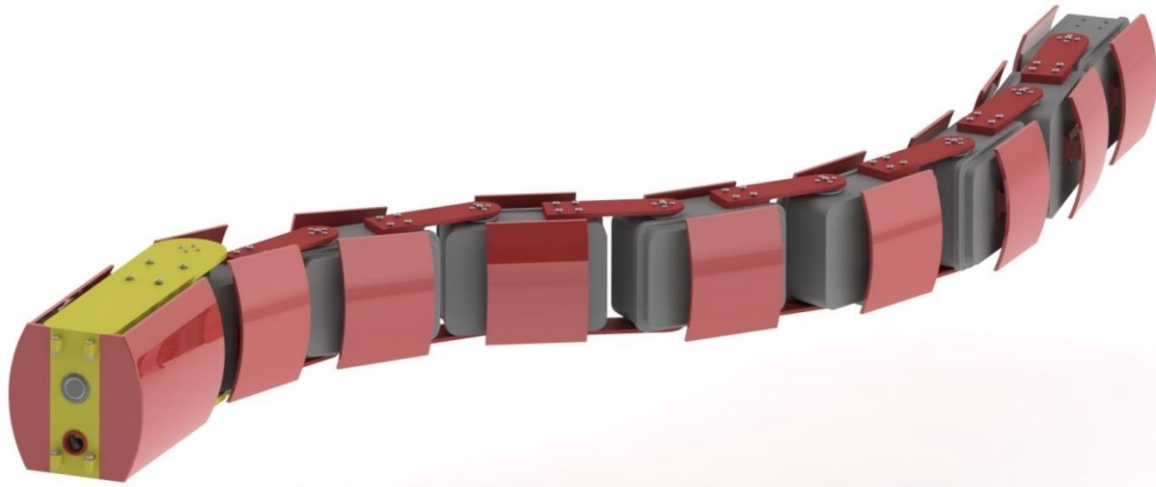


Figure 3.7: CAD of assembly with the cover.



## 4. Modeling of an aquatic snake robot

In the literature, many works have been done regarding terrestrial snake robots [53], [54] but only a few can be found regarding the aquatic and amphibious snake robots. Kinematic models developed for the terrestrial snake robot can be used also be used for the aquatic snake robot [55]. But modeling the dynamics becomes complex since interaction with the fluid needed to be taken to account. Some approaches have been made to develop a dynamic model neglecting effect due to reasonable assumptions [56]. There are some works that have been done to present more sophisticated dynamic modeling [57].

### 4.1. Kinematic Model

The mathematical model presented below was influenced by the work of Liljebäck et al [58] and the work of Liljebäck et al was based on works [53] and [54]. This model was originally presented for the terrestrial snake robot but since the mechanism is valid for both the terrestrial and aquatic robots it can be used for the aquatic snake robot. This model was developed for the motion of the snake robot in the 2D plane.

Figure 4.1 represent a simplified diagram of an ASR with  $N$  links. Analyzing the 2D planar problem, it has  $N + 2$  degree of freedoms. The center of mass (CM) of each link is denoted by  $(x_i, y_i)$  with the reference to the global frame of reference. A local reference system is placed on the top of the CM of the link, where the  $x$  axis coincide with the link and the  $y$  axis is normal to the link. The positive direction of the  $x$  axis coincides with the positive direction of the  $x$  axis of the global frame of reference when the *link angle* is zero. It is possible to assume that each link is identical, and the mass of each link is equal and given by  $m$  and length by  $d$ .

The angle defining the orientation of the link with respect to the global reference system is called *link angle* and it is denoted by  $\theta_i$ . There are  $N$  number of  $\theta_i$  values. In this derivation counterclockwise rotation with respect to the  $x$  axis of the global reference system is taken as positive.

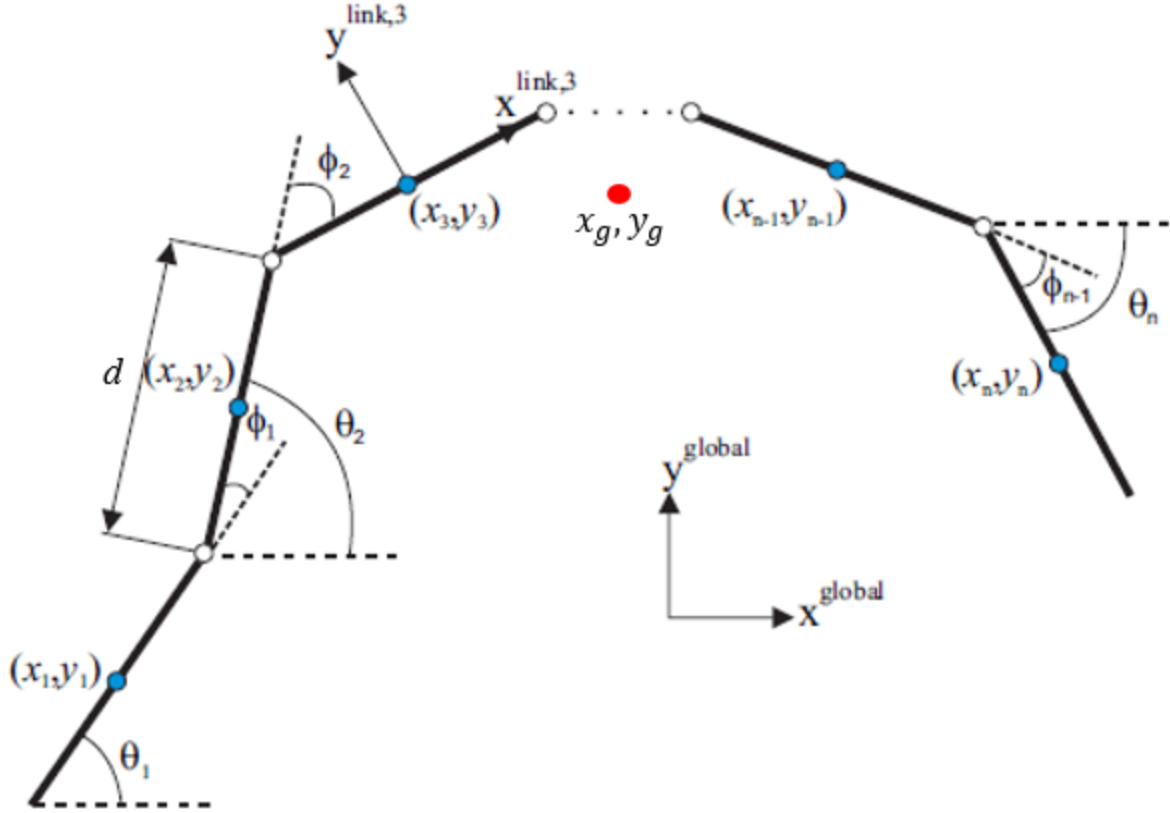


Figure 4.1: Simplified diagram of snake robot with N links.

The *Joint angle* is defined as the angle between the  $i^{th}$  link and its consecutive link. Since there are  $N$  number of links, it contains  $N-1$  number of joints and the joint angle of the  $i^{th}$  link is denoted by  $\phi_i$ . The  $i^{th}$  joint angle is given by equation 4.1.

$$\phi_i = \theta_i - \theta_{i-1} \quad (4.1)$$

The *head orientation* is denoted by the  $\theta_h$  and it is calculated as the average joint angles as shown in equation 4.2. There is no unique way of finding orientation, but it is influenced by the control objective.

$$\theta_h = \frac{1}{N} \sum_{i=1}^N \theta_i \quad (4.2)$$

The global center of mass of the ASR is denoted by the coordinates  $(x_g, y_g)$ . It can be found by using the center of mass coordinates of all the links defined in the global frame of reference and by calculating the mass weighted average as shown in equation 4.3.

$$\begin{aligned}x_g &= \frac{\sum_{i=1}^N mx_i}{N \sum_{i=1}^N m} \\y_g &= \frac{\sum_{i=1}^N mx_i}{N \sum_{i=1}^N m}\end{aligned}\quad (4.3)$$

We can simplify equation 4.3 and it can be transformed into matrix which is used in the following derivation.

$$\mathbf{C} = \begin{bmatrix} x_g \\ y_g \end{bmatrix} = \begin{bmatrix} \frac{\sum_{i=1}^N x_i}{N} \\ \frac{\sum_{i=1}^N y_i}{N} \end{bmatrix} = \frac{1}{N} \begin{bmatrix} \mathbf{eX} \\ \mathbf{eY} \end{bmatrix} \quad (4.4)$$

Matrix's  $X$ ,  $Y$  and  $S$  are defined as follows.

$$\mathbf{X} = \begin{bmatrix} x_1 \\ \vdots \\ x_N \end{bmatrix}_{N \times 1} \quad (4.5)$$

$$\mathbf{Y} = \begin{bmatrix} y_1 \\ \vdots \\ y_N \end{bmatrix}_{N \times 1} \quad (4.6)$$

$$\mathbf{e} = [1 \quad \dots \quad 1]_{1 \times N} \quad (4.7)$$

The forward velocity of the ASR is denoted by  $v_s$  and it can be found using velocity of the CM of ASR along the head orientation. The above relationship is given by equation 4.8.

$$v_s = \dot{x}_g \sin \theta_h + \dot{y}_g \cos \theta_h \quad (4.8)$$

To calculate the velocity of each link it is possible to exploit holonomic constraints. Since each link is connected by a joint, we can write the relationship for each joint. This relation is given by equations 4.9 and 4.10.

$$x_{i+1} - x_i = \frac{d}{2} \cos \theta_i + \frac{d}{2} \cos \theta_{i+1} \quad (4.9)$$

$$y_{i+1} - y_i = \frac{d}{2} \sin \theta_i + \frac{d}{2} \sin \theta_{i+1} \quad (4.10)$$

Equations 4.9 and 4.10 can be applied to the whole ASR can be written in a matrix form.

$$\mathbf{D}\mathbf{X}^T + \frac{d}{2}\mathbf{A}\cos\boldsymbol{\theta} = 0 \quad (4.11)$$

$$\mathbf{D}\mathbf{Y}^T + \frac{d}{2}\mathbf{A}\sin\boldsymbol{\theta} = 0 \quad (4.12)$$

Where  $\mathbf{D}$  is a difference matrix and  $\mathbf{A}$  is an addition matrix.  $\boldsymbol{\theta}$  is a matrix containing all the *link angles* given by equation 4.15. Where the matrices  $\mathbf{D}$  and  $\mathbf{A}$  is given by equations 4.13 and 4.14. The matrix  $\sin\boldsymbol{\theta}$  and  $\cos\boldsymbol{\theta}$  is given by equation 4.16.

$$\mathbf{D} = \begin{bmatrix} 1 & -1 & 0 & 0 \\ 0 & \ddots & \ddots & 0 \\ 0 & 0 & 1 & -1 \end{bmatrix}_{(N-1) \times N} \quad (4.13)$$

$$\mathbf{A} = \begin{bmatrix} 1 & 1 & 0 & 0 \\ 0 & \ddots & \ddots & 0 \\ 0 & 0 & 1 & 1 \end{bmatrix}_{(N-1) \times N} \quad (4.14)$$

$$\boldsymbol{\theta} = \begin{bmatrix} \theta_1 \\ \vdots \\ \theta_N \end{bmatrix}_{N \times 1} \quad (4.15)$$

$$\begin{aligned} \cos\boldsymbol{\theta} &= \begin{bmatrix} \cos\theta_1 \\ \vdots \\ \cos\theta_N \end{bmatrix}_{N \times 1} \\ \sin\boldsymbol{\theta} &= \begin{bmatrix} \sin\theta_1 \\ \vdots \\ \sin\theta_N \end{bmatrix}_{N \times 1} \end{aligned} \quad (4.16)$$

In order to obtain the positions of the links we can combine equations 4.4, equation 4.11 and 4.12. This combination of equations that provide the coordinates of the CM of each link as a function of CM of ASR and link angles, which is given by equation 4.17. Matrix  $\mathbf{T}$  is the unifying matrix given by equation 4.18.

$$\mathbf{T}\mathbf{X} = \begin{bmatrix} -\frac{d}{2}\mathbf{A}\cos\boldsymbol{\theta} \\ x_g \end{bmatrix}_{N \times N} \quad (4.17)$$

$$\begin{aligned} \mathbf{T}\mathbf{Y} &= \begin{bmatrix} -\frac{d}{2}\mathbf{A} \sin \boldsymbol{\theta} \\ \mathbf{y}_g \end{bmatrix}_{N \times N} \\ \mathbf{T} &= \begin{bmatrix} \mathbf{D} \\ \mathbf{e} \\ \mathbf{N} \end{bmatrix}_{N \times N} \end{aligned} \quad (4.18)$$

By calculating the inverse of the matrix  $\mathbf{T}$ , we can calculate the position of the CM of each link, if the position of the CM of ASR and link angles are known. The inverse of the matrix  $\mathbf{T}$  given by equation 4.19. Further, equation 4.17 can be simplified as given by equation 4.20. Matrix  $\mathbf{K}$  can be calculated by using equation 4.21.

$$\mathbf{T}^{-1} = [\mathbf{D}^T (\mathbf{D}\mathbf{D}^T)^{-1} \mathbf{e}^T] \quad (4.19)$$

$$\begin{aligned} \mathbf{X} &= -\frac{d}{2}\mathbf{K}^T \cos \boldsymbol{\theta} + \mathbf{e}^T \mathbf{x}_g \\ \mathbf{Y} &= -\frac{d}{2}\mathbf{K}^T \sin \boldsymbol{\theta} + \mathbf{e}^T \mathbf{y}_g \end{aligned} \quad (4.20)$$

$$\mathbf{K} = \mathbf{A}^T (\mathbf{D}\mathbf{D}^T)^{-1} \mathbf{D} \quad (4.21)$$

The linear velocity of each link can be obtained by calculating the derivative of equation 4.20 with respect to time. These velocities are given by equation 4.22. The terms  $\mathbf{S}_\theta$  and  $\mathbf{C}_\theta$  are two diagonal matrices given by equations 4.23 and 4.24 respectively.  $\dot{\boldsymbol{\theta}}$  is the derivative of the matrix  $\boldsymbol{\theta}$ .

$$\begin{aligned} \dot{\mathbf{X}} &= -\frac{d}{2}\mathbf{K}^T \mathbf{C}_\theta \dot{\boldsymbol{\theta}} + \mathbf{e}^T \dot{\mathbf{x}}_g \\ \dot{\mathbf{Y}} &= -\frac{d}{2}\mathbf{K}^T \mathbf{S}_\theta \dot{\boldsymbol{\theta}} + \mathbf{e}^T \dot{\mathbf{y}}_g \end{aligned} \quad (4.22)$$

$$\mathbf{S}_\theta = \begin{bmatrix} \cos \theta_1 & 0 & 0 \\ 0 & \ddots & 0 \\ 0 & 0 & \cos \theta_N \end{bmatrix}_{N \times N} \quad (4.23)$$

$$\mathbf{C}_\theta = -\begin{bmatrix} \sin \theta_1 & 0 & 0 \\ 0 & \ddots & 0 \\ 0 & 0 & \sin \theta_N \end{bmatrix}_{N \times N} \quad (4.24)$$

By using equations 4.22 we can calculate the acceleration of each link. The acceleration of each link of the robot is given by equation 4.25.

$$\begin{aligned}\ddot{\mathbf{X}} &= -\frac{d}{2} \mathbf{K}^T (\mathbf{S}_\theta \dot{\theta} + \mathbf{C}_\theta \ddot{\theta}) + \mathbf{e}^T \ddot{x}_g \\ \ddot{\mathbf{Y}} &= -\frac{d}{2} \mathbf{K}^T (\mathbf{C}_\theta \dot{\theta} + \mathbf{S}_\theta \ddot{\theta}) + \mathbf{e}^T \ddot{y}_g\end{aligned}\quad (4.25)$$

## 4.2. Dynamic Model

Modeling the forces acting on the body of the ASR is complex with respect to the overall rigid motion. To obtain the precise calculation of fluid forces, the Navier-Stokes equation must be solved, but since they take a lot of computational time and power, many researchers have used analytically simplified forms of equations.

Taylor [59] and Lighthill [60] have done work on analytical models of fluid forces. They are respectively known as resistive and reactive models, based on different sets of assumptions. The resistive model can be used for the swimmers with a low Reynold number and low velocity. The reactive model can be used in the case of the large swimmer. The ASR falls in between these two cases[57]. McIsaac [56] has presented a dynamic model which accounts for the fluid drag forces in his model but neglects the fluid moments. Gravdahl [57] argues that fluid moments are negligible but in calculating the power consumption they have a significant effect. The dynamic model presented below was influenced by the work of Gravdahl et al [17] and in their work, Morison's equation [61], [62] has been used in modeling the hydrodynamic forces.

In modeling the forces, to simplify the problem some assumptions and approximations are made, and they are stated below.

1. Each link of the ASR is approximated as an elliptical cylinder
2. Fluid effects induced by the corners of the robot are neglected
3. The fluid is assumed to be viscous, incompressible and irrotational in the inertia frame.
4. The robot is assumed to be neutrally buoyant where the gravitational force cancels the buoyant force.
5. The undisturbed flow in the global frame of reference is constant and irrotational
6. The relative velocity of each section of the link in the body frame is equal to relative velocity of the center of mass of each link.

The fluid forces are expressed as a function of the relative velocity. Hence the relative velocity of the link  $i$  can be given by equation 4.26. To calculate the relative velocity of the link, current velocity is needed with respect to the body reference frame. The transformation matrix used for the transformation of the current velocity is given by equation 4.27 and the transformed current velocity is given by equation 4.28.  $\dot{p}_i^{link,i}$  is the velocity of the link  $i$  in the body frame of reference. It can be obtained by multiplying the transpose of the transformation matrix with the velocity components in the global frame of reference.

$$v_{r,i}^{link,i} = \dot{p}_i^{link,i} - v_{c,i}^{link,i} \quad (4.26)$$

$$\mathbf{R}_{link,i}^{global} = \begin{bmatrix} \cos\theta_i & -\sin\theta_i \\ \sin\theta_i & \cos\theta_i \end{bmatrix} \quad (4.27)$$

$$v_{c,i}^{link,i} = (\mathbf{R}_{link,i}^{global})^T v_c \quad (4.28)$$

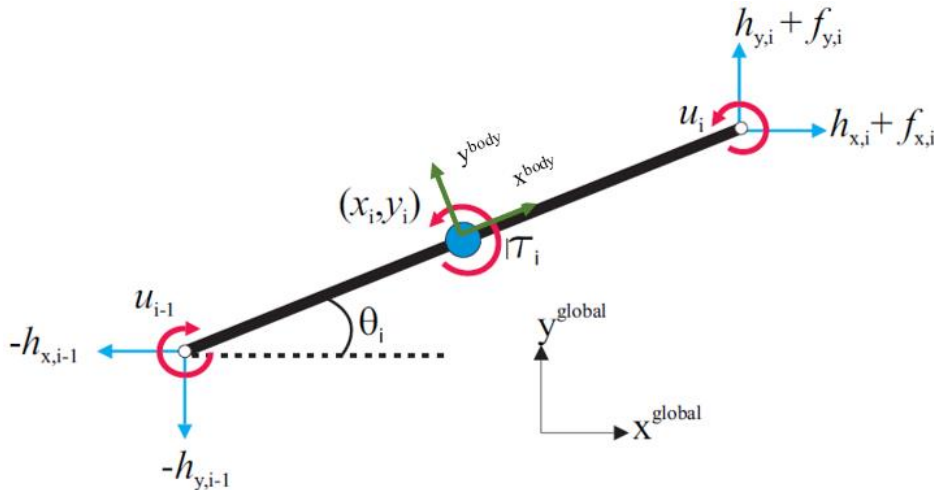


Figure 4.2: The internal and fluid forces acting on a link.

The fluid force exerted on the body of link  $i$  can be described by equation 4.29. In this equation, both added mass effect and fluid drag are considered. These effects can be decomposed into a fluid force and a fluid torque acting on the CM of the link as depicted in figure 4.2 [63], [64].  $\dot{v}_{r,i}^{link,i}$  is the relative acceleration of link in the body frame of reference. It can be found by using equation 4.30.  $\dot{v}_{c,i}^{link,i}$  is the acceleration of the current in the body frame of reference which is given by equation 4.31. Due to assumption 4, acceleration of the current in the body frame of reference has only the contribution of the derivative of rotation matrix. Terms  $V_{x,i}$  and  $V_{y,i}$  are the x and y

components of the current velocity acting on the link  $i$  in the global frame of the reference.

$$f_i^{link,i} = -\widehat{\mathbf{C}}_A \dot{v}_{r,i}^{link,i} - \widehat{\mathbf{C}}_D v_{r,i}^{link,i} - \widehat{\mathbf{C}}_D sgn(v_{r,i}^{link,i})(v_{r,i}^{link,i})^2 \quad (4.29)$$

$$\dot{v}_{r,i}^{link,i} = \ddot{p}_i^{link,i} - \dot{v}_{c,i}^{link,i} \quad (4.30)$$

$$\dot{v}_{c,i}^{link,i} = \frac{d}{dt} \left( (\mathbf{R}_{link,i}^{global})^T v_c \right) = \begin{bmatrix} -\sin\theta_i \dot{\theta}_i & \cos\theta_i \dot{\theta}_i \\ -\cos\theta_i \dot{\theta}_i & -\sin\theta_i \dot{\theta}_i \end{bmatrix} \begin{bmatrix} V_{x,i} \\ V_{y,i} \end{bmatrix} \quad (4.31)$$

Force on the link can be expressed as the function of  $x$ . Due to the assumption 5 we can skip the numerical calculation of the drag force due to nonlinear terms. Matrices  $\widehat{\mathbf{C}}_A$  and  $\widehat{\mathbf{C}}_D$  given by equation 4.32 and 4.33.  $c_t$  describe the drag force along the x axis and  $c_n$  describe the drag force along the y axis.  $\mu_t$  is the added mass effect along the x axis and  $\mu_n$  is the added mass effect along y axis.

$$\widehat{\mathbf{C}}_D = \begin{bmatrix} c_t & 0 \\ 0 & c_n \end{bmatrix} = \begin{bmatrix} \frac{1}{2} \rho \pi C_f \frac{(b+a)}{2} d & 0 \\ 0 & \frac{1}{2} \rho C_D 2ad \end{bmatrix} \quad (4.32)$$

$$\widehat{\mathbf{C}}_A = \begin{bmatrix} u_t & 0 \\ 0 & \mu_n \end{bmatrix} = \begin{bmatrix} 0 & 0 \\ 0 & \rho \pi C_A a^2 d \end{bmatrix} \quad (4.33)$$

Terms 2a and 2b are the major and the minor diameter of the approximated cylindrical link.  $d$  is the length of link.  $\rho$  is the density of the fluid. Terms  $C_f$  and  $C_D$  are the drag coefficient in the x and y direction of motion.  $C_A$  is the added mass coefficient. Added mass effect along the longitudinal direction can be neglected compared to the body mass [65].

The torque applied on the link by the fluids can be modelled through equation 4.34 [66]. Terms  $\lambda_1, \lambda_2$  and  $\lambda_3$  are variables that depend on the shape of body and the fluid characteristic.  $\lambda_1$  represent the added mass effect and the terms  $\lambda_2$  and  $\lambda_3$  represent the drag torque parameters. These terms are given by equations 4.35, 4.36 and 4.37 [57], [63], [64]. Term  $C_M$  is the added mass inertia coefficient.

$$\tau_i = -\lambda_1 \ddot{\theta}_i - \lambda_2 \dot{\theta}_i - \lambda_3 \dot{\theta}_i |\dot{\theta}_i| \quad (4.34)$$

$$\lambda_1 = \frac{1}{12} \rho \pi C_M (a^2 - b^2)^2 \frac{d^3}{8} \quad (4.35)$$

$$\lambda_2 = \frac{1}{6} \rho \pi C_f (a + b) \frac{d^3}{8} \quad (4.36)$$

$$\lambda_3 = \frac{1}{8} \rho \pi C_f (a + b) \frac{d^4}{16} \quad (4.37)$$

The fluid forces acting on link can be presented in the global frame of reference. For this purpose, transformation matrix is used as shown in equation 4.38.

$$f_i^{global} = \mathbf{R}_{link,i}^{global} f_i^{link,i} = \begin{bmatrix} \cos\theta_i & -\sin\theta_i \\ \sin\theta_i & \cos\theta_i \end{bmatrix} \begin{bmatrix} f_{x,i}^{link,i} \\ f_{y,i}^{link,i} \end{bmatrix} \quad (4.38)$$

Terms  $f_{x,i}^{link,i}$  and  $f_{y,i}^{link,i}$  are the x and y component of the fluid force in the body frame of reference. Solving equation 4.38 we can obtain equation 4.39. Terms  $V_{r_{x,i}}$  and  $V_{r_{y,i}}$  are given by equation 4.40. In equation 4.39,  $\dot{x}_i$  and  $\dot{y}_i$  are the velocity components of CM of the links in the global frame of reference.  $V_{x,i}$  and  $V_{y,i}$  are the velocity components of the currents acting on a link.

$$\begin{aligned} f_i^{global} = -\mathbf{R}_{link,i}^{global} & \left( \left( \hat{\mathbf{C}}_A \left( (\mathbf{R}_{link,i}^{global})^T \begin{bmatrix} \ddot{x}_i \\ \ddot{y}_i \end{bmatrix} \right. \right. \right. \\ & \left. \left. \left. - \begin{bmatrix} -\sin\theta_i \dot{\theta}_i & \cos\theta_i \dot{\theta}_i \\ -\cos\theta_i \dot{\theta}_i & -\sin\theta_i \dot{\theta}_i \end{bmatrix} \begin{bmatrix} V_{x,i} \\ V_{y,i} \end{bmatrix} \right) \right) \\ & + \left( \hat{\mathbf{C}}_D (\mathbf{R}_{link,i}^{global})^T \begin{bmatrix} \dot{x}_i - V_{x,i} \\ \dot{y}_i - V_{y,i} \end{bmatrix} \right) \\ & \left. + \left( \hat{\mathbf{C}}_D sgn \left( \begin{bmatrix} V_{r_{x,i}} \\ V_{r_{y,i}} \end{bmatrix} \right) \begin{bmatrix} V_{r_{x,i}}^2 \\ V_{r_{y,i}}^2 \end{bmatrix} \right) \right) \end{aligned} \quad (4.39)$$

$$\begin{bmatrix} V_{r_{x,i}} \\ V_{r_{y,i}} \end{bmatrix} = (\mathbf{R}_{link,i}^{global})^T \begin{bmatrix} \dot{x}_i - V_{x,i} \\ \dot{y}_i - V_{y,i} \end{bmatrix} \quad (4.40)$$

In order to assemble all the fluid forces on the all the links we can write them in a vector form. The effect of the fluid forces can be expressed as shown in equation 4.41.

$$\mathbf{f} = \begin{bmatrix} \mathbf{f}_x \\ \mathbf{f}_y \end{bmatrix} = \begin{bmatrix} \mathbf{f}_{Ax} \\ \mathbf{f}_{Ay} \end{bmatrix} + \begin{bmatrix} \mathbf{f}_{Dx}^L \\ \mathbf{f}_{Dy}^L \end{bmatrix} + \begin{bmatrix} \mathbf{f}_{Dx}^{NL} \\ \mathbf{f}_{Dy}^{NL} \end{bmatrix} \quad (4.41)$$

Terms  $\mathbf{f}_{Ax}$  and  $\mathbf{f}_{Ay}$  express the fluid force due to the added mass effect. Term  $\theta$  is a vector of link angles given by equation 4.42. Terms  $V_{x,1}$  and  $V_{y,1}$  are two diagonal matrices given by equations 4.43 and 4.44 respectively.

$$\begin{bmatrix} \mathbf{f}_{Ax} \\ \mathbf{f}_{Ay} \end{bmatrix} = - \begin{bmatrix} \mu_n(\mathbf{S}_\theta)^2 & -\mu_n \mathbf{S}_\theta \mathbf{C}_\theta \\ -\mu_n \mathbf{S}_\theta \mathbf{C}_\theta & \mu_n(\mathbf{C}_\theta)^2 \end{bmatrix} \begin{bmatrix} \ddot{\mathbf{X}} \\ \ddot{\mathbf{Y}} \end{bmatrix} - \begin{bmatrix} -\mu_n \mathbf{S}_\theta \mathbf{C}_\theta & \mu_n(\mathbf{S}_\theta)^2 \\ \mu_n(\mathbf{C}_\theta)^2 & \mu_n \mathbf{S}_\theta \mathbf{C}_\theta \end{bmatrix} \begin{bmatrix} V_x^a \\ V_y^a \end{bmatrix} \dot{\theta} \quad (4.42)$$

$$\mathbf{V}_x^a = \begin{bmatrix} V_{x,1} & 0 & 0 \\ 0 & \ddots & 0 \\ 0 & 0 & V_{x,N} \end{bmatrix} \quad (4.43)$$

$$\mathbf{V}_y^a = \begin{bmatrix} V_{y,1} & 0 & 0 \\ 0 & \ddots & 0 \\ 0 & 0 & V_{y,N} \end{bmatrix} \quad (4.44)$$

Terms  $\mathbf{f}_{Dx}^L$  and  $\mathbf{f}_{Dy}^L$  represent the linear fluid drag force and these terms are given by equation 4.45.  $\mathbf{V}_x$  and  $\mathbf{V}_y$  are the matrices of velocity components acting on all the links given by equations 4.46 and 4.47.

$$\begin{bmatrix} \mathbf{f}_{Dx}^L \\ \mathbf{f}_{Dy}^L \end{bmatrix} = \begin{bmatrix} c_t(\mathbf{C}_\theta)^2 + c_n(\mathbf{S}_\theta)^2 & (c_t - c_n)\mathbf{S}_\theta \mathbf{C}_\theta \\ (c_t - c_n)\mathbf{S}_\theta \mathbf{C}_\theta & c_t(\mathbf{S}_\theta)^2 + c_n(\mathbf{C}_\theta)^2 \end{bmatrix} \begin{bmatrix} \dot{\mathbf{X}} - \mathbf{V}_x \\ \dot{\mathbf{Y}} - \mathbf{V}_y \end{bmatrix} \quad (4.45)$$

$$\mathbf{V}_x = \begin{bmatrix} V_{x,1} \\ \vdots \\ V_{x,N} \end{bmatrix} \quad (4.46)$$

$$\mathbf{V}_y = \begin{bmatrix} V_{y,1} \\ \vdots \\ V_{y,N} \end{bmatrix} \quad (4.47)$$

The terms  $\mathbf{f}_{Dx}^{NL}$  and  $\mathbf{f}_{Dy}^{NL}$  represent the nonlinear drag force given by equation 4.48. The terms  $\begin{bmatrix} \mathbf{V}_{rx} \\ \mathbf{V}_{ry} \end{bmatrix}$  is given by equation 4.49.

$$\begin{bmatrix} \mathbf{f}_{Dx}^{NL} \\ \mathbf{f}_{Dy}^{NL} \end{bmatrix} = \begin{bmatrix} c_t \mathbf{C}_\theta & -c_n \mathbf{S}_\theta \\ c_t \mathbf{S}_\theta & c_n \mathbf{C}_\theta \end{bmatrix} \operatorname{sgn}\left(\begin{bmatrix} \mathbf{V}_{rx} \\ \mathbf{V}_{ry} \end{bmatrix}\right) \begin{bmatrix} \mathbf{V}_{rx}^2 \\ \mathbf{V}_{ry}^2 \end{bmatrix} \quad (4.48)$$

$$\begin{bmatrix} \mathbf{V}_{rx} \\ \mathbf{V}_{ry} \end{bmatrix} = \begin{bmatrix} \mathbf{C}_\theta & \mathbf{S}_\theta \\ -\mathbf{S}_\theta & \mathbf{C}_\theta \end{bmatrix} \begin{bmatrix} \dot{\mathbf{X}} - \mathbf{V}_x \\ \dot{\mathbf{Y}} - \mathbf{V}_y \end{bmatrix} \quad (4.49)$$

The compact equation containing the fluid torques of all the links can be written as shown in equation 4.50. The terms  $\Lambda_1$ ,  $\Lambda_2$  and  $\Lambda_3$  are given by the terms  $\lambda_1 \mathbf{I}_n$ ,  $\lambda_2 \mathbf{I}_n$  and  $\lambda_3 \mathbf{I}_n$  where  $I_n$  is an identity matrix.

$$\boldsymbol{\tau} = -\Lambda_1 \ddot{\boldsymbol{\theta}} - \Lambda_2 \dot{\boldsymbol{\theta}} - \Lambda_3 \dot{\boldsymbol{\theta}} |\dot{\boldsymbol{\theta}}| \quad (4.50)$$

The horizontal and vertical balance of force on the  $i^{th}$  link can be written as shown in equation 4.51. Moreover, a compact equation can be written for the all the links as shown in equation 4.52. Forces  $h_{x,i}$  and  $h_{y,i}$  are the internal forces in between the links. Terms  $\mathbf{h}_x$  and  $\mathbf{h}_y$  are column matrices of all the respective internal forces as shown in equation 4.53.

$$\begin{aligned} m\ddot{x}_i &= h_{x,i} - h_{x,i-1} + f_{x,i} \\ m\ddot{y}_i &= h_{y,i} - h_{y,i-1} + f_{y,i} \end{aligned} \quad (4.51)$$

$$\begin{aligned} m\ddot{\mathbf{X}} &= \mathbf{D}^T \mathbf{h}_x + \mathbf{f}_x \\ m\ddot{\mathbf{Y}} &= \mathbf{D}^T \mathbf{h}_y + \mathbf{f}_y \end{aligned} \quad (4.52)$$

$$\begin{aligned} \mathbf{h}_x &= \begin{bmatrix} h_{x,1} \\ \vdots \\ h_{x,N-1} \end{bmatrix} \\ \mathbf{h}_y &= \begin{bmatrix} h_{y,1} \\ \vdots \\ h_{y,N-1} \end{bmatrix} \end{aligned} \quad (4.53)$$

The acceleration of CM of the snake robot can be obtained by differentiating twice equation 4.4 as shown in equation 4.54. Equation 4.52 can be substituted in equation 4.54 and obtain equation 4.55. In equation 4.55, summing the internal forces  $h_{x,i}$  and  $h_{y,i}$ , are cancelled out thus remain only the external forces. Equation 4.55 simply state that having summed all the external forces, we can obtain the acceleration of the CM by dividing that sum by the total mass.

$$\begin{bmatrix} \ddot{x}_g \\ \ddot{y}_g \end{bmatrix} = \frac{1}{N} \begin{bmatrix} e \ddot{X} \\ e \ddot{Y} \end{bmatrix} \quad (4.54)$$

$$\begin{bmatrix} \ddot{x}_g \\ \ddot{y}_g \end{bmatrix} = \frac{1}{Nm} \begin{bmatrix} e & [0] \\ [0] & e \end{bmatrix} \begin{bmatrix} f_x \\ f_y \end{bmatrix} \quad (4.55)$$

Similarly, we can write the torque balance around the CM of the link as given by equation 4.56. Further all equations of each link can be expressed in a matrix form as shown by equation 4.57. In order to solve the terms  $\mathbf{h}_x$  and  $\mathbf{h}_y$ , we can use equations 4.52 and multiplying equation by D and solving it for  $\mathbf{h}_x$  and  $\mathbf{h}_y$  as given by equations 4.58 and 4.59. The term  $u_i$  represents the internal torque in between the links.  $\mathbf{u}$  is a column matrix of all the internal torques given by equation 4.60.

$$\begin{aligned} J\ddot{\theta}_i &= u_i - u_{i-1} - \frac{d}{2} \sin\theta_i (h_{x,i} + h_{x,i-1}) \\ &\quad + \frac{d}{2} \cos\theta_i (h_{y,i} + h_{y,i-1}) + \tau_i \end{aligned} \quad (4.56)$$

$$J\ddot{\boldsymbol{\theta}} = \mathbf{D}^T \mathbf{u} - \frac{d}{2} \mathbf{S}_\theta \mathbf{A}^T \mathbf{h}_x + \frac{d}{2} \mathbf{C}_\theta \mathbf{A}^T \mathbf{h}_y + \boldsymbol{\tau} \quad (4.57)$$

$$\begin{aligned} \mathbf{h}_x &= (\mathbf{D}\mathbf{D}^T)^{-1} \mathbf{D} (m\ddot{X} + \mu_n (\mathbf{S}_\theta)^2 \ddot{X} - \mu_n \mathbf{S}_\theta \mathbf{C}_\theta \ddot{Y} - \mu_n \mathbf{S}_\theta \mathbf{C}_\theta V_x^a \dot{\boldsymbol{\theta}} \\ &\quad - \mu_n (\mathbf{S}_\theta)^2 V_y^a \dot{\boldsymbol{\theta}} - \mathbf{f}_{Dx}^{NL} - \mathbf{f}_{Dx}^L) \end{aligned} \quad (4.58)$$

$$\begin{aligned} \mathbf{h}_y &= (\mathbf{D}\mathbf{D}^T)^{-1} \mathbf{D} (m\ddot{Y} + \mu_n \mathbf{S}_\theta \mathbf{C}_\theta \ddot{X} - \mu_n (\mathbf{C}_\theta)^2 \ddot{Y} - \mu_n (\mathbf{C}_\theta)^2 V_x^a \dot{\boldsymbol{\theta}} \\ &\quad - \mu_n \mathbf{S}_\theta \mathbf{C}_\theta V_y^a \dot{\boldsymbol{\theta}} - \mathbf{f}_{Dy}^{NL} - \mathbf{f}_{Dy}^L) \end{aligned} \quad (4.59)$$

$$\mathbf{u} = \begin{bmatrix} u_1 \\ \vdots \\ u_{N-1} \end{bmatrix} \quad (4.60)$$

By differentiating equations 4.11 and 4.12 we can obtain equation 4.61. We can obtain equation 4.62, by taking the second derivative of equation 4.4 and substituting its  $x$  and  $y$  components into the second derivative of equation 4.20.

$$\begin{aligned} \mathbf{D}\ddot{\mathbf{X}} &= \frac{d}{2} \mathbf{A}(\mathbf{C}_\theta \dot{\theta}^2 + \mathbf{S}_\theta \ddot{\theta}) \\ \mathbf{D}\ddot{\mathbf{Y}} &= \frac{d}{2} \mathbf{A}(\mathbf{S}_\theta \dot{\theta}^2 - \mathbf{C}_\theta \ddot{\theta}) \end{aligned} \quad (4.61)$$

$$\begin{aligned} \ddot{\mathbf{X}} &= \frac{d}{2} \mathbf{H}(\mathbf{C}_\theta \dot{\theta}^2 + \mathbf{S}_\theta \ddot{\theta}) \\ \ddot{\mathbf{Y}} &= \frac{d}{2} \mathbf{H}(\mathbf{C}_\theta \dot{\theta}^2 + \mathbf{S}_\theta \ddot{\theta}) \end{aligned} \quad (4.62)$$

$$\mathbf{H} = \left( \mathbf{I}_N - \frac{\mathbf{e}\mathbf{e}^T}{N} \right)^{-1} \mathbf{K}^T \quad (4.63)$$

By inserting equations 4.58 and 4.59 into equation 4.57 and replacing the terms  $\mathbf{D}\ddot{\mathbf{X}}$  and  $\mathbf{D}\ddot{\mathbf{Y}}$  with equation 4.61 and replacing the terms  $\ddot{\mathbf{X}}$  and  $\ddot{\mathbf{Y}}$  with 4.62 we can obtain equation 4.64. The terms  $\mathbf{M}_\theta, \mathbf{W}_\theta, \mathbf{V}_\theta$  and  $\mathbf{V}$  is given by equations 4.65, 4.66, 4.67 and 4.68 respectively.

$$\begin{aligned} \mathbf{M}_\theta \ddot{\theta} + \mathbf{W}_\theta \dot{\theta}^2 + \mathbf{V}_\theta \dot{\theta} + \Lambda_3 \dot{\theta} |\dot{\theta}| - \frac{d}{2} \mathbf{S}_\theta \mathbf{K} (\mathbf{f}_{Dx}^{NL} + \mathbf{f}_{Dx}^L) \\ + \frac{d}{2} \mathbf{C}_\theta \mathbf{V} (\mathbf{f}_{Dy}^{NL} + \mathbf{f}_{Dy}^L) = \mathbf{D}^T \mathbf{u} \end{aligned} \quad (4.64)$$

$$\begin{aligned} \mathbf{M}_\theta &= J + m \left( \frac{d}{2} \right)^2 \mathbf{S}_\theta \mathbf{V} \mathbf{S}_\theta + m \left( \frac{d}{2} \right)^2 \mathbf{C}_\theta \mathbf{Y} \mathbf{V} + \Lambda_1 \\ &+ \left( \frac{d}{2} \right)^2 \mathbf{S}_\theta \mathbf{K} \mu_n (\mathbf{S}_\theta)^2 \mathbf{H} \mathbf{S}_\theta + \left( \frac{d}{2} \right)^2 \mathbf{S}_\theta \mathbf{K} \mu_n \mathbf{S}_\theta \mathbf{C}_\theta \mathbf{H} \mathbf{C}_\theta \\ &+ \left( \frac{d}{2} \right)^2 \mathbf{C}_\theta \mathbf{K} \mu_n \mathbf{S}_\theta \mathbf{C}_\theta \mathbf{H} \mathbf{S}_\theta + \left( \frac{d}{2} \right)^2 \mathbf{S}_\theta \mathbf{K} \mu_n (\mathbf{C}_\theta)^2 \mathbf{H} \mathbf{C}_\theta \end{aligned} \quad (4.65)$$

$$\begin{aligned}
\boldsymbol{W}_\theta = & m \left( \frac{d}{2} \right)^2 \boldsymbol{S}_\theta \boldsymbol{V} \boldsymbol{C}_\theta - m \left( \frac{d}{2} \right)^2 \boldsymbol{C}_\theta \boldsymbol{V} \boldsymbol{C}_\theta + \left( \frac{d}{2} \right)^2 \boldsymbol{S}_\theta \boldsymbol{K} \mu_n (\boldsymbol{S}_\theta)^2 \boldsymbol{H} \boldsymbol{C}_\theta \\
& - \left( \frac{d}{2} \right)^2 \boldsymbol{S}_\theta \boldsymbol{K} \mu_n \boldsymbol{S}_\theta \boldsymbol{C}_\theta \boldsymbol{H} \boldsymbol{S}_\theta + \left( \frac{d}{2} \right)^2 \boldsymbol{C}_\theta \boldsymbol{K} \mu_n \boldsymbol{S}_\theta \boldsymbol{C}_\theta \boldsymbol{H} \boldsymbol{C}_\theta \\
& - \left( \frac{d}{2} \right)^2 \boldsymbol{C}_\theta \boldsymbol{K} \mu_n (\boldsymbol{C}_\theta)^2 \boldsymbol{H} \boldsymbol{S}_\theta
\end{aligned} \tag{4.66}$$

$$\begin{aligned}
\boldsymbol{V}_\theta = & \Lambda_2 - \frac{d}{2} \boldsymbol{S}_\theta \boldsymbol{K} \mu_n \boldsymbol{S}_\theta \boldsymbol{C}_\theta \boldsymbol{V}_x^a - \frac{d}{2} \boldsymbol{S}_\theta \boldsymbol{K} \mu_n (\boldsymbol{S}_\theta)^2 \boldsymbol{V}_y^a \\
& - \frac{d}{2} \boldsymbol{C}_\theta \boldsymbol{K} \mu_n (\boldsymbol{C}_\theta)^2 \boldsymbol{V}_x^a - \frac{d}{2} \boldsymbol{C}_\theta \boldsymbol{K} \mu_n \boldsymbol{S}_\theta \boldsymbol{C}_\theta \boldsymbol{V}_y^a
\end{aligned} \tag{4.67}$$

$$\boldsymbol{V} = \boldsymbol{A}^T (\boldsymbol{D} \boldsymbol{D}^T)^{-1} \boldsymbol{A} \tag{4.68}$$

# 5. Control algorithm

In this chapter, we are going to investigate into control algorithms of the aquatic snake robot. In section 5.1, we are presenting the state of the art of control algorithms, and classification is presented to identify them. In section 5.2, we describe in detail two different control algorithms that are implemented on the aquatic snake robot. In section 5.3, we describe the method we used to implement the control algorithms that we discussed in section 5.2.

## 5.1 State of art of Control algorithm

There have been several works done for the control of snake robots. The control systems used in terrestrial snake robots can be used also in the aquatic snake robot with little modifications. Compared to the work of control algorithm of the aquatic snake robots, there are many works done on the terrestrial snake robot. The state of the art of control methods of the snake robots can be categorized into mainly two different categories. They are as,

- feedforward control
- feedback control.

### 5.1.1 Feedforward control

The feedforward control method is applied to the snake robot to generate the motion on the snake robot according to the user. This method is difficult to be used with autonomous driving since it is working without the feed of the sensors data. Based on the sensor data, the user can control the snake robot. Feedforward control can be categorized into 3 main types. They are as,

- Sine approach
- Model approach
- Central Pattern Generator approach

### 5.1.1.1 Sine Approach

The sine-based approach uses a simple time-indexed sine-based function for generating the traveling waves. This method was one of the first control methods to be developed. Hirose [28] had worked on modeling of the motion rhythm of the snake and he presented a serpenoid curve in which the snakes take its body along. This curve is given by equation 5.1 on the cartesian plane.

$$x(s) = \int_0^s \cos(a\cos(b\sigma) + c\sigma) d\sigma \quad y(s) = \int_0^s \sin(a\cos(b\sigma) + c\sigma) d\sigma \quad (5.1)$$

Terms  $a$ ,  $b$  and  $c$  are parameters of the curve.  $\sigma$  is the variable along the curve.  $a$  represent the amplitude of the curve,  $b$  specifies the period of the curve, and  $c$  is used to turn the curve for a certain direction. Figure 5.1 shows different serpenoid curves for different parameters.

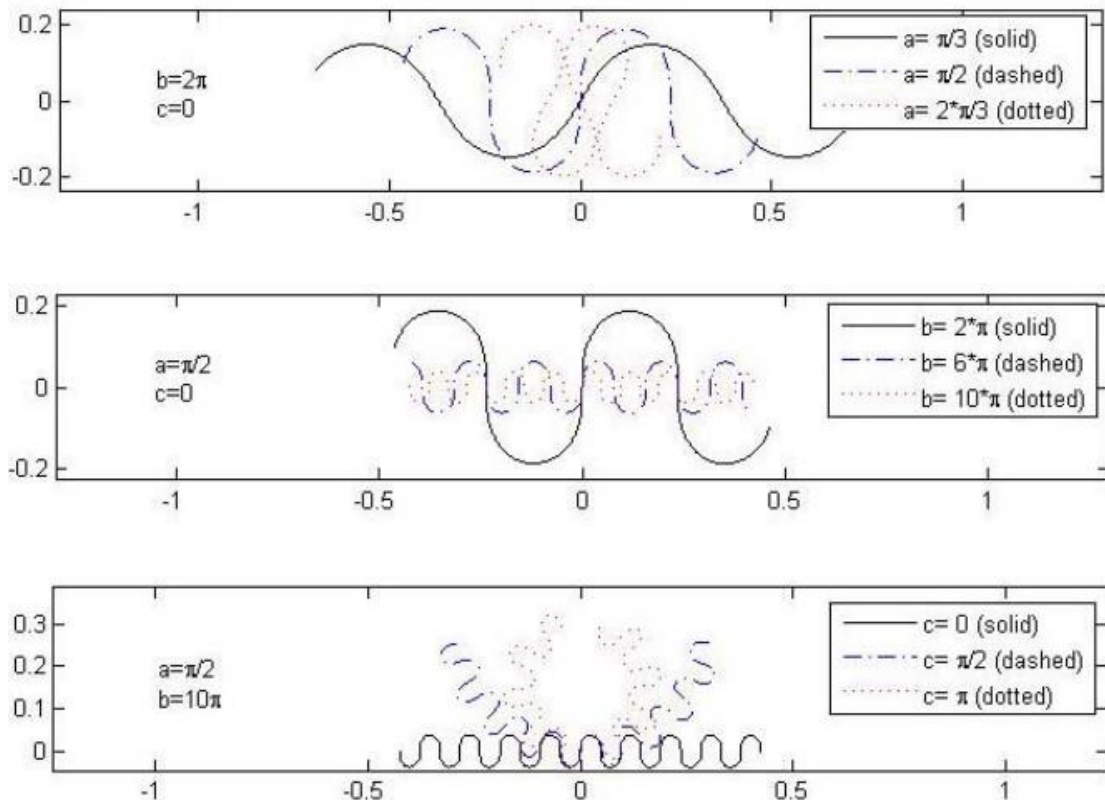


Figure 5.1: Serpenoid curve for different input parameters.

Snake robot with  $N$  number of links can achieve the above curve by passing a sin wave along its actuated joint. To achieve this phenomenon,  $N-1$  joints are moved in a sine wave with a constant shift at each joint. Since sine is the based mathematical function for the above generation it is known as a sine-based approach. Originally

this was used on the land snakes but later it was successfully used also on aquatic snake robots [57].

Other than the serpenoid curve there have been several works done on finding efficient and modified curves. Ma had introduced a new curve known as the serpentine curve [67]. Mahboob and Deghani have presented a modified serpenoid curve [68].

This method is simple and easy to implement but it is blind to the environment. The sine-based functions make it difficult to integrate sensory feedback signals. By using this method, we can simply modify the amplitude, frequency, and wavelength. But if we try to modify the above parameters online it will try to give jerky movements in the transition. One of the solutions for the above problem is filtering but the solution loses the simplicity of the sine-based approach.

#### 5.1.1.2 *Model Approach*

The model-based approach uses the kinematics or dynamics model of the robot to design control laws for the gait generation. Ostrowski and Burdick had worked on a kinematic model to control the snake robot. It was originally developed for the terrestrial snake robot, but it can be adapted for the underwater snake robot [69]. Matsuno and Suenaga had worked on a kinematic model to control a 3D snake robot [70]. Zhang et al have presented a control scheme-based dynamic model for an underwater snake robot [71]. McIsaac and Ostrowski had worked on a dynamic model for the motion control of a snake robot [56].

Control laws can be based on sine functions, but the use of the model approach can give the fastest and the best gait. The disadvantages of this method are that the performance of the model deteriorates when the model is not accurate this can happen when the environment is not compatible with the model. This method is not so good when operated by humans.

#### 5.1.1.3 *Central Pattern Generator*

Central pattern generator (CPG) is a biomimetic approach for the control of the snake robot [72], [73]. CPG are neural networks in charge of generating rhythmic movements such as swimming, flying, and walking. Ouyang et al have presented a CPG model as a coupled equation, which they had used for the locomotion generator [74]. This method uses traveling waves as a limit cycle. Therefore, this kind of implementation can change the gaits smoothly. Crespi states that the use of CPG model makes it difficult to implement different patterns and it is difficult to control the properties such as amplitude, frequency, and wavelength since parameters are not explicitly defined [75].

### 5.1.2 Feedback control

The feedback control system is used to control the snake robot based on several sensory feedbacks. In this control approach, the snake robot can travel precisely on a generated path and even autonomous drive based on the feedback of the sensors. Compared to the feedforward control system, the work done in the feedback system is minimum. Feedback controls remain an open question, and it is the spearhead of the snake control research.

Kelasidi et al have used the underwater sensors to identify the snake robot's position and perform feedback control on the assigned path for the snake robot. Qualisys camera systems were used to identify the position of the snake robot. To facilitate the identification light-reflective marks were placed on the snake robot. They had used a kinematic model to generate the gait pattern and therefore the path of the snake robot can be easily modified by the feedback system. Figure 5.2 shows an overview of the implemented system by Kelasidi et al[76].

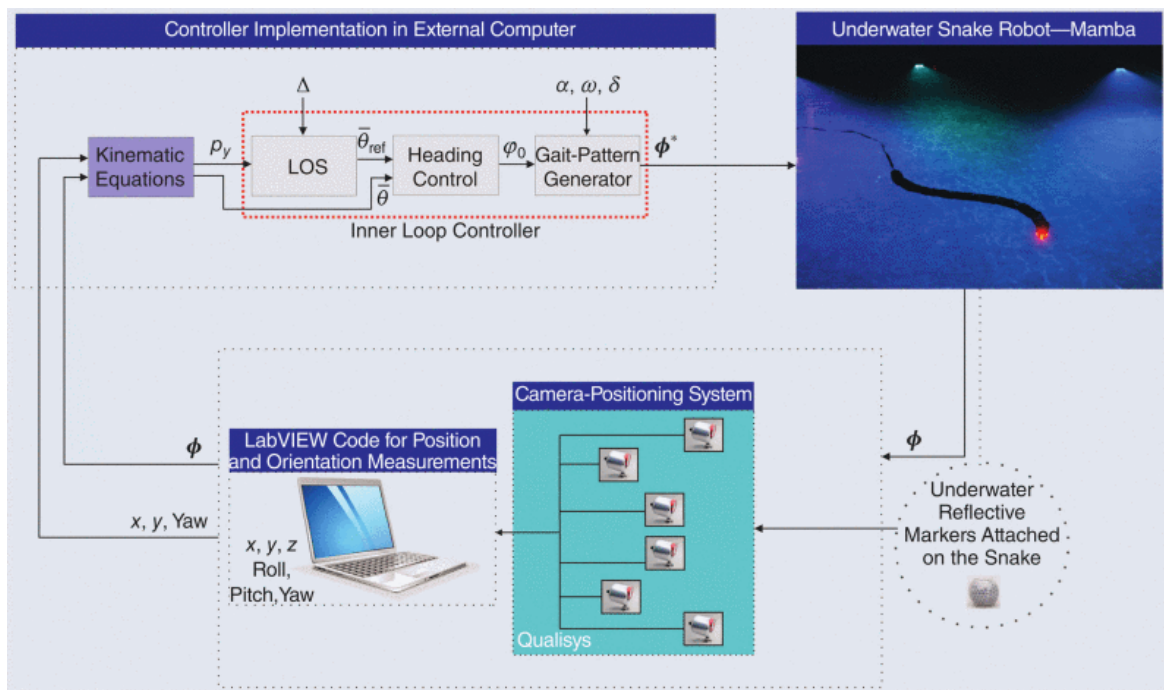


Figure 5.2: Feedback system implemented by Kelasidi et al.

McIsaac et al had worked on an eel robot and had implemented a feedback system. The sensors they had used were cameras. They had used images to identify the position of their snake robot and had implemented a position feedback system. They had generated the gaits using a kinematic model they had developed [56].

Bayraktaroglu et al had worked on a feedback system to perform the motion of a snake robot. This robot is operated on land, and it is not waterproof. To implement the motion, they had used an algorithm based on the lateral touchpoints and their robot is equipped with switches that act as touch sensors. The motion of the snake robot is based on the activation and deactivation of these touchpoints [31].

Tanaka et al had developed a whole-body collision avoiding system for a terrestrial snake robot. For this, they had used the range sensors on the snake robot. Using Hector SLAM software with the data of Laser Range Finder a map of the obstacle is obtained. This map was used to navigate through the obstacle[77].

Zhao et al had achieved autonomous navigation on land using Micro-Electromechanical-System and Inertial-Measurement-Units. They had developed a kinematic model and had used Extended-Kalman-Filter for position estimation. They have implemented a feedback system for autonomous driving based on the position feedback. They had tested this control algorithm on a snake robot they had built for several movements such as moving straight, turning, moving in a circle, etc [78].

## 5.2 Implemented Control Algorithm

Researchers have used different methods to achieve the motion of the aquatic snake robot. The motion generation of ASRs can be divided into mainly 2 different phases. The first is the momentum generation phase and the second is the steering phase [56]. In this thesis, we had used and tested two different types of control algorithms to generate two swimming gaits. They are as follows,

- Lateral Undulation
- Eel-like motion

### 5.2.1 Lateral undulation

The lateral undulation also known as the serpentine movement is the most used gait in both terrestrial and underwater snake robots. In this gait, a traveling wave is passed along the body of the snake robot. This traveling wave at a given instance reassembles serpentine curve which was discussed in section 5.1.1.1. This gait can be implemented through equation 5.2. Hence the construction of links due to the angles from equation 5.2 can be presented as the discretized form of the serpentine curve.

$$\phi_i = A \sin(\omega t + i\varphi) \quad (5.2)$$

The subscript  $i$  represent the  $i^{th}$  the actuated joint of the snake robot and there are  $N - 1$  actuated joints in a snake robot with  $N$  number of links.  $A$  represents the

amplitude of the serpentine curve and  $\omega$  represents the frequency of the traveling wave.  $\varphi$  is the constant phase difference between the links. By changing the sign of the  $\omega$ , we can change the direction of the traveling wave. If it is negative, it means it is traveling towards the end of the body and the propulsion is forward, and if it is positive vice versa.

Equation 5.2 can be used for linear propulsion. Steering is an important aspect of the motion of the snake robot. McIsaac and Ostrawski have presented two methods to achieve maneuver [79]. They are as,

- Constant offset method
- Constant hold method

#### 5.2.1.1 Constant offset method

The constant offset method is a method used to change the direction of the snake robot. It uses a phase offset to rotate the snake robot. This offset can be introduced into equation 5.1 as shown in equation 5.3.

$$\phi_i = A \sin(\omega t + i\varphi) + \varphi_{offset} \quad (5.3)$$

The offset in the traveling wave will cause an uneven thrust and it will cause the snake robot to rotate. This maneuver can be done without having the aquatic snake robot gain its initial momentum gain. But above maneuver does not mimic, how the biological sea snakes behave.

#### 5.2.1.2 Constant hold method

The constant hold method is a technique used to steer the aquatic snake robot. This technique mimics the steering of the biological sea snake. The biological sea snakes can coil, and it does it with a small forward inertial moment. In aquatic snake robot, to achieve this gait, we must systematically control the waveform of the aquatic snake robot.

To generate a coil in the snake, a hold must be passed along the body of the ASR. To achieve this phenomenon, we hold the sine wave when a joint angle achieves its maximum or minimum angle, the respective angle is held for a fixed duration of time. The fact that whether it's the maximum or minimum angle to be held, depends on the turn direction that needed to be achieved. By changing the time of hold we can adjust the turn radius. The algorithm to implement this gait is shown in figure 5.3.

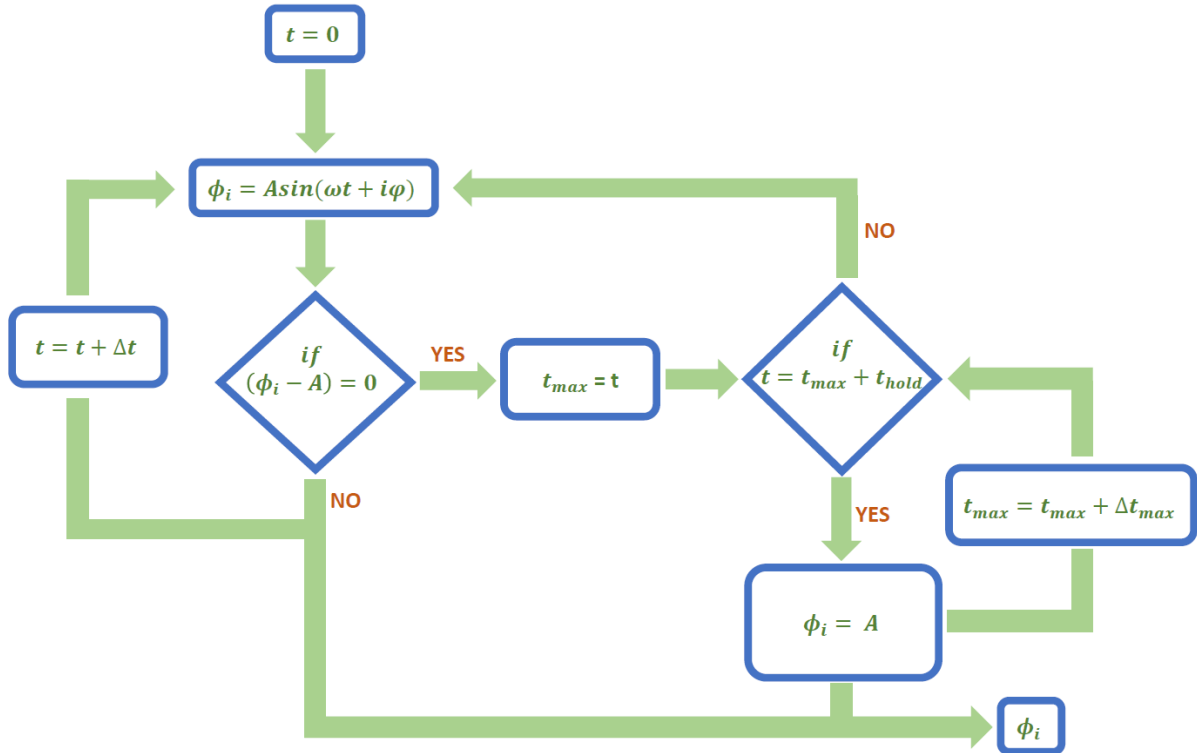


Figure 5.3: The algorithm for the constant hold method steering.

The next important maneuver in the Lateral undulation is the stop of the aquatic snake robot. If we stop the movement of the joint of the snake robot it does not stop the movement of the snake immediately since it has inertial momentum. We can reduce time to a complete stop by reversing the direction of the traveling wave which is fed to the aquatic snake robot.

### 5.2.2 Eel motion

The eel-like motion closely resembles the lateral undulation, but the aquatic snake robot keeps its head oriented in one direction while in the Lateral undulation the head is moved along with the body as another module. Eel motion can be achieved by increasing the amplitude of the oscillation starting from the head. Therefore, equation 5.2 can be modified as shown in equation 5.4 to achieve the eel motion.

$$\phi_i = A \left( \frac{N-i}{N+1} \right) \sin(\omega t + i\varphi) \quad (5.4)$$

The term  $A \left( \frac{N-i}{N+1} \right)$  corresponds to the increasing amplitude starting from the first actuated joint. Term  $i$  represents the  $i^{th}$  actuated joint of the snake robot and there are  $N - 1$  actuated joints in a snake robot with  $N$  links. Term  $\omega$  represents the

frequency of the traveling wave and  $\varphi$  is the phase offset between each actuated joint. The steering of the snake robot can be achieved using both the methods that were discussed in 5.2.1.1 and 5.2.1.2. Further, to stop the snake robot the traveling wave reversing technique can be used.

In the literature, there have been attempts to try the gaits of terrestrial snake robots on the aquatic snake robots [22]. Yu et al have tried to implement the gaits such as Lateral undulation, Concertina, Sidewinding, Arc-shape rolling, S-shape rolling, and Helical rolling on an aquatic snake robot. They have found that the efficiency of all the terrestrial gaits is low except for the Lateral undulation.

### 5.2.3 Simulation

Simulation for the above-discussed swimming gaits was performed using MATLAB. In performing this simulation, the kinematic model was considered and to observe the gait patterns and progressions a reasonable velocity was assumed.

#### 5.2.3.1 Lateral undulation

Using equation 5.1 we can stimulate the gait pattern for the lateral undulation straight motion. Figure 5.4 represents the angles generated by a MATLAB code for 4 actuated joints. The plot is generated for 20 seconds. The parameters used in the above simulation are given in table 5.1.

Parameter	Value	Unit
Amplitude	40	Degrees
Wave frequency	$\frac{\pi}{6}$	rads <sup>-1</sup>
Phase	$\frac{\pi}{6}$	rad

Table 5.1: Parameters of simulation for lateral undulation straight motion.

We can simulate the shape of the robot using the data of the joints of the robot and the kinematic model. Figure 5.5 shows the progression of the snake robot simulated for 9 links and the length of a segment ( $l$ ) set to 150mm which approximates the link of our aquatic snake robot. To obtain the progression, it was assumed that the center segment of the ASR moves along the horizontal direction at a velocity of  $\frac{l}{2} \text{ ms}^{-1}$ .

As it is evident in figure 5.4 Angle 4 has a sudden jump from  $0^\circ$  to  $40^\circ$ . This can damage the robot and can result in jerky motion at the beginning of the snake robot's motion. To solve this issue, we had multiplied equation 5.2 by a decreasing exponential term as given by equation 5.5.

$$\phi_i = (1 - e^{-\lambda t}) A \sin(\omega t + i\varphi) \quad (5.5)$$

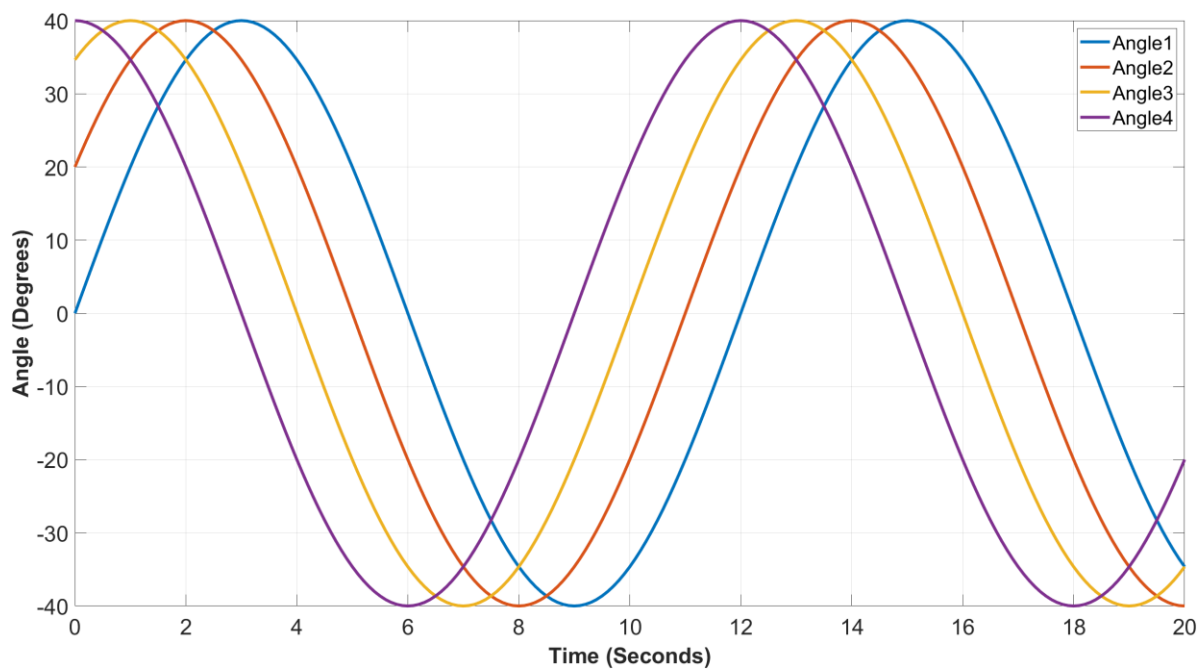


Figure 5.4: The joint angle variation with respect to time for lateral undulation straight motion.

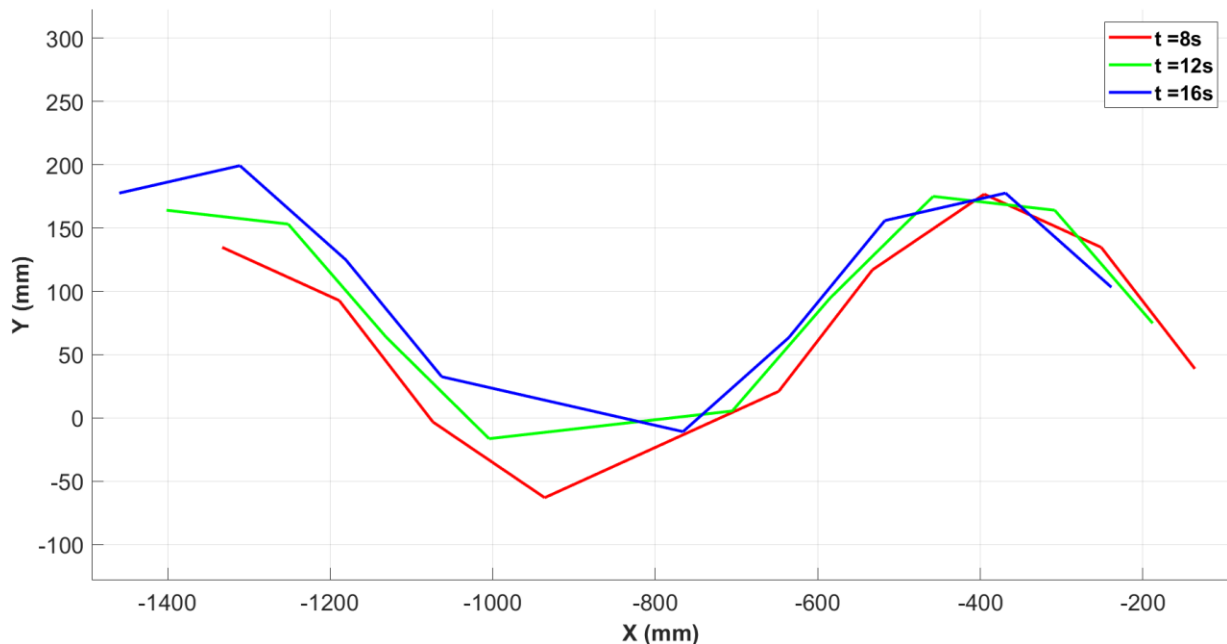


Figure 5.5: The simulation of progression of the ASR for lateral undulation motion.

Its effect is present at the beginning of the motion of the ASR and will fade away with the time giving a pure lateral undulation motion. Behavior of 4 joint angles to time is shown by figure 5.6. By changing the value of the  $\lambda$  we can change the intensity of the smoothening effect. In this simulation, we had used  $\lambda = 0.5$ .

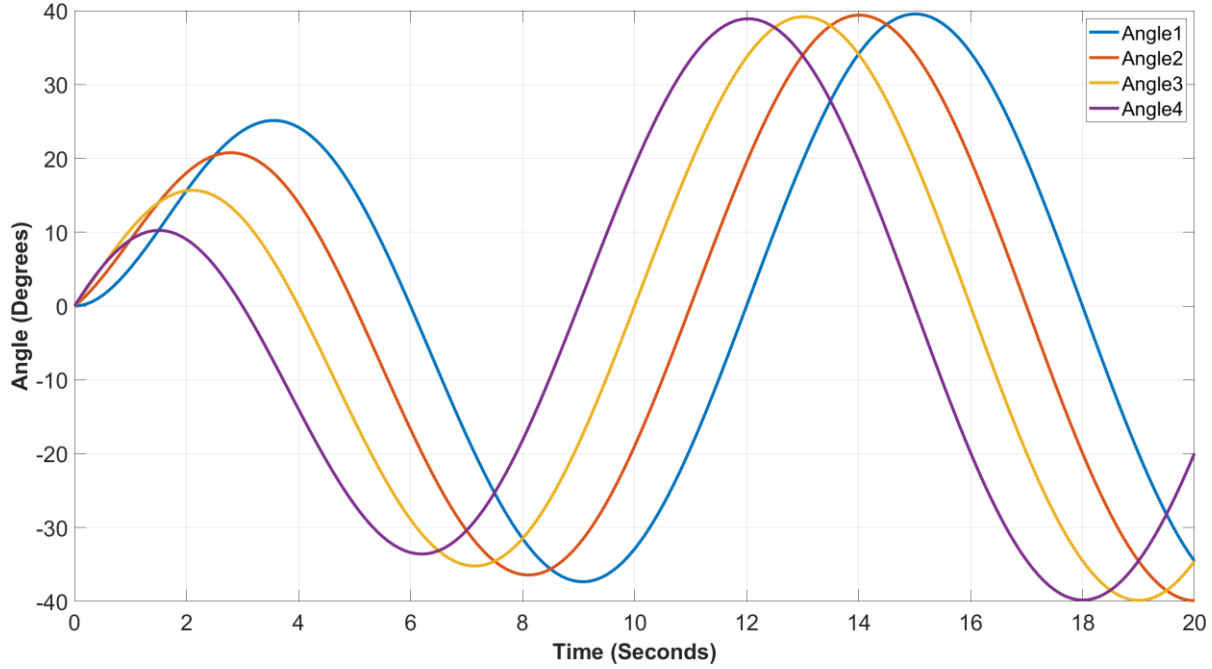


Figure 5.6: The joint angle variation with decreasing exponential function for lateral undulation motion.

Further, simulation was done for the steering of the ASR. Figure 5.6 shows a progression of the ASR turning at a radius of 800mm with the constant offset method. The values of the parameters are given in table 5.2

Parameter	Value	Unit
Amplitude	20	Degrees
Wave frequency	$\frac{\pi}{4}$	$rads^{-1}$
Phase	$\frac{\pi}{6}$	rad
Turning Offset	$\frac{\pi}{18}$	rad

Table 5.2: Parameters of simulation for constant offset method steering of lateral undulation.

Further, it was assumed that it would take 30 seconds to complete the maneuver. To have a smooth transition of the turning maneuver, the offset is multiplied by the

Heaviside function with smoothing coefficient  $k = 0.3$  and the max offset is delayed by  $t_{delay} = 12s$ . The modified equation is given by equation 5.6.

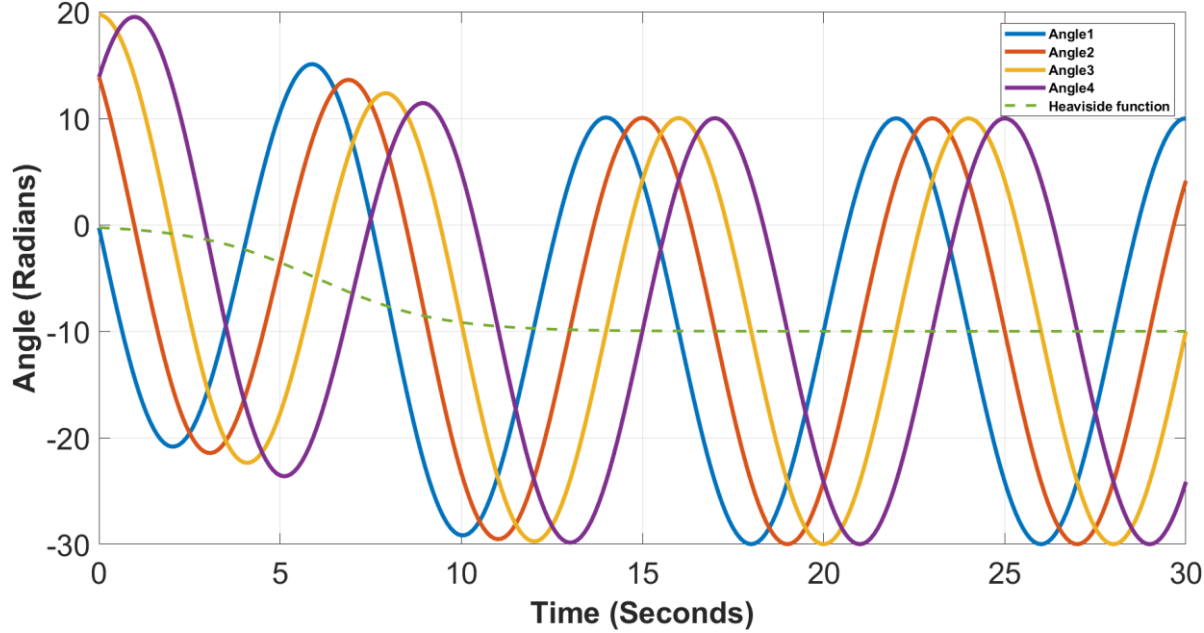


Figure 5.7: The joint angle variation to time in steering phase with constant offset method for lateral undulation motion.

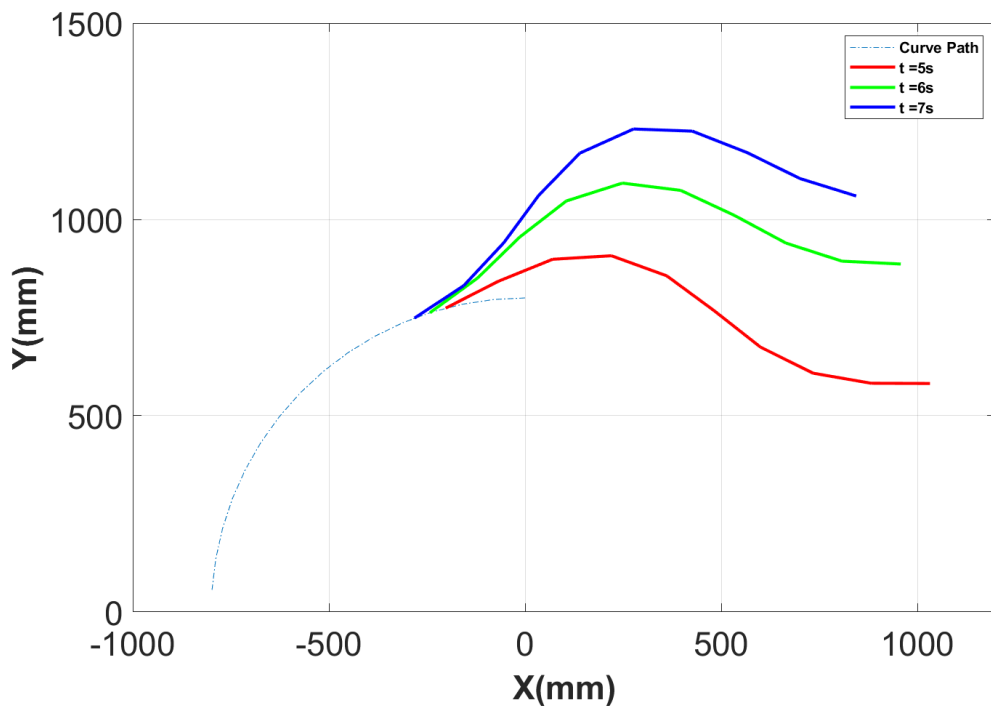


Figure 5.8: The progression of ASR in steering phase with constant offset method for lateral undulation motion.

$$\phi_i = A \sin(\omega t + i\varphi) + \left( \frac{\varphi_{offset}}{1 + e^{-2k(t - \frac{t_{delay}}{2})}} \right) \quad (5.6)$$

The constant offset turning gait with the modification can be seen in figure 5.7. In figure 5.7, it is shown the behavior of 4 consecutive joint angles and its smooth transition from the motion generating phase to the steering phase. Figure 5.8 shows the progression of the snake robot in time intervals of [5s to 7s].

A simulation was performed for the steering phase with the constant hold method. The values of the parameters of the stimulation are given in table 5.3. Figure 5.9 shows the variation of the 4 consecutive joint angles respective to time performing the constant hold steering maneuver. When the joint angle is at its minimum, the minimum angle is kept hold for 1 sec.

Parameter	Value	Unit
Amplitude	20	Degrees
Wave frequency	$\frac{\pi}{2}$	rads <sup>-1</sup>
Phase	$\frac{\pi}{6}$	rad

Table 5.3: Parameters of simulation for constant offset method steering of lateral undulation.

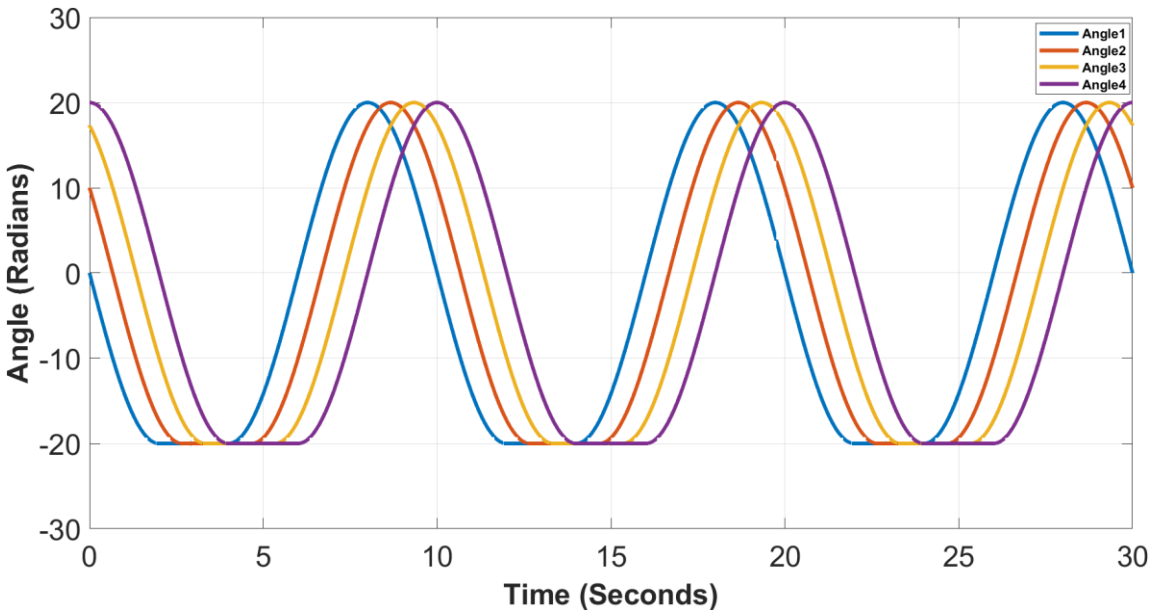


Figure 5.9: The joint angle variation in constant hold steering method for lateral undulation motion.

Figure 5.10 represents the progression of the snake robot performing the turning motion using the constant hold method. Figure 5.10a represents the ASR when the hold is not passed along the body of the robot for the time intervals of [12s to 14s]. Figure 5.10b represents the ASR when the hold is passed along the snake robot for the time intervals of [16s to 18s].

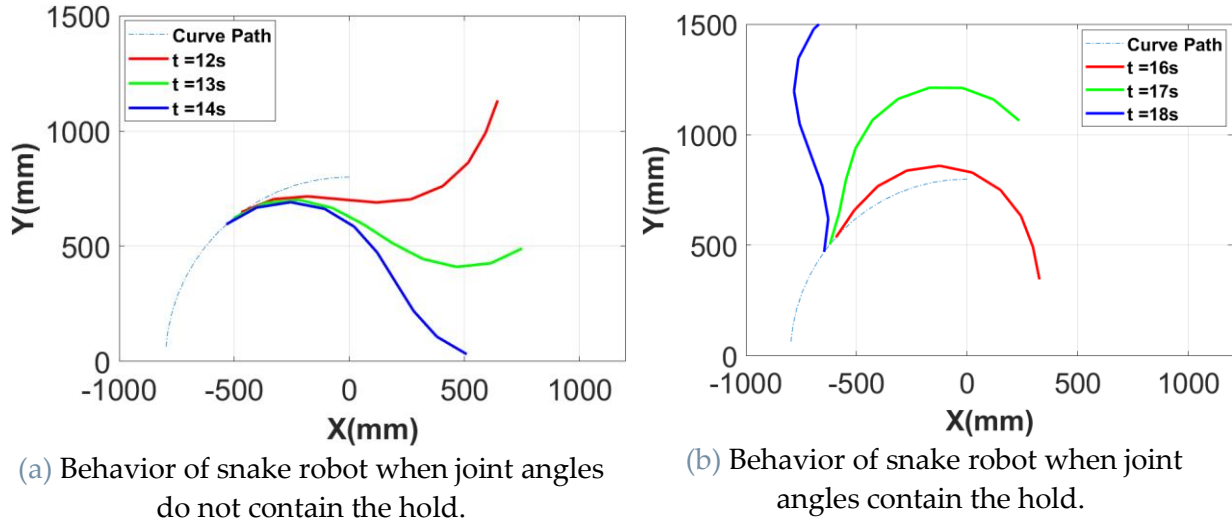


Figure 5.10: Progression of ASR performing constant hold steering method for lateral undulation motion.

### 5.2.3.2 Eel-like motion

Using equation 5.4 we can stimulate the eel-like motion for driving straight. Figure 5.11 represents the angles generated by a MATLAB code for 5 joints. As it is evident in figure 5.10, the amplitude of the angle of the oscillation increases with each module. The ninth module has the maximum oscillation amplitude. The plot in figure 5.11 is generated for 20 seconds. The parameters used in the above simulation are given in table 5.4.

Parameter	Value	Unit
Amplitude	40	Degrees
Wave frequency	$\frac{\pi}{6}$	$rads^{-1}$
Phase	$\frac{\pi}{6}$	rad

Table 5.4: Parameters of simulation for eel-like straight motion.

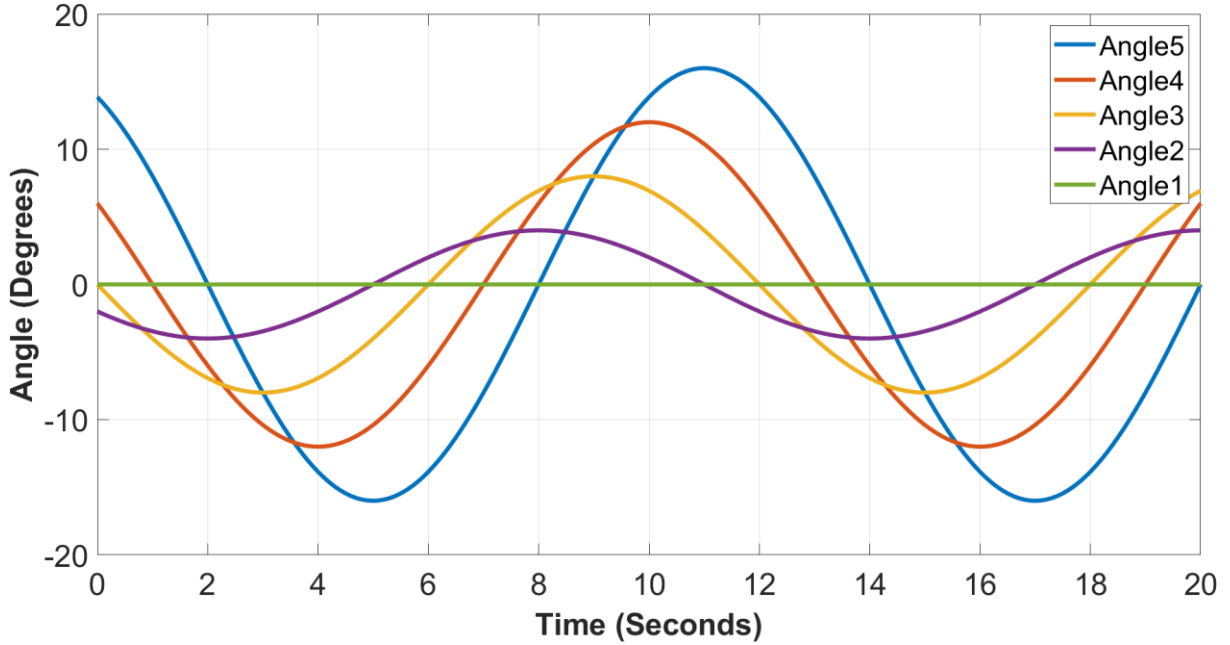


Figure 5.11: The joint angle variation by time for eel-like straight motion.

The shape of the ASR for given times can be generated using the kinematic model. Figure 5.12 shows the image of the progression of the ASR. In generating figure 5.12, we considered 9 links, and each link is 150mm long. To obtain the progression it was assumed that the velocity of the ASR is about  $\frac{l}{2} \text{ ms}^{-1}$ , where  $l$  is the length of a segment of the ASR.

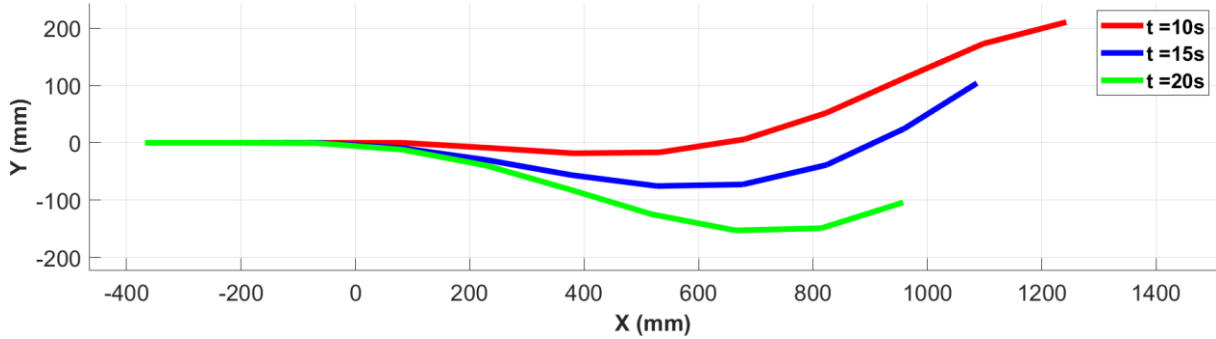


Figure 5.12: The simulation of progression of the ASR for eel-like motion.

Similar to lateral undulation, to avoid sudden jump of joint angles from zero to higher angles in the last modules, the decreasing exponential term is introduced. This problem does not exist for the first few modules but to have consistency all the target angles are multiplied by the decreasing exponential term. The modified equation 5.4 is given in equation 5.7.

$$\phi_i = (1 - e^{-\lambda t}) A \left( \frac{N-i}{N+1} \right) \sin(\omega t + i\varphi) A \sin(\omega t + i\varphi) \quad (5.7)$$

Figure 5.13 shows the joint angles of the first five modules after the smoothening effect. As it is evident in figure 5.13, the effect of the smooth start will disappear with time. Since equation 5.7 gradually increase the oscillation of the modules, ASR does not make any jerky motions at the beginning of the motion. By changing the value of the  $\lambda$  we can change the intensity of the smoothening effect. The  $\lambda$  that was used in this simulation was 0.5.

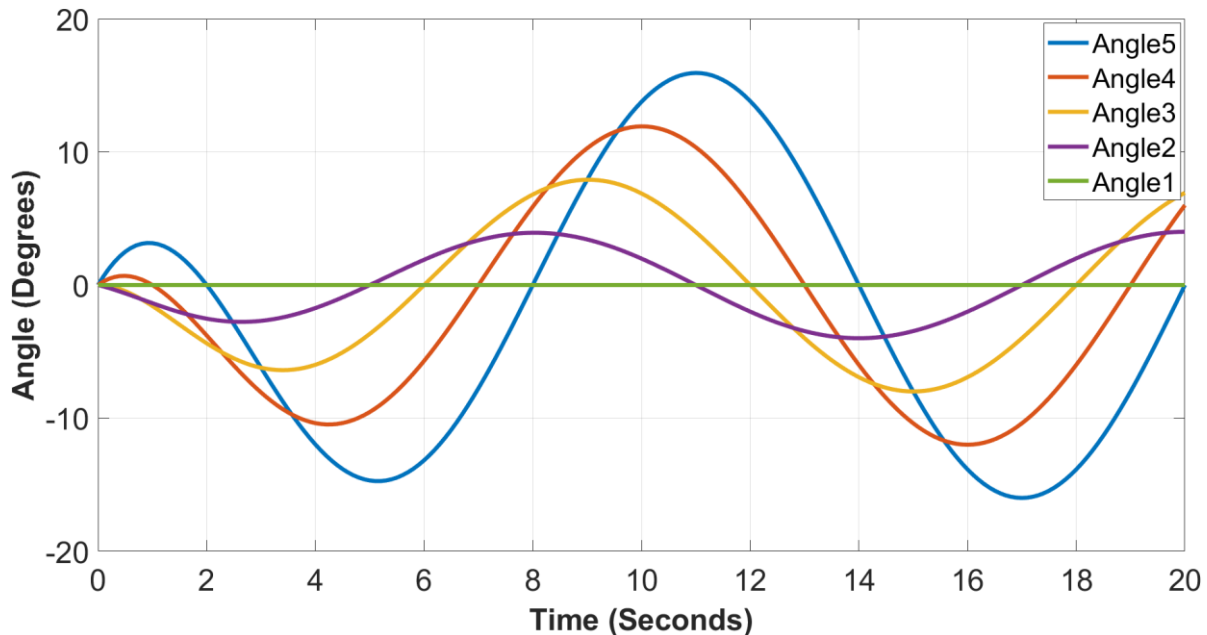


Figure 5.13: The joint angle variation with decreasing exponential function for eel-like motion.

A simulation was done for the steering of the ASR. Figure 5.14 shows the progression of the ASR turning at a radius of 800mm with the constant offset method. The values of the parameters are given in table 5.5

Parameter	Value	Unit
Amplitude	20	Degrees
Wave frequency	$\frac{\pi}{4}$	rads <sup>-1</sup>
Phase	$\frac{\pi}{6}$	rad
Turning Offset	$\frac{\pi}{18}$	rad

Table 5.5: Parameters of simulation for constant offset method steering of eel-like motion.

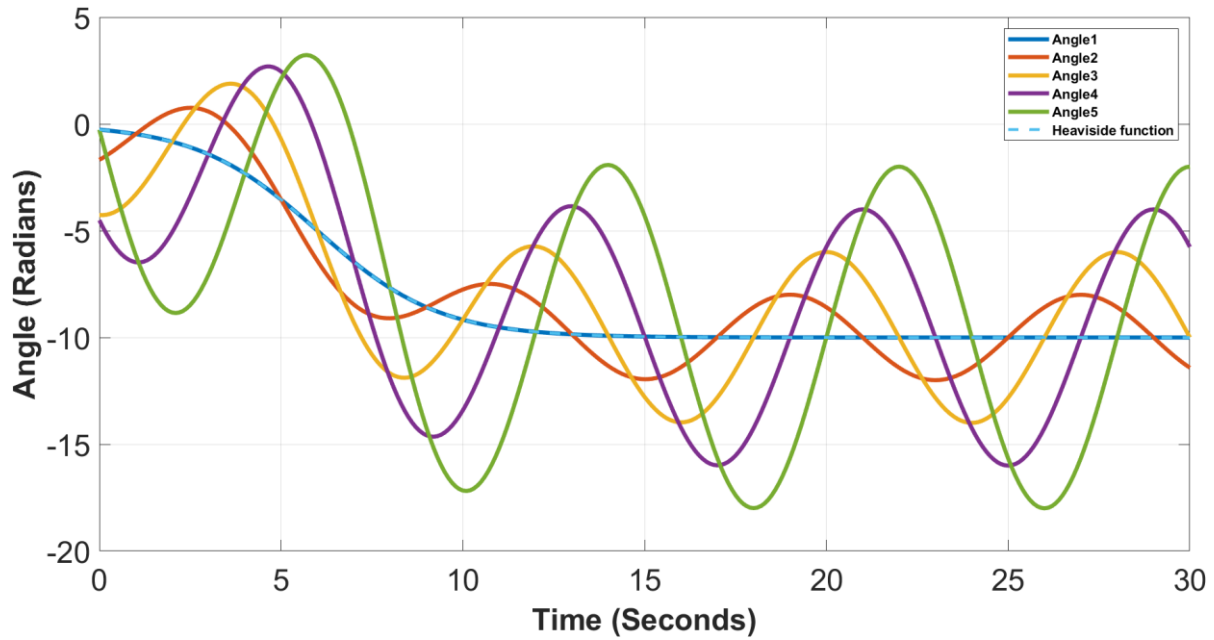


Figure 5.14: The joint angle variation with time in steering phase with constant offset method for eel like motion.

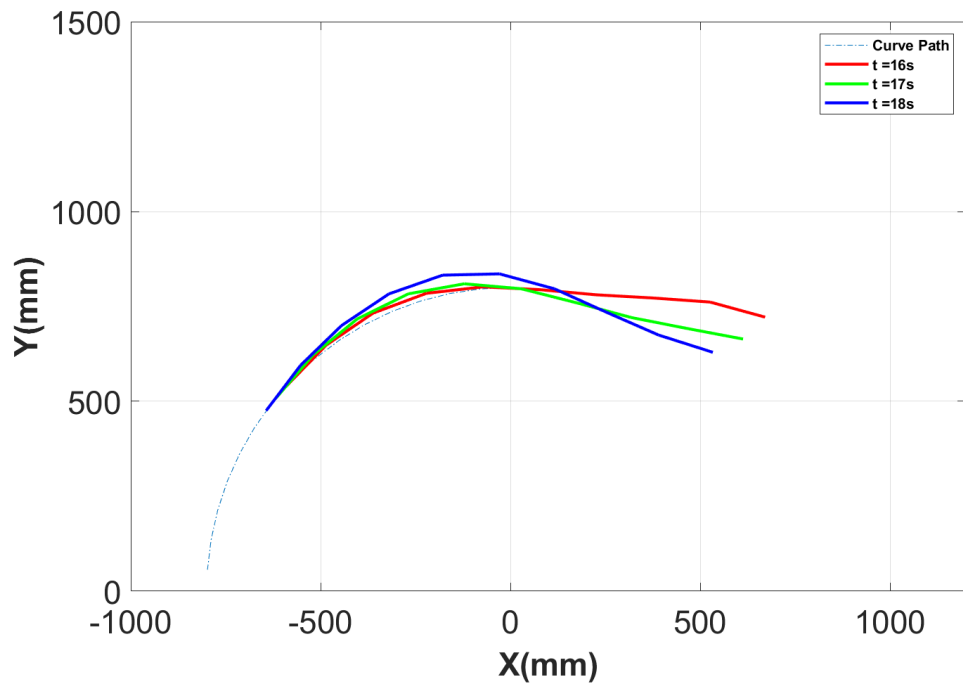


Figure 5.15: The progression of ASR in steering phase with constant offset method for eel-like motion.

To complete this maneuver, it was assumed that it would take 30 seconds. To have a smooth transition of the turning maneuver, the offset is multiplied by the Heaviside

function with smoothing coefficient  $k = 0.3$  and the max offset is delayed by  $t_{delay} = 12s$ . The modified equation is given by equation 5.8.

$$\phi_i = A \left( \frac{N - i}{N + 1} \right) \sin(\omega t + i\varphi) + \left( \frac{\varphi_{offset}}{1 + e^{-2k(t - \frac{t_{delay}}{2})}} \right) \quad (5.8)$$

The effect of the modified equation can be seen in figure 5.14. In figure 5.14, it is shown behavior of 5 consecutive joint angles and its smooth transition from the motion generating phase to steering phase. The figure 5.15 shows the progression of the snake robot in time intervals of [16s to 17s].

A simulation was performed for the steering phase with the constant hold method. The values of the parameters of the simulation are given in table 5.6

Parameter	Value	Unit
Amplitude	20	Degrees
Wave frequency	$\frac{\pi}{4}$	$rads^{-1}$
Phase	$\frac{\pi}{6}$	rad

Table 5.6: Parameters of simulation for constant offset method steering of eel-like motion.

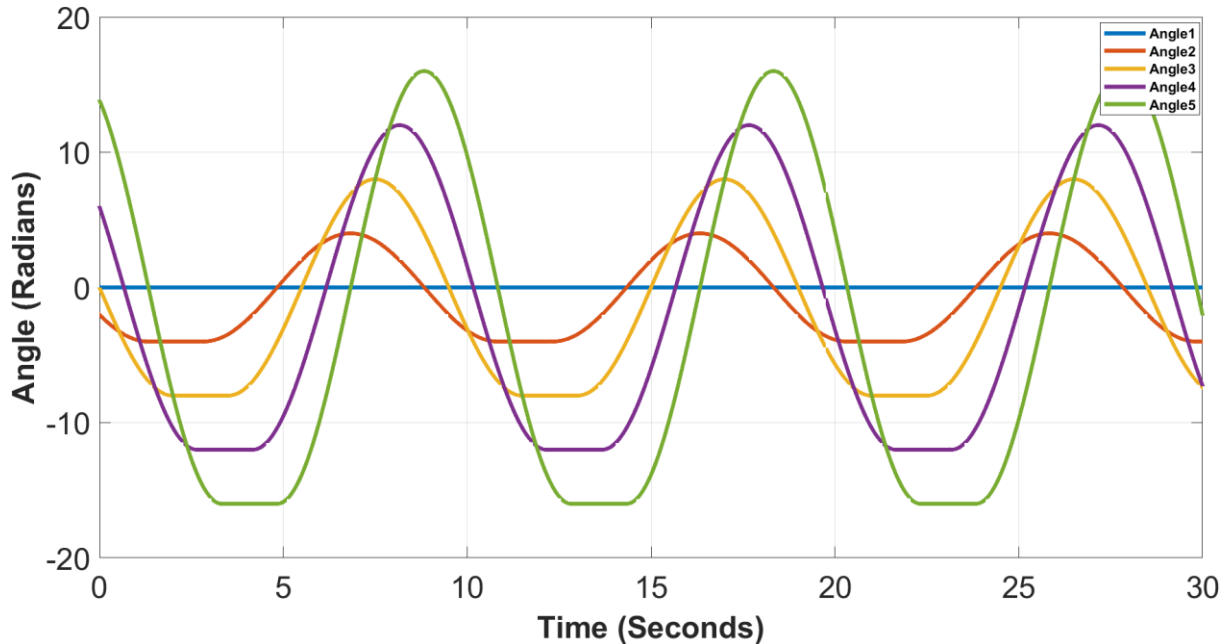


Figure 5.16: The joint angle variation in constant hold steering method for eel-like motion.

Figure 5.16 shows the variation of the 5 consecutive joint angles respective to time performing the constant hold steering maneuver. When the joint angle is at its minimum, the minimum angle is kept hold for 1.5 sec. In performing the simulation for the eel-like motion turning using the constant offset method, we encountered several numerical issues. In identifying the minimum value of the sine function, we had to use different values of intensity for each target angle. This was done to avoid overestimation and underestimation of the minimum value.

Figure 5.17 shows the ASRs progression while performing the constant hold turning method. Figure 5.17a shows the behavior of the ASR when the hold is not passed along the snake robot. Figure 5.17b represents the snake robot when a hold is passed along the body of the ASR.

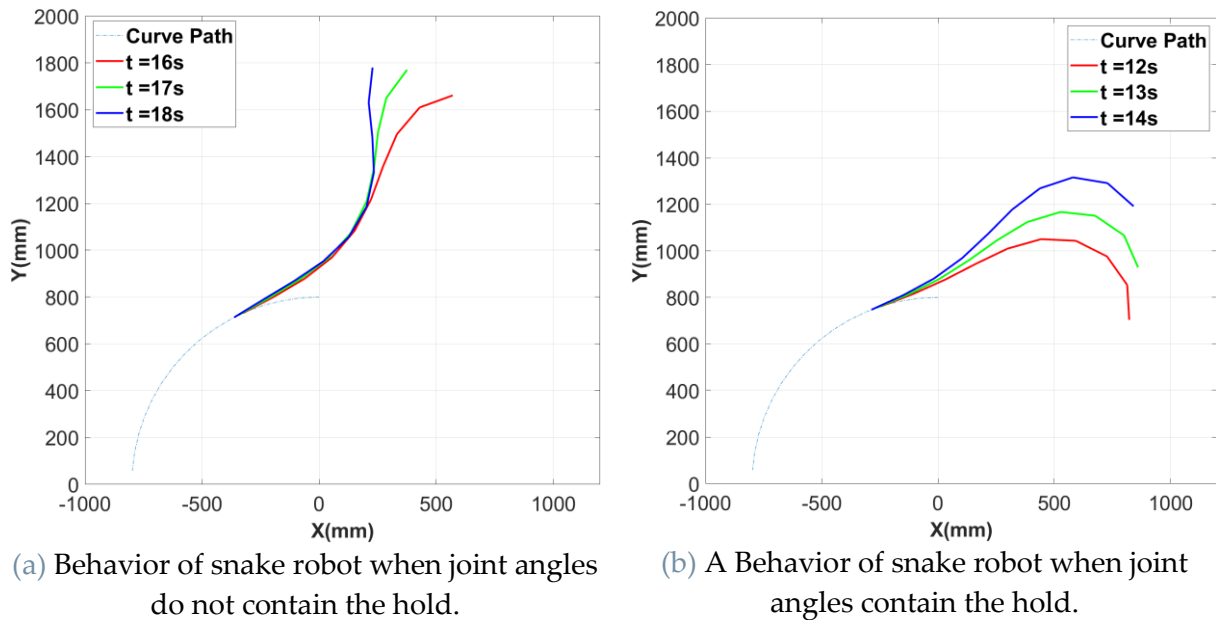


Figure 5.17: Progression of ASR performing constant hold steering method for eel-like motion.

### 5.3 Gait implementation

This sub-chapter discusses how the above-discussed motion control was implemented in the aquatic snake robot. This implementation was done for both swimming gaits which are lateral undulation and eel-like motion. The target angles were generated using the functions discussed in subchapters 5.1 and 5.2. The target angle generating system is known as the High-Level Feedforward System and it is discussed in 5.3.1. An internal feedback system is implemented on the module to

rotate the servomotor to its target angle, and it is described in 5.3.2. This aspect of the control is known as the Low-Level Feedback System.

### 5.3.1 High level feedforward system

The high-level feedforward system is implemented in the ASR to generate the target angles that are necessary for the generation of the serpentine curve using the modules. The high-level feedforward system can generate the target angles for the lateral undulation and eel-like motion patterns for both the steering and the straight drive phase.

The instruction for the Arduino Mega is received through the Bluetooth module by an external device. The Bluetooth module can be connected to Bluetooth terminal software on a PC or Mobile. Arduino Mega is programmed such that, by sending appropriate characters we can move the ASR according to the user's desire. Through the Bluetooth terminal software, the user can turn the sensor on and off so the user can visualize the sensor's data on the Bluetooth terminal software. Further, the Bluetooth module can be connected to MATLAB and perform autonomous or semi-autonomous navigation based on the internal and external sensors.

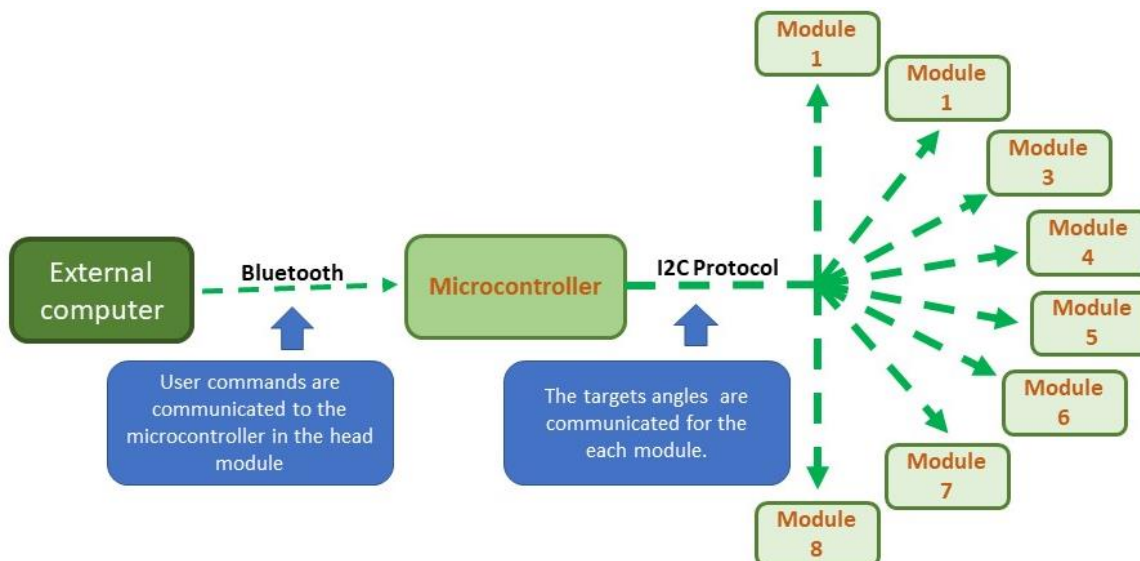


Figure 5.18: The Block diagram of the implemented system.

The target angles for every 8 modules are generated by the Arduino Mega present inside the head module for every 0.1 milliseconds. For this purpose, a timer is used to trigger the function based on the predetermined motion. These target angles are transmitted to the modules through the I2C connection. Arduino Mega is programmed such that the gait patterns can be changed from eel-like motion to

lateral undulation based on the received characters from the Bluetooth terminal software. The ASR can be moved forward, turn left or right, and stopped based on the received commands from the Bluetooth terminal software. Further, a function is built into the Arduino Mega to adjust the proportional gain in the low-level feedback system. To avoid the jerk motion at the beginning of the motion and turning of the ASR, the smoothening techniques discussed in 5.2.3.1 and 5.2.3.2 were implemented. Decreasing exponential smoothening technique was also used to stop the motion of ASR. Figure 5.18 shows an overall block diagram of the implemented system.

### 5.3.2 Low level feedback system

The low-level feedback system runs a feedback system to achieve the target angle received by the high-level feedforward system. Figure 5.19 represents the implemented feedback system on the 8<sup>th</sup> module and the rest of the modules have a similar system.

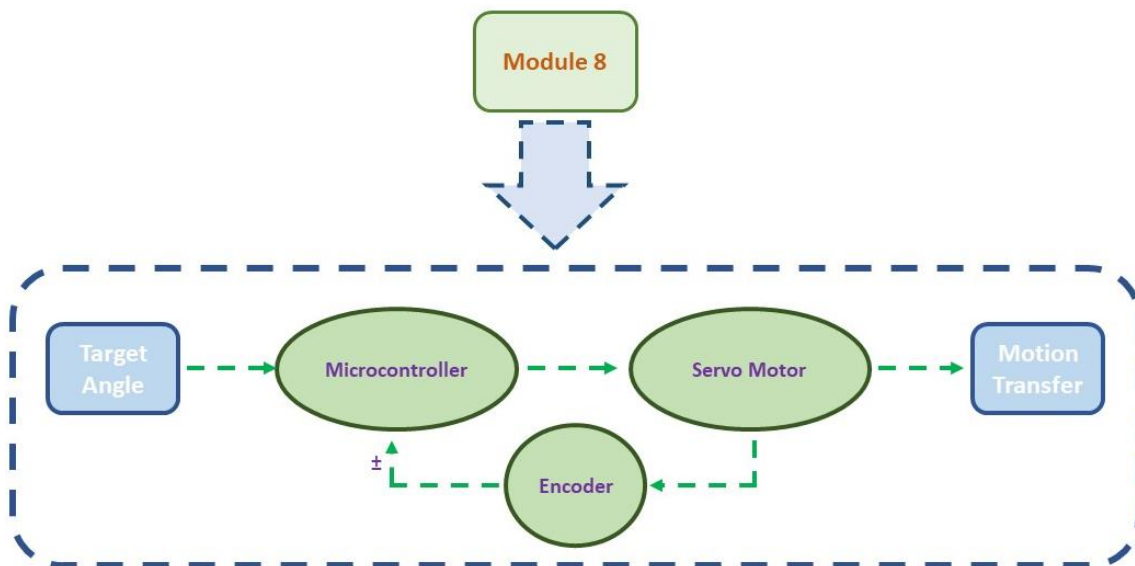


Figure 5.19: The Block diagram of the implemented low-level feedback system in module.

The FeeTech FB5311M-360 is equipped with an inbuilt magnetic encoder. By using this encoder, a PD control is implemented through the microcontroller inside the module. The proportional gain is set to 5 and the derivative gain is set 2. In theory, the PID controller must produce a better result on the position control of the servo motor. But due to the inconsistent noise in the encoder, it was experienced that the Integral regulator contributes to the instability more than stability.

The noise observed in the data from the encoder is consistent and not symmetric for the data. Further depending on the change of servo speed the content of noise changes. Figure 5.20 shows the untreated data of the encoder when the servo motor is on an oscillator motion between the angles 60 and -60 at about 0.5 Hz as shown in figure 5.21.

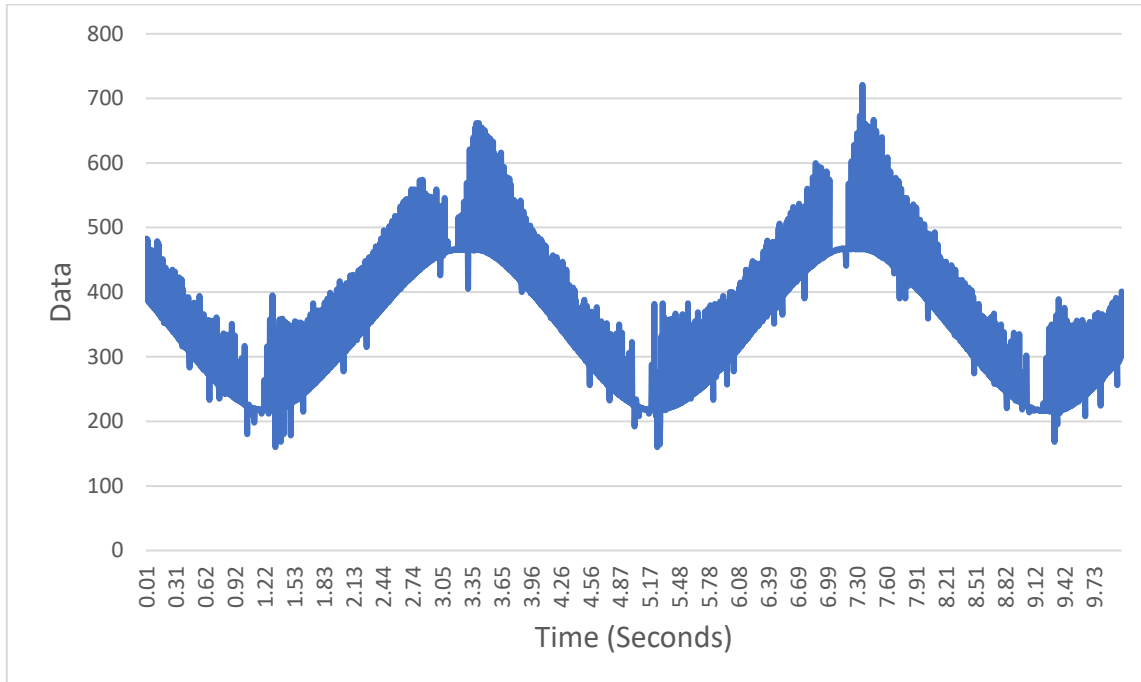


Figure 5.20: The untreated encoder data from servomotor.

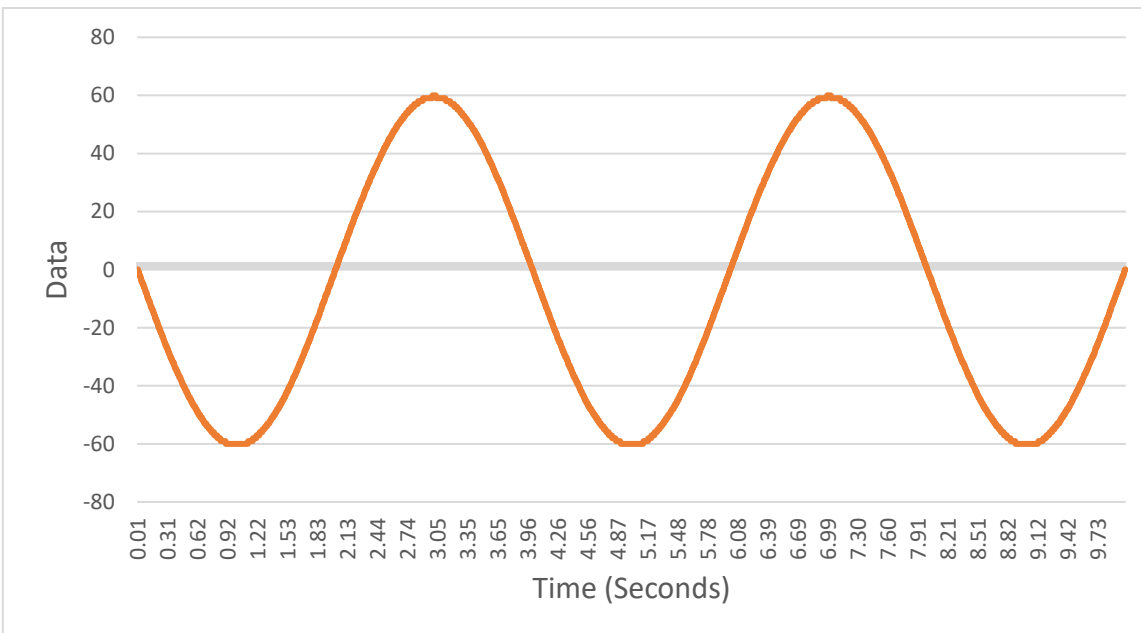


Figure 5.21: Oscillating angle generated based on time.

To tackle the above problem two kind of solutions were used. The first solution is the implementation of a low pass filter, and the other is the minimum value selection function.

### 5.3.2.1 Low pass filter

The low pass filter was used to filter the high-frequency noise in the encoder. This filter is implemented using equation 5.9 which is given in the LaPlace domain. Term  $\omega_o$  is the pole frequency. Equation 5.9 is discretized by the sampling frequency of 1000 Hz and the discrete transfer function is found using the Tustin method. Equation 5.10 presents the discrete transfer function.

$$H(s) = \frac{\omega_o}{s + \omega_o} \quad (5.9)$$

$$H(z) = \frac{b_0 + b_1 z^{-1} + b_2 z^{-2} + \dots}{1 - a_1 z^{-1} - a_2 z^{-2} + \dots} \quad (5.10)$$

Using the coefficient of the discrete transfer function we can build equation necessary for the filtering as shown in equation 5.11.  $y(n)$  is the filtered data of the encoder and  $x(n)$  is the untreated data from the encoder.

$$\begin{aligned} y(n) = & a_1 y(n-1) + a_2 y(n-2) + \dots \\ & + b_0 x(n) + b_1 x(n-1) + \dots \end{aligned} \quad (5.11)$$

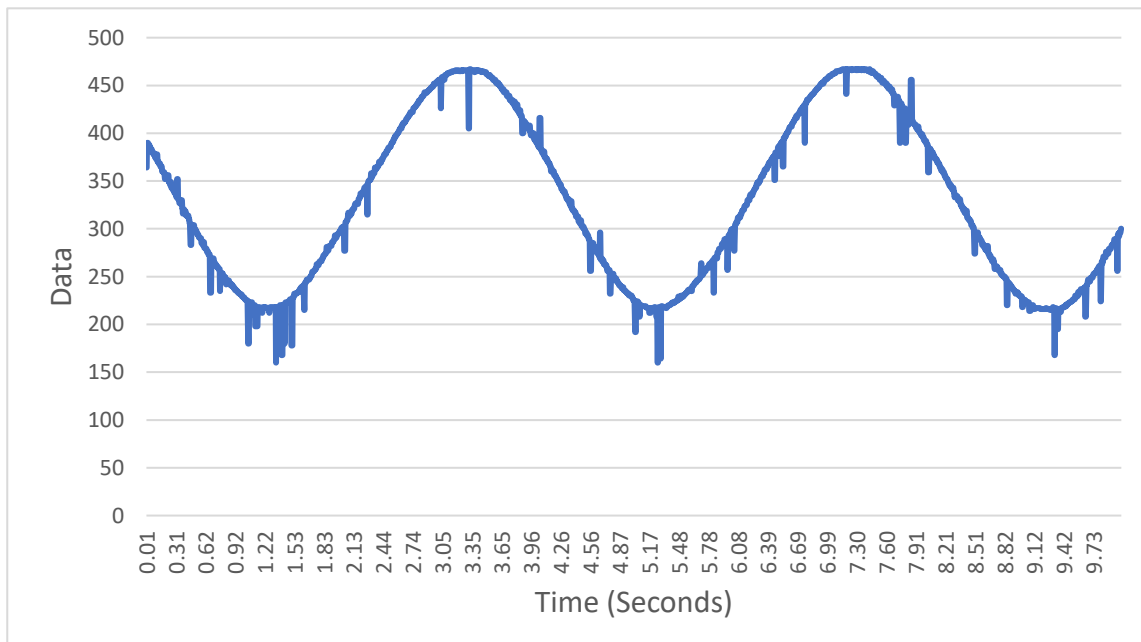


Figure 5.22: The encoder data after the low pass filter implementation.

In this thesis, we calculate the coefficient for different pole frequencies. Pole frequency set the cut-off frequency and we use the trial-and-error method to find the best cut-off frequency. In our case, it was found to be 10 Hz. Figure 5.22 shows the filtered signal of the encoder data through the low pass filter at the cut-off frequency of 10 Hz.

### 5.3.2.2 Minimum value function

Although the low pass filter removes a significant amount of noise, it is not able to remove all the noise. As it is evident in figure 5.22 there are some areas with significantly higher data values and lower values. These peaks and valleys are producing an uneven rotation velocity on the servo motor. To tackle the above problem, we created a function that records the 400 values of data of the encoder and selects the minimum data out of those 400 values. This array of 400 is renewed with the newest data and the oldest data is eliminated out of the array. Figure 5.23 shows the filtered data of the low-pass filtered data of encoder using the above process.

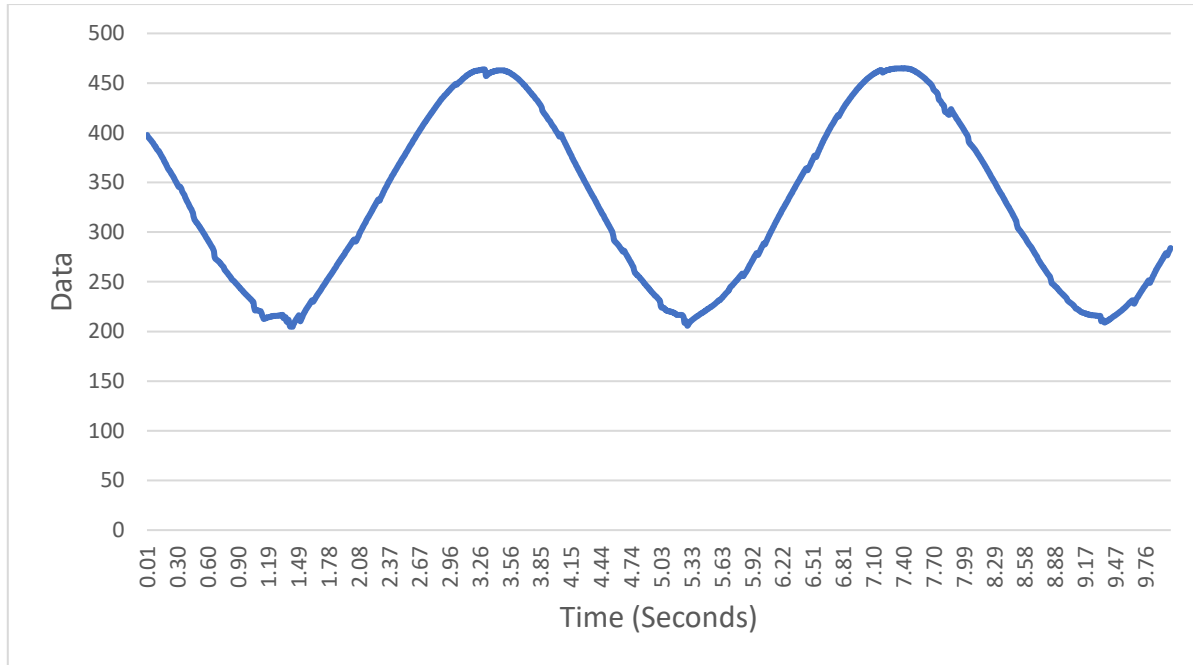


Figure 5.23: The encoder data filtered through both the low pass filter and the minimum value function.

Figure 5.24 shows the both the set of data from the filter and unfiltered signal. As it is evident these methods were able to reduce a significant amount of noise, but it has introduced a slight phase shift.

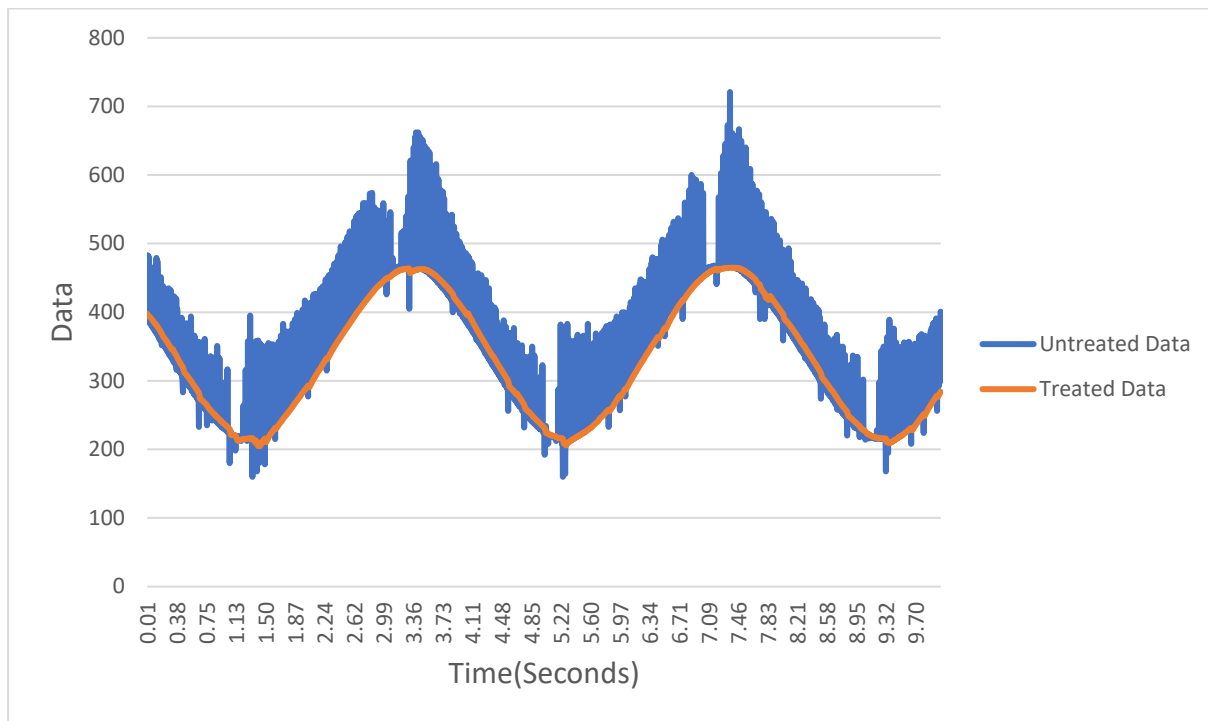


Figure 5.24: Fully treated data and untreated data.

## 6. Construction of the robot and the Experimental tests

ASR was constructed and experimented with the motion control algorithms. In subchapter 6.1 we discuss the fused deposition modeling used for the construction of the ASR. In subchapter 6.2, we discuss the construction of the head module. In subchapter 6.3, we discuss the construction of the module. In subchapter 6.4 we discuss the assembly of the ASR. In subchapter 6.5, we discuss the performed experimental activities.

### 6.1 Fused deposition modeling.

Fused deposition modeling is a process that lay fused material layer by layer by using a precise computer numerical control system. To perform this task the machine requires a sliced model of the component. Using this technology, the outer cover of the robot's head module is manufactured. Further, the brackets to hold the servomotor, spacers, and the extended arm for motion transfer are manufactured by using this manufacturing technology.

The designed components of the ASR are converted into stereography format. Then we have imported the file into the Slicer software Z-Suite v2.21 and oriented the component on the base of the printer in the best configuration for the printing. The orientation of the components on the 3D printer is very important since it affects the strength of the components and the surface quality of the printed components. Later we generated a Z code file that is readable by the printer. This file is specific for the selected 3D printing machine.

In manufacturing, we used the 3D printer Zortax M200 shown in figure 3.6, and the material used was Acrylonitrile-butadiene-styrene (ABS).



**Figure 6.1:** Zortrax M200 printer.

The process parameters chosen on the printer are crucial since they can affect the printing quality and the speed of the printing. The process parameters used in the printer are given in table 6.1. To improve the surface quality of the printed components, they were polished with acetone. Painting the printed components with acetone gives a shining surface. The servo bracket printed was able to counter the torque of the servo motor, hence the strength of the printed components was reasonable.

Parameters	Values
Layer thickness	0.14mm
Infill density	20%
Fan speed	80%
First layer gap	0.44mm
Nozzle diameter	0.4mm
First layer density	120%

**Table 6.1:** Parameters of additive manufacturing.

This technology is relatively cheap and versatile with respect to alternative manufacturing processes. But there is a catch to using this technology. The printing is very slow hence a large component can take up to hours. In this project, it took roughly 40 hours to print the head module of the robot. Therefore, in mass production and in large components it is not a viable production technology. This technology is compatible with a limited number of materials. The quality of the

manufacturing is influenced by environmental conditions such as humidity and temperature.

## **6.2 Head assembly**

The head assembly consists of all the electronic components and the outer cover to protect them. The outer cover of the snake robot is printed in the segment due to the dimension restriction of the printer. These components are assembled using permanent glue and the part that need to be taken apart are assembled using screws. Further, the bracket to attach the outermost cover is glued to the outer cover of the head module.

The sensors and other components are placed inside the assembled outer cover. All the sensors needed to be connected to the microcontroller and powered by the same battery. The electronic components were soldered with the connectors to assemble them in the space-restricted environment. Since it is hard to take off the battery to charge it each time, a separate circuit and a mechanism were built inside the head module. Due to this mechanism, the battery can be charged through a USB adapter. The charger module can produce the current and voltage cycle that need to charge the battery. This practice allows us to have higher battery life per charge and overall life of the battery. Figure 6.2 represents the circuit diagram of the head module.

To communicate with the Arduino Mega from an external device Bluetooth module HC-05 is used and its baud rate is set to 115200. This baud rate is the system-defined baud rate of the Arduino Mega to reprogram the microcontroller through the Bluetooth module. Further, to facilitate this feature, the Bluetooth module is needed to be connected to the Arduino Mega through a special circuit as shown in figure 6.2. This feature is very handy since the same Bluetooth module can be used to communicate to the microcontroller as well as to reprogram it. Also due to this feature, we can program the ASR without opening the cover of the ASR to access the microcontroller. The Bluetooth module is powered through a 5v current.

The ultrasonic sensor and the IMU sensor can be powered using the battery directly since their operational voltage is compatible with the battery voltage of 6 volts. The data acquainted from the sensors is transferred to an external device through the Bluetooth serial connection. IMU sensor is communicating the Arduino Mega through the I2C connection and the data is updated at a frequency of 50Hz. The ultrasonic sensor is triggered at a frequency of 100Hz. Based on the time for the echo the distance for the object is calculated.

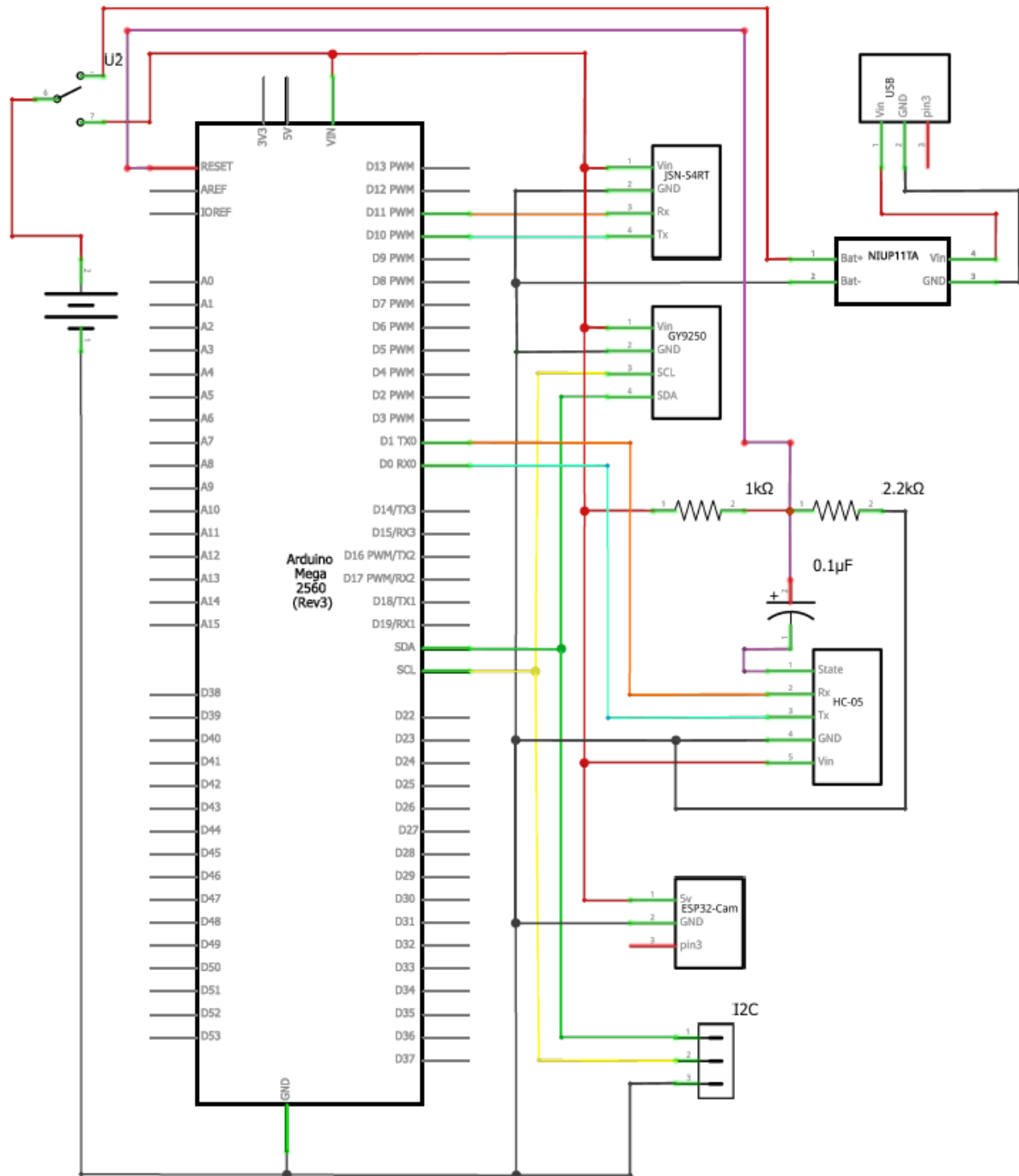


Figure 6.2: Circuit diagram of the head module.

The camera module is powered through a 6v current from the battery. The camera module is not integrated into the Arduino Mega and operates separately. This camera module got a microcontroller and hence it can be programmed to operate

through the Wi-Fi connection. Once the camera module is paired to a Wi-Fi stay paired to that Wi-Fi hotspot even when it is restarted. To acquire the images from the camera module we need to visit the IP address of the camera through a web browser of an external device that is connected to the same Wi-Fi network. The IP address carries to a web page where color images can be acquired through the camera. Further, several modifications can be done to the image such as increasing the resolution, rotating the image, etc. Increasing the resolution of the image decrease the refresh rate of the image. At the maximum resolution, the camera module has a refresh rate 15 fps.



Figure 6.3: Image taken from the camera module ESP32-CAM.

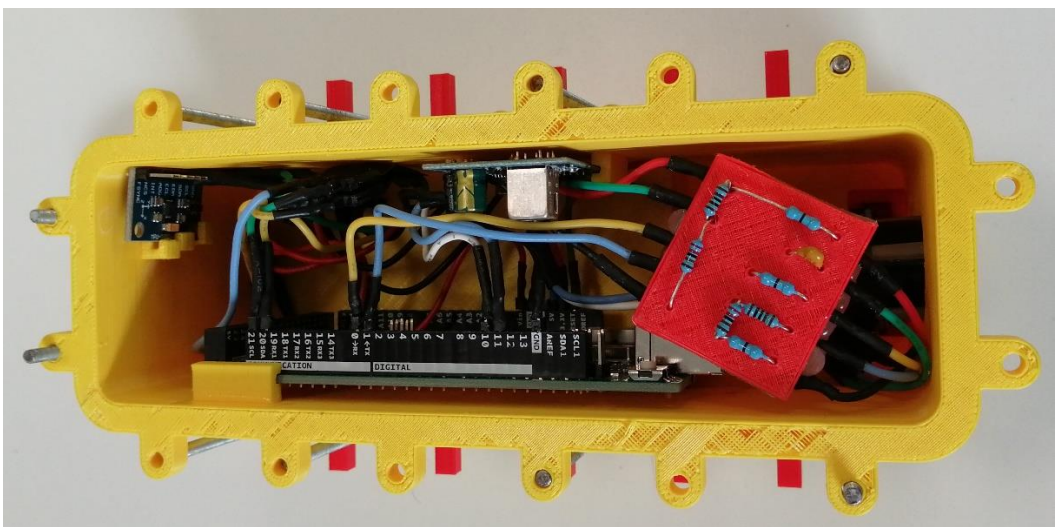


Figure 6.4: Internal components of the head module.

The head module contains wires with the connectors used to attach to the following module. Therefore, the head module can be connected to the rest of the modules through these connectors. Figure 6.4 shows the internal components of the assembled head module. Figure 6.5 shows the external view of the assembled head module. The physical properties of the head module are given in table 6.2.

Properties	Values
Mass	558g
Length	260mm
Width	80mm
Height	120mm

Table 6.2: Physical properties of head module.

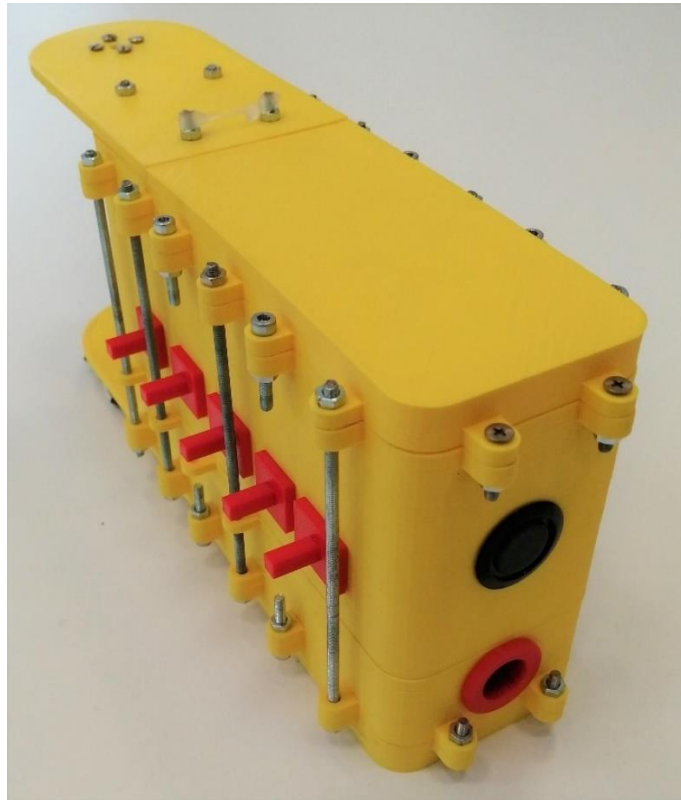


Figure 6.5: The assembled head module.

### 6.3 Module assembly

Depending on the dimensions of the buoyancy calculation, a manufactured box with the lid is brought. This box was manufactured with ABS material. Then the holes and openings that are necessary for the function of the module were made by drilling.

The servomotor was placed on the servo bracket, and it was fixed to the bracket using the M3 screws. Then the bracket was placed inside the box such that the shaft of the servo motor peaked out of the drilled holes in the box.

Properties	Values
Mass	365g
Length	75mm
Width	195 mm
Height	95mm

Table 6.3: Physical properties of the module.

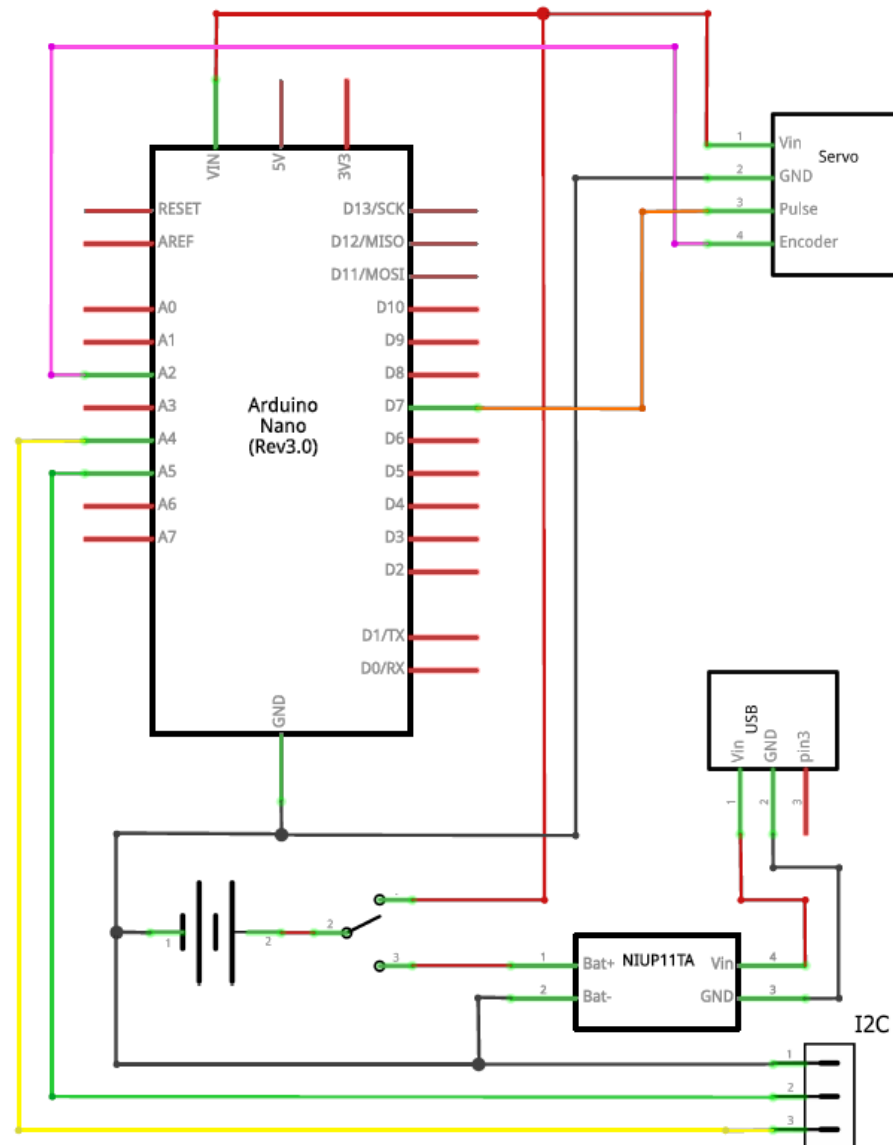


Figure 6.6: Circuit diagram of the module.

Figure 6.6 shows the circuit diagram of the module. Both the Arduino Nano and the servomotor was powered directly through the 6v battery. Similar to the head module all the electronic components were soldered to the male and female connectors respectively so they can be assembled easily in the small space of the module box. 3D printed spacers and the components were used to hold the electronics. The charging mechanism for the battery was built similar to the head module due to the same reasons. The physical properties of the module are given in table 6.3.

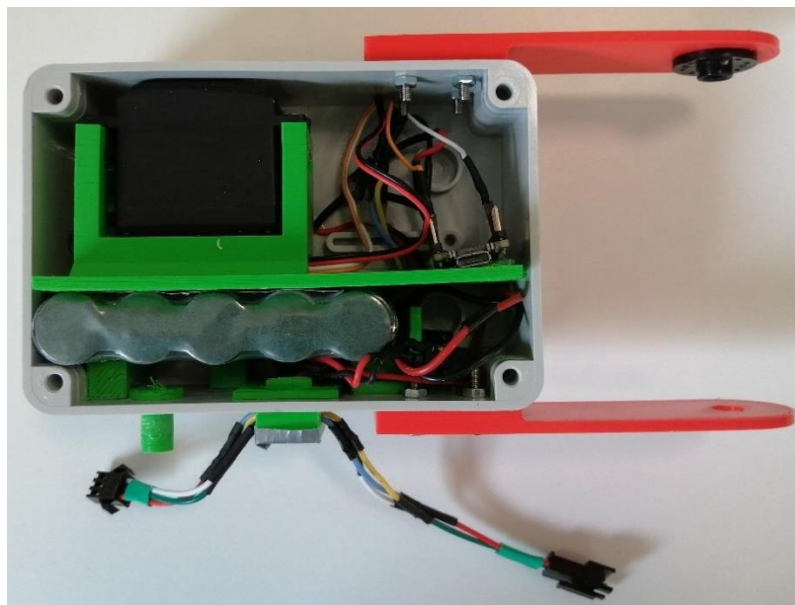


Figure 6.7: Internal components of the module.

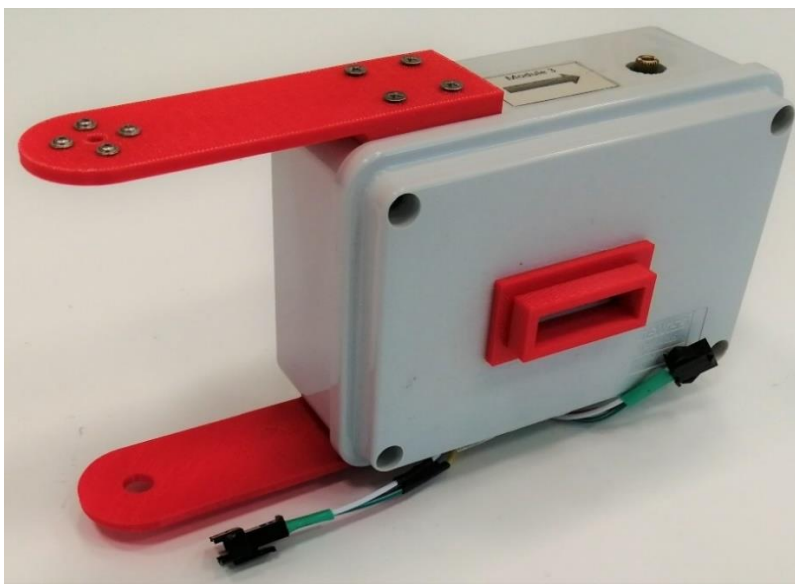


Figure 6.8: The assembled module.

Figure 6.7 shows the internal components of the module. Some of the 3D printed parts were glued to the box and while the removable components are fixed through 3mm machine screws. Figure 6.8 shows the assembled version of the module. As evident in figure 6.8 two connectors were left out of the box to connect the consecutive modules.

## 6.4 Snake Robot Assembly

The aquatic snake robot was assembled using the head module and the other 8 modules. The modules are rotated 180 degrees along its longitudinal direction for the even number of the modules. This is done so because then the lid of the box does not bring nonsymmetric feature in assembling the robot. When making the hole and printing the components this fact was taken to account. The servomotor bracket for the even number of the modules is mirrored with respect to the bracket of the odd number of the modules.

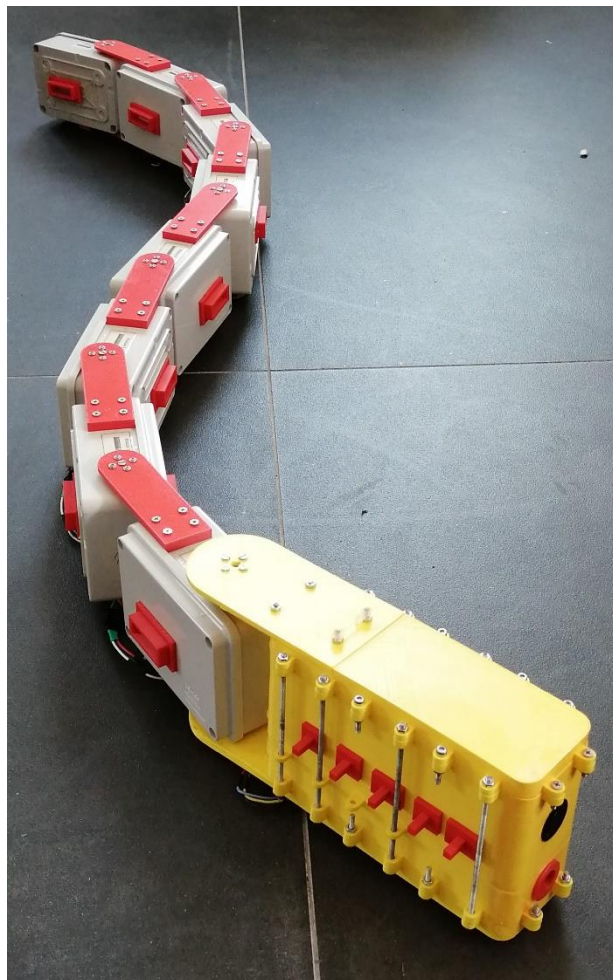


Figure 6.9: The assembled snake robot.

The modules were connected using the extended arm. For this purpose, a bracket was used. This bracket was mounted on the extended arm with 2.5mm screws. When connecting the modules one to another, we make sure that the servomotor was at the zero-degree position, otherwise, the oscillation moment will have an unintentional offset. Figure 6.9 shows the assembled aquatic snake robot.



(a) Top view of the snake robot.

(b) Front view of the snake robot.

Figure 6.10: The assembled snake robot.

After assembling the modules and the head, the circuits in the modules and the head module were integrated through the connectors. The I2C protocol is established using these connectors. The all-Arduino Nano and the Arduino Mega boards must have a common ground wire for the I2C protocol to work.

After assembling the modules and the head module, the cover which was designed to increase the esthetic appeal is installed. Figure 6.10 shows the snake robot with the outermost cover. Further, to waterproof the ASR, a flexible cover was made from polythene. This cover can be easily opened and closed by a zipper. Thanks to this feature the ASR can be taken out for charging and placed back in when it is needed to be tested. Figure 6.11 shows the snake robot with the polythene cover built to make it waterproof.



Figure 6.11: The assembled ASR with the waterproofing polythene cover.

## 6.5 Experimental tests

The aquatic snake robot had been tested in an aquatic environment to test the two different swimming gaits we proposed. The aquatic snake robot did not sink into water as we expected. Therefore, it affected the stability of the ASR in the water. To solve this issue, we added weights to the snake robot. Table 6.4 shows the weights added to each module. Small lead pieces were used to add weights and they have

been glued on the backside of the outermost cover of the ASR as shown in figure 6.12.

Component	Values
Head Module	362g
Module	161g
Total Weight	1650g

Table 6.4: Added extra mass for the snake robot.

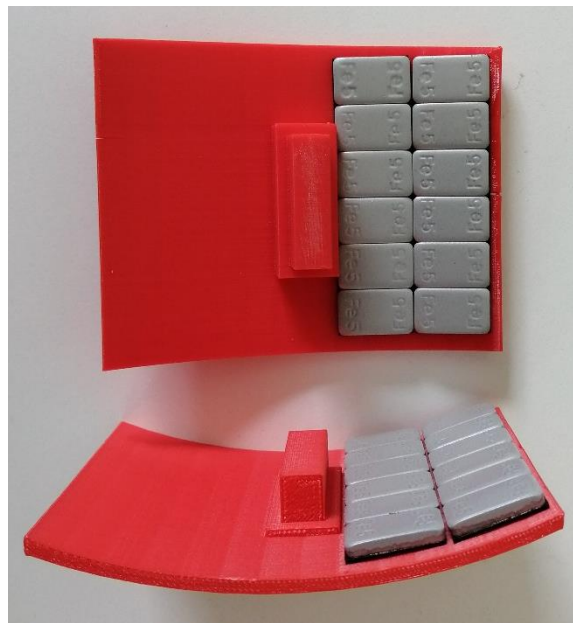


Figure 6.12: The added weights for the snake robot.

### 6.5.1 Eel-Like motion

We tested the aquatic snake robot performing the eel-like motion in an aquatic environment. We had changed the parameters necessary to perform the eel-like motion by using the wireless programming method of Arduino Mega which was discussed in subchapter 6.2. After reprogramming the Arduino Mega, we had paired and connected to the HC-05 Bluetooth module using a mobile phone. We had placed the aquatic snake robot in the water and by using the Bluetooth terminal application available in the mobile phone we had controlled the features such as forward motion, sensors activation/deactivation, etc.

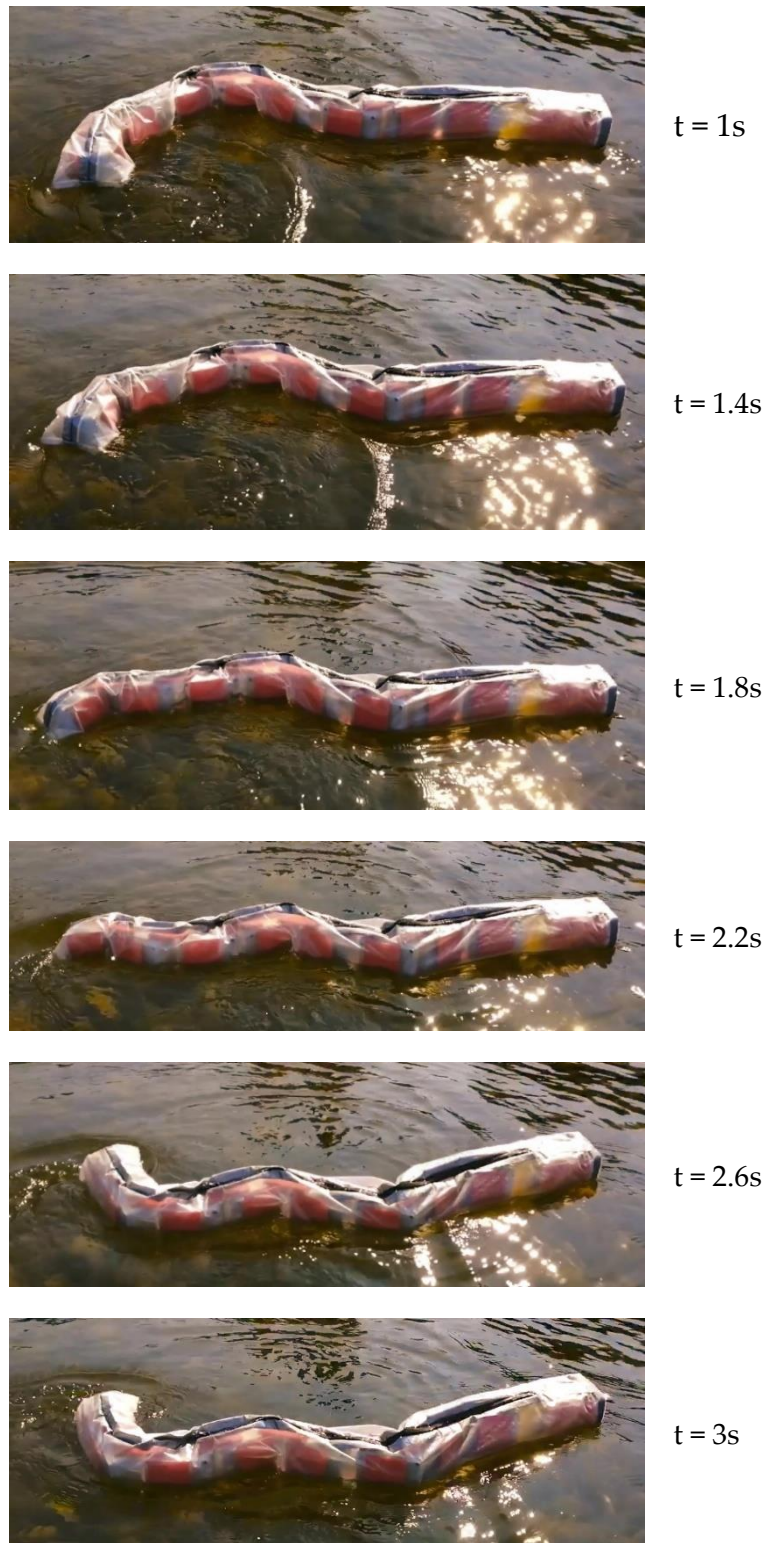


Figure 6.13: Aquatic snake robot performing the eel-like motion.

Parameters	Values
Angular Velocity	$\frac{\pi}{3} \text{ rads}^{-1}$
Phase shift	$-\frac{\pi}{18} \text{ rad}$
Amplitude	$\frac{\pi}{6} \text{ rad}$

Table 6.5: Experimental parameters for the eel-like motion.

Figure 6.13 shows images of the ASR performing the eel-like motion in time intervals of 0.4 seconds. As it is evident in figure 6.13, the last modules are actively performing the serpentine movement and the first module has a low amplitude of oscillation with respect to others. Table 6.5 shows the parameters we had used in the experimental activities. With the parameters give in table 6.5 we were available to achieve a speed roughly about  $4 \text{ cms}^{-1}$ .

# 7. Conclusion and future development

## 7.1 Conclusion

In this dissertation, we started with the design of the aquatic snake robot influenced by the design requirements. The aquatic snake robot was designed to be modular, slightly buoyant, power distributed, waterproof, and remotely operable. The design of the ASR is composed of two parts, they are head module and the module. The assembly of the ASR is composed of 1 head module and 8 modules. Several sensors such as a camera, UV sensor, and IMU sensor were included in the design of the aquatic snake robot. The data from the sensors can be transmitted to an operator or an external computer by using Bluetooth modules. These data can be used to assist the operator to navigate the ASR. Further, they can be used for autonomous navigation and semi-autonomous navigation.

A kinematic model and a dynamic model were presented, which can be used to study aquatic snake robots. Inspired by the state of art, the motion control that can be implemented to generate two different swimming gaits were developed. Equations to perform two different swimming gaits were presented. These swimming gaits were known as lateral undulation and eel-like motion. Using these equations and motion control techniques, ASR can be driven straight or turned. A simulation was performed on both lateral undulation and eel-like motion using the presented equations. Using the kinematic model, the behavior of the ASR was presented for both swimming gaits.

The aquatic snake robot was manufactured to test our motion control algorithms. All the electronic components that were used in the ASR had been pre-soldered with the connectors. We had changed the default settings of the electronic components such as the camera and Bluetooth module to serve our purpose. The fused deposition modeling was used to manufacture the cover of the head module and several other components. The head module was assembled with sensors and electronic components. A suitable module cover was brought and manufactured according to the design. The modules were assembled using the 3D-printed elements and electronic components. The ASR is assembled using the preassembled modules and

the head module. An outermost cover was fixed to the ASR to support the waterproofing polythene and to improve the esthetic aspect. A waterproofing flexible cover was made from polythene and a zipper. Zipper was included to remove and place the ASR easily.

ASR was experimented with the eel-like motion in an aquatic environment. Weights were added to the ASR to solve the problem of higher buoyant force. Wireless communication of ASR was tested at a distance of 30m. The ASR responded properly to the user commands such as motion generation and sensor activation and deactivation. We experimented with different parameters until we obtain the best straight propulsion. The aquatic snake robot performing the eel-like motion was able to achieve a velocity of roughly about  $4\text{cms}^{-1}$ . Based on the experimental result it can be concluded that the motion control we presented can be used for the control of the aquatic snake robot.

## 7.2 Future development

Future work is done on experimenting with the ASR. The lateral undulation and the turning needed to have experimented. Based on the sensors available on the ASR, obstacle avoidance driving can be tested. ASR can be improved to build a better version in the future. By using smaller batteries and the servo motors we can reduce the size of the module and therefore the total dimension of the aquatic snake robot. ASR with smaller dimensions has an advantage in accessing narrow and constrained spaces. Better sensors with better precision and accuracy can be used in motion control and obtaining data. Using the sensors available onboard and utilizing external sensors high-level feedback system can be implemented. This high-level feedback system can be used for activities such as path correction, performing CPG, autonomous driving, etc.





## Bibliography

- [1] E. Sherratt, A. R. Rasmussen, and K. L. Sanders, "Trophic specialization drives morphological evolution in sea snakes," *Royal Society Open Science*, vol. 5, no. 3, p. 172141, 2018, doi: 10.1098/rsos.172141.
- [2] S. A. Minton, "Lethal toxicity of venoms of snakes from the Coral Sea," *Toxicon*, vol. 21, no. 6, pp. 901–902, 1983.
- [3] P. Hutchings, M. Kingsford, and O. Hoegh-Guldberg, *The Great Barrier Reef: biology, environment and management*. Csiro publishing, 2019.
- [4] S. Lawrence, *The encyclopedia of animals: a complete visual guide*. Univ of California Press, 2004.
- [5] J. Stidworthy, D. McDougal, and others, *Snakes of the world by John Stidworthy; illustrated by Dougal MacDougal*. Grosset & Dunlap, 1974.
- [6] N. S. Barrett, *Poisonous Snakes*. Franklin Watts, 1991.
- [7] J. B. GRAHAM, W. R. LOWELL, I. R. A. RUBINOFF, and J. MOTTA, "Surface and Subsurface Swimming of the Sea Snake *Pelamis Platurus*," *Journal of Experimental Biology*, vol. 127, no. 1, pp. 27–44, Jan. 1987, doi: 10.1242/jeb.127.1.27.
- [8] F. Alvarez and A. Celis, "On the Occurrence of *Conchoderma virgatum* and *Dosima fascicularis* (Cirripedia, Thoracica) on the Sea Snake, *Pelamis platurus* (Reptilia, Serpentes) in Jalisco, Mexico," *Crustaceana*, vol. 77, no. 6, pp. 761–764, 2004, [Online]. Available: <http://www.jstor.org/stable/20105754>
- [9] V. Udyawer, C. Goiran, O. Chateau, and R. Shine, "Swim with the tide: Tactics to maximize prey detection by a specialist predator, the greater sea snake (*Hydrophis major*)," *PLOS ONE*, vol. 15, no. 10, Oct. 2020, doi: 10.1371/journal.pone.0239920.
- [10] A. R. Rasmussen, "Sea snakes," *FAO species identification guide for fishery purposes. The living marine resources of the Western Central Pacific*, vol. 6, pp. 3987–4008, 2001.

- [11] K. E. Carpenter and V. H. Niem, *The living marine resources of the western Central Pacific: 1. Seaweeds, corals, bivalves and gastropods*. 1998.
- [12] J. M. Mehrtens, *Living snakes of the world in color*, no. 598.12 M4. 1987.
- [13] F. Brischoux and R. Shine, "Morphological adaptations to marine life in snakes," *Journal of Morphology*, vol. 272, no. 5, pp. 566–572, 2011, doi: <https://doi.org/10.1002/jmor.10933>.
- [14] H. W. Parker and A. G. C. Grandison, "Snakes-a natural history," *Natural History*, p. 124pp, 1977.
- [15] J. A. Campbell, W. W. Lamar, E. D. Brodie, and others, *The venomous reptiles of the western hemisphere*, vol. 1, no. 2. Comstock Pub. Associates Ithaca [NY], 2004.
- [16] D. R. KARNS, J. C. MURPHY, H. K. VORIS, and J. S. SUDDETH, "Comparison of semi-aquatic snake communities associated with the Khorat Basin, Thailand," *Tropical Natural History*, vol. 5, no. 2, pp. 73–90, 2005.
- [17] J. K. Hopkins, B. W. Spranklin, and S. K. Gupta, "A survey of snake-inspired robot designs," vol. 4, no. 2, p. 21001, Jan. 2009, doi: 10.1088/1748-3182/4/2/021001.
- [18] M. Sfakiotakis, D. M. Lane, and J. B. C. Davies, "Review of fish swimming modes for aquatic locomotion," *IEEE Journal of Oceanic Engineering*, vol. 24, no. 2, pp. 237–252, 1999, doi: 10.1109/48.757275.
- [19] A. Ming, T. Ichikawa, W. Zhao, and M. Shimojo, "Development of a sea snake-like underwater robot," in *2014 IEEE International Conference on Robotics and Biomimetics (ROBIO 2014)*, 2014, pp. 761–766. doi: 10.1109/ROBIO.2014.7090423.
- [20] E. Kelasidi, P. Liljebäck, K. Y. Pettersen, and J. T. Gravdahl, "Experimental investigation of efficient locomotion of underwater snake robots for lateral undulation and eel-like motion patterns," *Robotics and Biomimetics*, vol. 2, no. 1, p. 8, 2015, doi: 10.1186/s40638-015-0029-4.
- [21] C. Stefanini *et al.*, "A compliant bioinspired swimming robot with neuro-inspired control and autonomous behavior," *Proceedings - IEEE International Conference on Robotics and Automation*, pp. 5094–5098, 2012, doi: 10.1109/ICRA.2012.6224948.
- [22] S. Yu, S. Ma, B. Li, and Y. Wang, "An amphibious snake-like robot: Design and motion experiments on ground and in water," in *2009 International Conference on Information and Automation*, 2009, pp. 500–505. doi: 10.1109/ICINFA.2009.5204975.

- [23] A. Ming, T. Ichikawa, W. Zhao, and M. Shimojo, "Development of a sea snake-like underwater robot," in *2014 IEEE International Conference on Robotics and Biomimetics (ROBIO 2014)*, 2014, pp. 761–766. doi: 10.1109/ROBIO.2014.7090423.
- [24] H. Ohno and S. Hirose, "Study on slime robot (proposal of slime robot and design of slim slime robot)," in *Proceedings. 2000 IEEE/RSJ International Conference on Intelligent Robots and Systems (IROS 2000) (Cat. No.00CH37113)*, 2000, vol. 3, pp. 2218–2223 vol.3. doi: 10.1109/IROS.2000.895298.
- [25] M. Mori and S. Hirose, "Development of active cord mechanism ACM-R3 with agile 3D mobility," in *Proceedings 2001 IEEE/RSJ International Conference on Intelligent Robots and Systems. Expanding the Societal Role of Robotics in the the Next Millennium (Cat. No.01CH37180)*, 2001, vol. 3, pp. 1552–1557 vol.3. doi: 10.1109/IROS.2001.977200.
- [26] M. Mori and S. Hirose, "Three-dimensional serpentine motion and lateral rolling by active cord mechanism ACM-R3," in *IEEE/RSJ International Conference on Intelligent Robots and Systems*, 2002, vol. 1, pp. 829–834 vol.1. doi: 10.1109/IRDS.2002.1041493.
- [27] W. Zhu, X. Guo, and Y. Fang, "Design of a modular snake robot and control with Internet of Things," Oct. 2017. doi: 10.1109/CAC.2017.8242884.
- [28] S. Hirose, "Snake-like locomotors and manipulators," *Biologically inspired robots*, 1993.
- [29] S. Chigasaki, M. Mori, H. Yamada, and S. Hirose, "Design and control of amphibious Snake-like Robot ACM-R5," *Nippon Kikai Gakkai Robotikusu, Mekatoronikusu Koenkai Koen Ronbunshu (CD-ROM)*, vol. 43, 2005.
- [30] A. Crespi and A. J. Ijspeert, "AmphiBot II: An amphibious snake robot that crawls and swims using a central pattern generator," in *Proceedings of the 9th international conference on climbing and walking robots (CLAWAR 2006)*, 2006, no. CONF, pp. 19–27.
- [31] Z. Y. Bayraktaroglu, "Snake-like locomotion: Experimentations with a biologically inspired wheel-less snake robot," *Mechanism and Machine Theory*, vol. 44, no. 3, pp. 591–602, 2009, doi: <https://doi.org/10.1016/j.mechmachtheory.2008.08.009>.
- [32] M. Yim, "New locomotion gaits," in *Proceedings of the 1994 IEEE International Conference on Robotics and Automation*, 1994, pp. 2508–2514 vol.3. doi: 10.1109/ROBOT.1994.351134.

- [33] M. Yim, D. G. Duff, and K. D. Roufas, "Walk on the wild side [modular robot motion]," *IEEE Robotics Automation Magazine*, vol. 9, no. 4, pp. 49–53, 2002, doi: 10.1109/MRA.2002.1160071.
- [34] R. Worst and R. Linnemann, "Construction and operation of a snake-like robot," in *Proceedings IEEE International Joint Symposia on Intelligence and Systems*, 1996, pp. 164–169. doi: 10.1109/IJSIS.1996.565065.
- [35] C. Wright *et al.*, "Design of a modular snake robot," in *2007 IEEE/RSJ International Conference on Intelligent Robots and Systems*, 2007, pp. 2609–2614. doi: 10.1109/IROS.2007.4399617.
- [36] M. S. M. Jasni, R. E. Samin, and B. S. K. Ibrahim, "Biological Inspired Inspection Underwater Robot (SNAKEY)," *Procedia Engineering*, vol. 41, pp. 1058–1064, 2012, doi: <https://doi.org/10.1016/j.proeng.2012.07.283>.
- [37] A. Crespi, A. Badertscher, A. Guignard, and A. J. Ijspeert, "AmphiBot I: an amphibious snake-like robot," *Robotics and Autonomous Systems*, vol. 50, no. 4, pp. 163–175, 2005, doi: <https://doi.org/10.1016/j.robot.2004.09.015>.
- [38] A. Kuwada, S. Wakimoto, K. Suzumori, and Y. Adomi, "Automatic pipe negotiation control for snake-like robot," *IEEE/ASME International Conference on Advanced Intelligent Mechatronics, AIM*, pp. 558–563, 2008, doi: 10.1109/AIM.2008.4601721.
- [39] P. Liljebäck, Ø. Stavdahl, K. Y. Pettersen, and J. T. Gravdahl, "Mamba - A waterproof snake robot with tactile sensing," in *2014 IEEE/RSJ International Conference on Intelligent Robots and Systems*, 2014, pp. 294–301. doi: 10.1109/IROS.2014.6942575.
- [40] H. Kimura and S. Hirose, "Development of Genbu : Active wheel passive joint articulated mobile robot," in *IEEE/RSJ International Conference on Intelligent Robots and Systems*, 2002, vol. 1, pp. 823–828 vol.1. doi: 10.1109/IRDS.2002.1041492.
- [41] H. Yamada and S. Hirose, "Development of practical 3-dimensional active cord mechanism ACM-R4," *Journal of Robotics and Mechatronics*, vol. 18, no. 3, pp. 305–311, 2006.
- [42] K. Wang, W. Gao, and S. Ma, "Snake-Like Robot with Fusion Gait for High Environmental Adaptability: Design, Modeling, and Experiment," *Applied Sciences*, vol. 7, no. 11, 2017, doi: 10.3390/app7111133.
- [43] Y. Takagi, M. Ishikawa, and K. Osuka, "Development and Control Experiment of a Snake-Like Robot with Controllable Side-Thrust Links \*\*This work was supported by JST CREST Grant Number JP-MJCR14D5, Japan.," *IFAC-*

- PapersOnLine*, vol. 52, no. 15, pp. 229–234, 2019, doi: <https://doi.org/10.1016/j.ifacol.2019.11.679>.
- [44] J. K. Hopkins, B. W. Spranklin, and S. K. Gupta, "A survey of snake-inspired robot designs," vol. 4, no. 2, p. 21001, Jan. 2009, doi: 10.1088/1748-3182/4/2/021001.
- [45] I.-L. G. Borlaug, K. Y. Pettersen, and J. T. Gravdahl, "Comparison of two second-order sliding mode control algorithms for an articulated intervention AUV: Theory and experimental results," *Ocean Engineering*, vol. 222, p. 108480, 2021, doi: <https://doi.org/10.1016/j.oceaneng.2020.108480>.
- [46] J. Sverdrup-Thygeson, E. Kelasidi, K. Y. Pettersen, and J. T. Gravdahl, "The underwater swimming manipulator - a bio-inspired AUV," in *2016 IEEE/OES Autonomous Underwater Vehicles (AUV)*, 2016, pp. 387–395. doi: 10.1109/AUV.2016.7778701.
- [47] E. Kelasidi, K. Y. Pettersen, A. M. Kohl, and J. T. Gravdahl, "An Experimental Investigation of Path Following for an Underwater Snake Robot with a Caudal Fin \*\*Research partly funded by VISTA - a basic research program in collaboration between The Norwegian Academy of Science and Letters, and Statoil, and partly supported by the Research Council of Norway through its Centres of Excellence funding scheme, project no. 223254-NTNU AMOS.," *IFAC-PapersOnLine*, vol. 50, no. 1, pp. 11182–11190, 2017, doi: <https://doi.org/10.1016/j.ifacol.2017.08.1242>.
- [48] A. M. Kohl, E. Kelasidi, A. Mohammadi, M. Maggiore, and K. Y. Pettersen, "Planar maneuvering control of underwater snake robots using virtual holonomic constraints," vol. 11, no. 6, p. 65005, Nov. 2016, doi: 10.1088/1748-3190/11/6/065005.
- [49] A. M. Kohl, E. Kelasidi, A. Mohammadi, M. Maggiore, and K. Y. Pettersen, "Planar maneuvering control of underwater snake robots using virtual holonomic constraints," vol. 11, no. 6, p. 65005, Nov. 2016, doi: 10.1088/1748-3190/11/6/065005.
- [50] Z. Zuo, Z. Wang, B. Li, and S. Ma, "Serpentine locomotion of a snake-like robot in water environment," in *2008 IEEE International Conference on Robotics and Biomimetics*, 2009, pp. 25–30. doi: 10.1109/ROBIO.2009.4912974.
- [51] C. Wright *et al.*, "Design of a modular snake robot," *IEEE International Conference on Intelligent Robots and Systems*, pp. 2609–2614, 2007, doi: 10.1109/IROS.2007.4399617.

- [52] C. Wright *et al.*, "Design and architecture of the unified modular snake robot," *Proceedings - IEEE International Conference on Robotics and Automation*, pp. 4347–4354, 2012, doi: 10.1109/ICRA.2012.6225255.
- [53] M. Saito, M. Fukaya, T. Iwasaki, and others, "Modeling, analysis, and synthesis of serpentine locomotion with a multilink robotic snake," *IEEE control systems magazine*, vol. 22, no. 1, pp. 64–81, 2002.
- [54] S. Ma, "Analysis of Creeping Locomotion of Snakes and Snaks-like Robots," in *Proceedings of 2001 International Workshop on Bio-Robotics & Teleoperation*, 2001, vol. 67.
- [55] K. Y. Pettersen, "Snake robots," *Annual Reviews in Control*, vol. 44, pp. 19–44, 2017, doi: <https://doi.org/10.1016/j.arcontrol.2017.09.006>.
- [56] K. A. McIsaac and J. P. Ostrowski, "Motion planning for anguilliform locomotion," *IEEE Transactions on Robotics and Automation*, vol. 19, no. 4, pp. 637–652, 2003, doi: 10.1109/TRA.2003.814495.
- [57] E. Kelasidi, K. Y. Pettersen, J. T. Gravdahl, and P. Liljeback, "Modeling of underwater snake robots," in *2014 IEEE International Conference on Robotics and Automation (ICRA)*, 2014, pp. 4540–4547. doi: 10.1109/ICRA.2014.6907522.
- [58] P. Liljeback, K. Y. Pettersen, Ø. Stavdahl, and J. T. Gravdahl, *Snake robots: modelling, mechatronics, and control*. Springer, 2013.
- [59] G. I. Taylor, "Analysis of the swimming of long and narrow animals," *Proceedings of the Royal Society of London. Series A. Mathematical and Physical Sciences*, vol. 214, no. 1117, pp. 158–183, 1952.
- [60] M. J. Lighthill, "Large-amplitude elongated-body theory of fish locomotion," *Proceedings of the Royal Society of London. Series B. Biological Sciences*, vol. 179, no. 1055, pp. 125–138, 1971.
- [61] J. R. Morison, J. W. Johnson, and S. A. Schaaf, "The force exerted by surface waves on piles," *Journal of Petroleum Technology*, vol. 2, no. 05, pp. 149–154, 1950.
- [62] O. Faltinsen, *Sea loads on ships and offshore structures*, vol. 1. Cambridge university press, 1993.
- [63] A. J. Wiens and M. Nahon, "Optimally efficient swimming in hyper-redundant mechanisms: control, design, and energy recovery," vol. 7, no. 4, p. 46016, Nov. 2012, doi: 10.1088/1748-3182/7/4/046016.
- [64] W. Khalil, G. Gallot, O. Ibrahim, and F. Boyer, "Dynamic Modeling of a 3-D Serial Eel-Like Robot," in *Proceedings of the 2005 IEEE International Conference on*

- Robotics and Automation*, 2005, pp. 1270–1275. doi: 10.1109/ROBOT.2005.1570290.
- [65] J. N. Newman, *Marine hydrodynamics*. The MIT press, 2018.
  - [66] K. Klaka, J. D. Penrose, R. R. Horsley, and M. R. Renilson, “Hydrodynamic tests on a plate in forced oscillation,” *Ocean engineering*, vol. 34, no. 8–9, pp. 1225–1234, 2007.
  - [67] S. Ma, “Analysis of snake movement forms for realization of snake-like robots,” in *Proceedings 1999 IEEE International Conference on Robotics and Automation (Cat. No.99CH36288C)*, 1999, vol. 4, pp. 3007–3013 vol.4. doi: 10.1109/ROBOT.1999.774054.
  - [68] M. Dehghani and M. J. Mahjoob, “A modified serpenoid equation for snake robots,” in *2008 IEEE International Conference on Robotics and Biomimetics*, 2009, pp. 1647–1652. doi: 10.1109/ROBIO.2009.4913248.
  - [69] J. Ostrowski and J. Burdick, “Gait kinematics for a serpentine robot,” in *Proceedings of IEEE International Conference on Robotics and Automation*, 1996, vol. 2, pp. 1294–1299 vol.2. doi: 10.1109/ROBOT.1996.506885.
  - [70] F. Matsuno and K. Suenaga, “Control of redundant 3D snake robot based on kinematic model,” in *2003 IEEE International Conference on Robotics and Automation (Cat. No.03CH37422)*, 2003, vol. 2, pp. 2061–2066 vol.2. doi: 10.1109/ROBOT.2003.1241897.
  - [71] A. Zhang, S. Ma, B. Li, M. Wang, X. Guo, and Y. Wang, “Adaptive controller design for underwater snake robot with unmatched uncertainties,” *Science China Information Sciences*, vol. 59, no. 5, May 2016, doi: 10.1007/s11432-015-5421-8.
  - [72] J. Conradt and P. Varshavskaya, “Distributed central pattern generator control for a serpentine robot,” in *Proceedings of the International Conference on Artificial Neural Networks (ICANN)*, 2003, pp. 338–341.
  - [73] D. P. Tsakiris, M. Sfakiotakis, and A. Vlakidis, “Biomimetic centering for undulatory robots,” in *The First IEEE/RAS-EMBS International Conference on Biomedical Robotics and Biomechatronics (BioRob 2006)*, 2006, pp. 744–749.
  - [74] W. Ouyang, W. Liang, C. Li, H. Zheng, Q. Ren, and P. Li, “Steering motion control of a snake robot via a biomimetic approach,” *Frontiers of Information Technology & Electronic Engineering*, vol. 20, no. 1, Jan. 2019, doi: 10.1631/FITEE.1800554.

- [75] A. Crespi and A. J. Ijspeert, "Online optimization of swimming and crawling in an amphibious snake robot," *IEEE Transactions on Robotics*, vol. 24, no. 1, pp. 75–87, 2008.
- [76] E. Kelaṣidi, K. Y. Pettersen, A. M. Kohl, and J. T. Gravdahl, "An Experimental Investigation of Path Following for an Underwater Snake Robot with a Caudal Fin," *IFAC-PapersOnLine*, vol. 50, no. 1, pp. 11182–11190, Jul. 2017, doi: 10.1016/J.IFACOL.2017.08.1242.
- [77] M. Tanaka, K. Kon, and K. Tanaka, "Range-Sensor-Based Semiautonomous Whole-Body Collision Avoidance of a Snake Robot," *IEEE Transactions on Control Systems Technology*, vol. 23, no. 5, pp. 1927–1934, Sep. 2015, doi: 10.1109/TCST.2014.2382578.
- [78] X. Zhao, L. Dou, Z. Su, and N. Liu, "Study of the Navigation Method for a Snake Robot Based on the Kinematics Model with MEMS IMU," *Sensors 2018, Vol. 18, Page 879*, vol. 18, no. 3, p. 879, Mar. 2018, doi: 10.3390/S18030879.
- [79] K. A. Melsaac and J. P. Ostrowski, "A geometric approach to anguilliform locomotion: modelling of an underwater eel robot," in *Proceedings 1999 IEEE International Conference on Robotics and Automation (Cat. No. 99CH36288C)*, 1999, vol. 4, pp. 2843–2848.





# List of Figures

Figure 0.1: Simulation of snake robot working on underwater pipes.....	2
Figure 1.1: The distribution of the Yellow-Bellied Sea snake around the world. ....	5
Figure 1.2: Different species of Sea snakes .....	6
Figure 1.3: Ventral scales of Snakes and Sea Kraits.....	6
Figure 1.4: Skeleton of a snake.....	7
Figure 1.5: A Sea snake performing lateral undulation. ....	8
Figure 1.6: An Eel performing an eel like motion.....	9
Figure 2.1: Different Snake Robots developed by Hirose.....	12
Figure 2.2: Snake robot developed by Bayraktaroglu.....	13
Figure 2.3: Snakey robot developed by Wakimoto et al. ....	13
Figure 2.4: Different Snake Robots developed by Hirose.....	14
Figure 2.5: Snake robot which can elongate, developed by Wang et al. ....	15
Figure 2.6: ACM-R5 amphibious snake robot, developed by Hirose et al.....	16
Figure 2.7: Mamba snake robot with passive propellers.....	17
Figure 2.8: Snake robot developed by Ma et al. ....	17
Figure 2.9: AmphiBot family robots, developed by Crespi et al. ....	18
Figure 2.10: Snakey robot, developed by Jasni et al. ....	18
Figure 2.11: Snake robots, developed by Wright et al.....	19
Figure 2.12: Snake robot with active propellers.....	20
Figure 3.1: Different number of the links in a robot.....	22

Figure 3.2: Exploded view of Head .....	24
Figure 3.3: CAD head assembled. ....	27
Figure 3.4: Module CAD exploded view .....	27
Figure 3.5: CAD of the assembled module .....	29
Figure 3.6: CAD of assembly. ....	30
Figure 3.7: CAD of assembly with the cover.....	31
Figure 4.1: Simplified diagram of snake robot with N links.....	34
Figure 4.2: The internal and fluid forces acting on a link.....	39
Figure 5.1: Serpenoid curve for different input parameters. ....	48
Figure 5.2: Feedback system implemented by Kelasidi et al. ....	50
Figure 5.3: The algorithm for the constant hold method steering.....	53
Figure 5.4: The joint angle variation with respect to time for lateral undulation straight motion.....	55
Figure 5.5: The simulation of progression of the ASR for lateral undulation motion.	55
Figure 5.6: The joint angle variation with decreasing exponential function for lateral undulation motion. ....	56
Figure 5.7: The joint angle variation to time in steering phase with constant offset method for lateral undulation motion.....	57
Figure 5.8: The progression of ASR in steering phase with constant offset method for lateral undulation motion. ....	57
Figure 5.9: The joint angle variation in constant hold steering method for lateral undulation motion. ....	58
Figure 5.10: Progression of ASR performing constant hold steering method for lateral undulation motion. ....	59
Figure 5.11: The joint angle variation by time for eel-like straight motion.....	60
Figure 5.12: The simulation of progression of the ASR for eel-like motion.....	60
Figure 5.13: The joint angle variation with decreasing exponential function for eel-like motion.....	61
Figure 5.14: The joint angle variation with time in steering phase with constant offset method for eel like motion.....	62

Figure 5.15: The progression of ASR in steering phase with constant offset method for eel-like motion. ....	62
Figure 5.16: The joint angle variation in constant hold steering method for eel-like motion. ....	63
Figure 5.17: Progression of ASR performing constant hold steering method for eel-like motion.....	64
Figure 5.18: The Block diagram of the implemented system. ....	65
Figure 5.19: The Block diagram of the implemented low-level feedback system in module. ....	66
Figure 5.20: The untreated encoder data from servomotor.....	67
Figure 5.21: Oscillating angle generated based on time. ....	67
Figure 5.22: The encoder data after the low pass filter implementation.....	68
Figure 5.23: The encoder data filtered through both the low pass filter and the minimum value function.....	69
Figure 5.24: Fully treated data and untreated data. ....	70
Figure 6.1: Zortax M200 printer. ....	72
Figure 6.2: Circuit diagram of the head module.....	74
Figure 6.3: Image taken from the camera module ESP32-CAM.....	75
Figure 6.4: Internal components of the head module. ....	75
Figure 6.5: The assembled head module.....	76
Figure 6.6: Circuit diagram of the module. ....	77
Figure 6.7: Internal components of the module. ....	78
Figure 6.8: The assembled module. ....	78
Figure 6.9: The assembled snake robot. ....	79
Figure 6.10: The assembled snake robot. ....	80
Figure 6.11: The assembled ASR with the waterproofing polythene cover. ....	81
Figure 6.12: The added weights for the snake robot. ....	82
Figure 6.13: Aquatic snake robot performing the eel-like motion. ....	83



## List of Tables

Table 3.1: List of components used in head module.....	24
Table 3.2: List of components used in the module.....	28
Table 3.3: The specifications of the servo motor.....	28
Table 5.1: Parameters of simulation for lateral undulation straight motion.....	54
Table 5.2: Parameters of simulation for constant offset method steering of lateral undulation.....	56
Table 5.3: Parameters of simulation for constant offset method steering of lateral undulation.....	58
Table 5.4: Parameters of simulation for eel-like straight motion.....	59
Table 5.5: Parameters of simulation for constant offset method steering of eel-like motion.....	61
Table 5.6: Parameters of simulation for constant offset method steering of eel-like motion.....	63
Table 6.1: Parameters of additive manufacturing.....	72
Table 6.2: Physical properties of head module.....	76
Table 6.3: Physical properties of the module.....	77
Table 6.4: Added extra mass for the snake robot.....	82
Table 6.5: Experimental parameters for the eel-like motion.....	84



## 2. Acknowledgements

I would like to thank Prof. Simone Cinquemani for giving me the opportunity to work on this thesis and guiding me throughout the thesis. I would also like to thank Dot. Bianchi Giovanni for the help and guidance throughout my thesis.

